Millimeter-wave generation using hybrid silicon photonics

Journal of Optics

TOPICAL REVIEW

Millimeter-wave generation using hybrid silicon photonics

To cite this article: Iterio Degli-Eredi *et al* 2021 *J. Opt.* **23** 043001

IOP Publishing Journal of Optics
J. Opt. **23** (2021) 043001 (37pp) https://doi.org/10.1088/2040-8986/abc312

Topical Review

Millimeter-wave generation using hybrid silicon photonics

Iterio Degli-Eredi[1], Pengli An[1], Jacob Drasbæk[1], Hakimeh Mohammadhosseini[1], Lars Nielsen[1], Peter Tønning[1], Simon Rommel[2], Idelfonso Tafur Monroy[2,3] and Martijn J R Heck[1,4]

[1] Aarhus University, Department of Engineering, Aarhus, Denmark
[2] Eindhoven University of Technology, Eindhoven, The Netherlands
[3] Technical University of Denmark, Department of Photonics Engineering, Lyngby, Denmark
[4] Eindhoven University of Technology, Eindhoven, The Netherlands

E-mail: ideglieredi@eng.au.dk

Received 9 March 2020, revised 6 July 2020
Accepted for publication 20 October 2020
Published 8 March 2021

Abstract

Technological innovation with millimeter waves (mm waves), signals having carrier frequencies between 30 and 300 GHz, has become an increasingly important research field. While it is challenging to generate and distribute these high frequency signals using all-electronic means, photonic techniques that transfer the signals to the optical domain for processing can alleviate several of the issues that plague electronic components. By realizing optical signal processing in a photonic integrated circuit (PIC), one can considerably improve the performance, footprint, cost, weight, and energy efficiency of photonics-based mm-wave technologies. In this article, we detail the applications that rely on mm-wave generation and review the requirements for photonics-based technologies to achieve this functionality. We give an overview of the different PIC platforms, with a particular focus on hybrid silicon photonics, and detail how the performance of two key components in the generation of mm waves, photodetectors and modulators, can be optimized in these platforms. Finally, we discuss the potential of hybrid silicon photonics for extending mm-wave generation towards the THz domain and provide an outlook on whether these mm-wave applications will be a new milestone in the evolution of hybrid silicon photonics.

Keywords: silicon photonics, hybrid silicon photonics, photonic integrated circuits, microwave photonics, millimeter-wave photonics

(Some figures may appear in colour only in the online journal)

1. Introduction

Millimeter wave (mm wave) signals, electronic signals having carrier frequencies between 30 GHz and 300 GHz, have become increasingly important for many applications such as telecommunications, radar and sensing. However, not only does it become less and less financially attractive to generate these high-frequency signals using only electronic components, but these devices are also negatively impacted by their limited frequency response [1–3]. For example, electronics-based mm-wave generators rely on frequency multiplication to achieve these high frequencies, but all-electronic frequency multipliers have limited output power and bandwidth. Moreover, the phase noise in the driving frequency is multiplied as well. These limitations can be overcome by employing photonics-based components, considering the far higher frequencies of optical waves and the availability of low-cost optical components. Indeed, frequency multiplication can

be achieved in the optical domain, as is shown by the optical fiber-based systems described in [4–7]. Nevertheless, fiber-based components are bulky, costly and require high mm-wave driving powers for efficient operation [8–11]. Assembling all these components into a useful product further reduces the reliability and mass-manufacturability of the device [8, 12].

As such, a solution to the issues that plague fiber-based devices is to integrate all of the necessary components for frequency multiplication, such as modulators and detectors, into a single optical chip. The field of integrated optics has been around for over 50 years, but it is only recently, with photonic integrated circuit (PIC) foundries offering multi-project wafer (MPW) services, that these integrated optical chips have become economically viable [13–15]. Indeed, foundries optimize their fabrication process largely through these MPW runs, enabling the realization of mass-manufacturable, high-yield and high-performance PICs as a result [16]. Achieving these objectives is necessary to enable the commercialization of integrated frequency multipliers and implement them in mm-wave technologies [17].

While different PIC technologies exist, we specifically focus on the CMOS-compatible silicon-on-insulator (SOI) platform in this paper [12, 18, 19]. The SOI platform has the advantage that its waveguides have a large refractive-index contrast between the core and the cladding, which enables the implementation of a large number of optical components such as filters, splitters etc., on a very small chip area [18, 20], achieving high functional density. The SOI platform also offers silicon–germanium (SiGe) high-speed photodetectors (PDs) with cutoff frequencies well beyond 30 GHz and plasma-dispersion-effect-based phase modulators or electro-absorption-based modulators [19, 21]. And while Si does not have a direct bandgap, thus lacking the ability to amplify light through stimulated emission and achieve on-chip lasing, this issue can be resolved by the heterogeneous integration of active III–V materials on SOI through the use of, for example, flip-chip bonding [22–24]. Since this technology also offers hybrid III–V/Si PDs and modulators, these components are not limited to SiGe or Si. These features make SOI an excellent platform for realizing on-chip mm-wave generation functionality.

Nevertheless, despite the tremendous potential of mm-wave generation in SOI, there is little to no overview of the current state of research and achievements in this field. As a result, there is also no clear outlook on which SOI-based technologies have the most potential to target applications that require mm-wave generation (in terms of their performance metrics), neither is there a clear outlook on emerging technologies in this field. We therefore believe it is crucial to list and discuss the latest techniques of SOI-based mm-wave generation and as such, in this review paper, we explain their importance in the framework of applications and target metrics. The paper is organized as follows: in section 2, we detail the existing and emerging applications for mm-wave systems, most notably in wireless communications, sensing and imaging and quantify the requirements for such systems to set the context and target metrics for the use of SOI photonics later on. In section 3, we list the main building blocks that are needed to enable photonics-based mm-wave generation and explain how bulk fiber-based off-the-shelf components can provide this functionality. We then explain which integrated photonics technologies are required to enable mm-wave generation on a chip in section 4 and provide a brief overview of the main integration platforms in this way. We make the case that SOI or hybrid SOI are the most advantageous platforms for this purpose and provide some examples of devices that have already been realized using the SOI platform. In sections 5 and 6, we discuss two key components for the generation of mm waves in detail: the high-power photodiode (PD) and the linear modulator. In particular, we will (1) review the relevant performance metrics of each component, (2) explain how one can optimize these metrics in the realm of the SOI platform and (3) discuss the current state of the art of the SOI-based PDs and modulators. Since the discussion in these sections still revolves around components operating in the mm wave band below 100 GHz, we will focus in section 7 on the opportunities to use SOI photonics for mm-wave generation beyond 100 GHz and into the terahertz (THz) regime. In particular, we provide a brief overview of the current techniques for THz generation and we then discuss three approaches to achieve this functionality on an SOI chip. Finally, in section 8, we conclude the paper with an outlook for the field, exploring whether mm-wave applications could be the next key application of silicon (Si) photonics after datacenter interconnects and telecommunications.

2. Applications and requirements for optically generated mm-wave signals

Mm waves have gained tremendous research interest in a wide range of applications in communications and sensing over the last two decades [25–33]. In this section, we will review these applications and discuss their performance metrics such as the signal and system requirements, i.e. the frequency, bandwidth, and power of the signal and the size, energy-efficiency, and cost of the system, as well as the applicable regulatory frameworks for photonics-based generation of mm-wave signals.

2.1. Applications

2.1.1. Communications. As the demand for high datarates continues to increase, spectrum allocations have been made available in the mm-wave range to address the capacity limits and spectrum shortages that plague wireless and mobile communication services in the common frequency bands below 6 GHz [27, 34–36]. Although, compared to traditional microwaves, mm waves suffer from a larger path loss, increased atmospheric attenuation, higher precipitation impact, and more restricted penetration through typical building materials [27–29, 35, 36], the introduction of multiple-input multiple-output signaling and beam shaping and steering, allows transmission in urban environments over the distances typically required for mobile fronthaul or local high-speed access [28, 36–38].

While mm waves are already employed in short-range wireless services and small-cell backhaul [38, 39], they will play a

key role in supporting the ambitious targets set for 5G mobile networks, i.e. the widespread availability of mm wavebands at around 30 GHz and beyond. As compared to 4G, mm-wave technology will enable a reduction of latency by a factor of 10, a hundred-fold increase in user data rate and connectivity density, a twenty-fold increase of peak data rates and area traffic capacity and more importantly, the possibility of progressing beyond these performances in future networks [27, 28]. When large distances can be bridged between the source, where the signal is generated, and the antenna, where the signal is converted to radio frequencies for radiation to free space, different functional splits between centralized and distributed network elements are enabled, which allows for novel distribution strategies for the dense deployment of pico- and microcell 5G base stations [2, 28, 40–43]. It is here that optically generated mm waves are especially interesting, considering the availability of low-loss optical fibers for distributing mm waves via optical signals [2, 28, 35, 44].

2.1.2. Sensing and imaging. Apart from communication networks, mm waves can also be employed in security, scanning, imaging, and spectroscopy applications; the non-destructive nature of this technology when used for analysis and inspection provides superior measurement quality and reduced measurement time, compared to other sensing and measurement technologies [31, 32, 45]. Mm-wave sensors provide specific advantages in many fields, resulting in considerable industry interest and a continuous expansion of the range of target applications [32].

In security screening and imaging, mm and THz waves have found their way into body scanners such as those employed at airports, as an addition to optical imaging, since they allow 'seeing through' clothes and polymers [32, 45], while their ability to penetrate poor weather allows advances in surveillance. In the industrial field, mm waves are currently used for structural monitoring, as well as material and process analysis [32, 45, 46].

In radar applications, such as vehicular and military radar, wireless positioning systems, and navigation aids, the use of mm waves combines high-precision measurement of distances and velocities with short measurement times [30–32, 46–48], while still being robust against many environmental influences as compared to other solutions such as LIDAR. This allows for applications in the military and automotive sectors [47, 48], but also in the analysis and control of industrial processes [46]. In vehicular radar, sensors at frequencies just below and within the lower third of the mm-wave spectrum have enabled automatic distance control, which will play an increasingly important role in the developments leading to autonomous driving [47].

2.1.3. Other emerging applications. Apart from its use in communication, sensing and imaging applications, mm-wave technology might also be employed as a medical treatment for pain relief. Low power density (typically below 10 mW cm^{-2}) mm-wave-based pain-relief treatments were popular in the USSR and several studies seem to indicate that there are therapeutic effects associated with these treatments [49, 50]. However, there is, as yet, no consensus about their effectiveness, the underlying physical mechanisms or the methodology itself (such as the power density, duration and frequency of the treatment) [51]. As such, more research and clinical tests are needed for this treatment to be accepted by the medical community and conform to medical standards [51].

While the communication applications discussed in this paper mainly focus on 5G and other telecom networks, mm waves can also be employed in virtual reality headsets due to their ability to reduce latency and offer higher bandwidths [52]. This also allows the processing of high-quality VR images to be moved to a remote computer instead of the processors inside the VR headsets, thus reducing their cost [52]. The same principle can be applied to enable wireless streaming of ultrahigh-resolution videos [53, 54]. Finally, another area that can benefit from mm-wave technology is wireless communication within data centers [55]. This development can improve the energy efficiency of data centers, as replacing the physical connectors between racks or other parts of the datacenter with wireless communication in the mm-wave range allows for more efficient cooling of all the servers and processors due to better air circulation, without impacting the bandwidth of the data transfer [55]. We expect these wireless technologies to become more and more mainstream in future years, considering the current technological developments towards 5G and WiGig [39, 56].

2.2. Requirements

Clearly, mm waves have immense technological potential. Combining mm waves with photonics and in particular, generating mm-wave signals through optical means, will further improve and extend the functionality of mm-wave-based devices. However, this technology can only be successful when certain requirements are met for both the mm-wave signals themselves, such as signal carrier frequency, quality, bandwidth, and power, and the hardware employed for signal generation, such as size, energy footprint, and cost.

2.2.1. Signal requirements. The requirements imposed on mm-wave signals not only depend on the target application and the required performance but are also impacted by regulatory provisions, such as spectrum assignment and signal-quality standards, e.g. in cases where mm-wave radiation might interfere with other systems.

2.2.1.1. Frequencies and tunability requirements. Figure 1 provides a summary of some of the recent mm-wave spectrum assignments and their target applications. Although there are different standards for naming the frequency bands, we will abide by the nomenclature of figure 1 throughout this review. For telecommunications and many radar applications, the lower part of the mm-wave spectrum, i.e. up to 100 GHz, is currently of the most interest. The generation of mm-wave signals in this frequency range must be able to precisely match the target frequency band, and typically be tunable to sub-bands

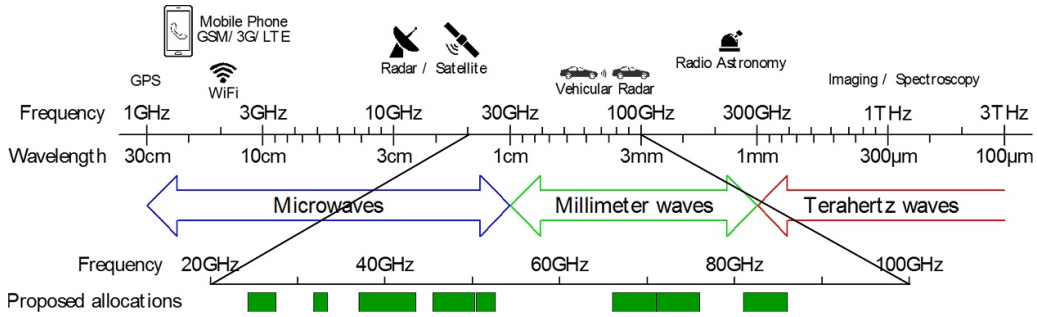

Figure 1. Applications and frequency allocations for (mobile) communications in the mm-wave range.

and/or channels therein during operation. This depends on the model employed for spectrum licensing and/or sharing as well as potential frequency multiplexing [28, 40, 41, 57]. Applications, e.g. radar, especially frequency-modulated continuous-wave (CW) radar, require mm-wave signals of high purity and with large instantaneous frequency [47, 48]. And with existing spectrum assignments as wide as 14 GHz around a center frequency of 64 GHz, tunability of more than 20% of the central frequency is required.

Sensing applications, such as spectroscopy and imaging, already routinely make use of the full mm-wave spectrum and frequencies beyond, i.e. into the THz range [31, 45]. The requirements are as diverse as the sensing applications themselves, including CW signals, modulated signals, pulsed signals, and frequency combs, as well as wideband noise [31]. On one hand, frequency-domain spectroscopy and imaging applications often require narrowband sources to be swept over large sections of, or even the whole, mm-wave spectrum (and often beyond, into the THz range) [31, 45]. On the other hand, time-domain spectroscopy requires sources that provide short pulses or frequency combs [31]. Finally, wideband mm-wave noise sources may be required to improve spatial resolution in imaging [31].

2.2.1.2. Bandwidth and modulation requirements. The interest in mm-wave signals for communications is largely stimulated by the availability of larger channel bandwidths of up to a few GHz. Any signal generation scheme must be able to support such modulation bandwidths. To achieve the required capacities, it must support complex modulation formats, i.e. the modulation of signal amplitude and phase [2, 28, 58]. Similarly, for high-speed frequency-modulated CW radar systems, instantaneous bandwidths of multiple GHz and repetition rates of hundreds of kHz are required [48].

2.2.1.3. Regulatory requirements. These requirements will mainly affect applications where a mm-wave signal is radiated into free space, such as 5G communications and radar. They set strict limits on the deviations allowed from the specified signal frequency and power. Specifically, for communication services in the mm wave band, the ITU-R mandates frequency stabilities within ± 150 ppm to ± 100 ppm of the target mm-wave frequency [59], while the requirements posed by standards for mobile networks may be even more stringent. For radar systems, the emission must be contained within the assigned band or deviations must be below 5000 ppm [59]. These regulatory requirements may be more stringent than the technical requirements for the successful operation of the application, as they are mainly driven by spectrum scarcity, even at mm-wave frequencies, and by the requirement for protection against interference. These stringent requirements for signal purity are likely to strongly influence applicable mm-wave generation schemes, especially for communications [37, 60].

2.2.1.4. Signal power requirements. The signal power required for mm-wave applications varies widely, ranging from below 1 mW to the region of multiple W. While for indoor and sensing applications the required power may be very low, for radar and telecommunications, significant levels of radiated power are required to achieve the necessary range and signal-to-noise ratio (SNR). While this may mandate overall radiated powers on the order of a few W, this does not necessarily directly translate into an equal power-output requirement from mm-wave signal generation or amplification, since with MIMO processing or analog beamforming from large antenna arrays, multiple mm-wave sources or chains combine to effectively form a concentrated radiated signal and thus radiation levels from each antenna element may be substantially lower [28]. The resulting requirements for mm-wave signal generation are therefore not only highly application specific but also vary, depending on the radiation and deployment strategy.

Finally, safety and health regulations impose strict limits on the radiated power levels, severely limiting the allowed radiated power levels or requiring large exclusion zones around radiating elements. While the permitted radiation levels may be as high as 10 W m^{-2} (ICNIRP guideline, USA, Canada, non-binding EU regulations) in some countries, others impose restrictions on power levels that are up to two orders of magnitude lower, i.e. 0.1 W m^{-2} (Poland, Bulgaria, Russia) [61, 62].

2.2.2. Size and energy footprint and cost. The actual target size and energy footprint for mm-wave generation depend on the type of target application, with larger footprints allowed in certain cases, e.g. stationary radar and industrial monitoring, while embedded sensing and mobile communications require extreme integration. For the vast majority of applications, however, the required sizes range from a few cubic millimeters

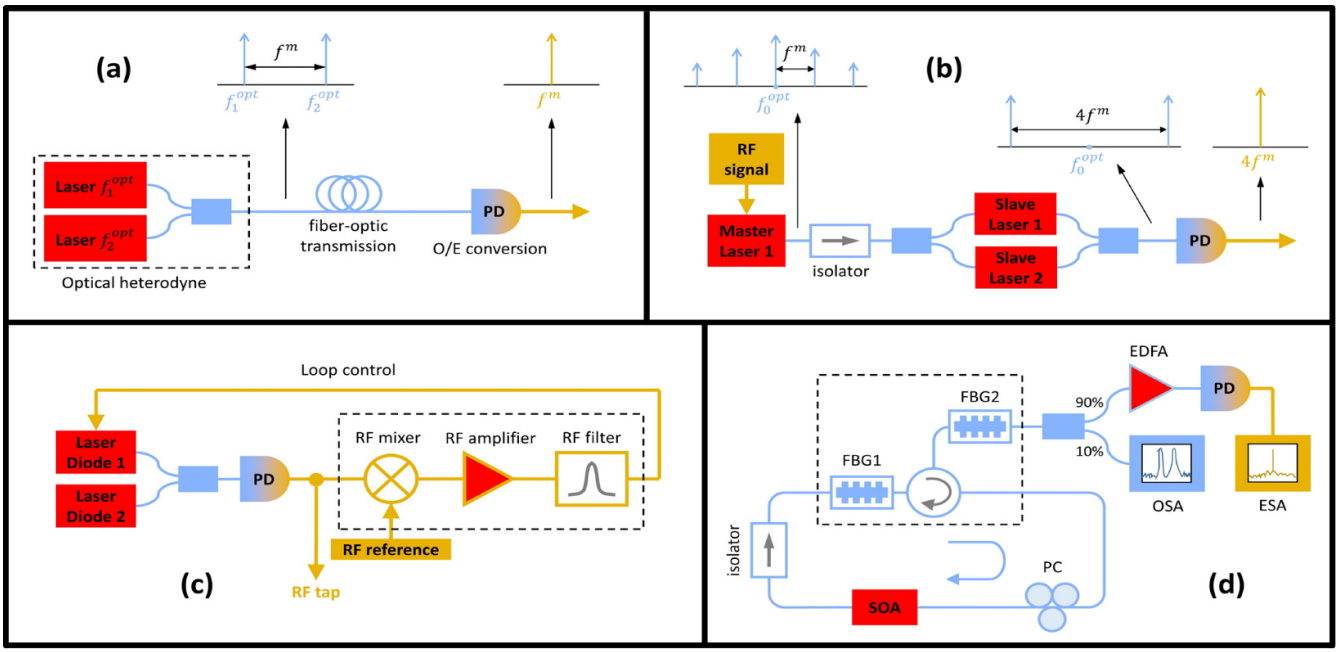

Figure 2. Mm-wave generation through the heterodyning of two lasers and methods of improving the performance. (a) Mm-wave signal generation by beating the output of two lasers with optical frequencies f_1^{opt} and f_2^{opt}, using an optical heterodyning technique. An opto-electrical (o/e) converter, the PD, demodulates the envelope or the beat signal of the optical signal to the electrical domain as a single mm-wave frequency. System configuration for microwave and mm-wave signal generation using (b) an optical-injection-locking technique, (c) an optical phase-locked loop (OPLL) technique and (d) a dual-wavelength laser source. (a) © 2011 IEEE. Reprinted, with permission, from [74]. (b)–(d) © 2009 IEEE. Reprinted, with permission, from [75].

to a few tens of cubic millimeters, necessitating co-packaging or complete integration [47, 63, 64]. Similarly, the constraints in regards to energy consumption are highly dependent on the environment in which the application will be employed, with the constraints for stationary applications being less stringent than for mobile, remote or autonomous devices [41].

Nevertheless, low-energy operation and a reduction in energy consumption are especially important considering the introduction of multiple-input multiple-output signaling or beamforming, with large transmitter and receiver arrays, at mobile base stations or other transmitting equipment. Since this necessitates densely integrated and highly efficient mm-wave signal chains [38, 40, 41], the mm-wave signal generation, analog signal processing functionality and potentially the radiating antenna need to be integrated on a total footprint of less than a few tens of square millimeters. Due to this reduction of the spatial footprint, these devices potentially have reduced energy consumption and unit cost [64]. This makes dense integration a prerequisite for the use of mm-wave signals and suggests mm-wave generation in integrated photonics as a key enabler in a wide range of applications.

Finally, apart from the devices themselves, the introduction of mm-waves to mobile and wireless communications also causes a paradigm shift in the way networks are built and operated, including radical changes in network architectures and control, as well as base station design and deployment [35, 41]. The large increase in the number of deployed base stations dictates a significant reduction in their energy consumption [35, 38, 41, 44], as well as the energy consumption of their front- and backhaul, where the latter requires a close tie-in with optical fiber [2].

While changes to network operation and resource assignment may improve energy usage, the main contribution to optimizing energy consumption and cost will still come from an appropriate design of the mm-wave devices themselves, at the very least through dense integration and cost-effective high-frequency packaging [64]. The recent advances in co-packaging or even the complete integration of full mm-wave front ends, including radiating antennas [64], have dramatically reduced the size and cost of mm-wave generation and processing devices, which makes the use of mm-wave signals feasible for the applications mentioned earlier. Combining mm-wave technology with photonics through PICs has the potential to achieve the target metrics at a lower cost and to extend their applicability.

3. Techniques for photonics-based mm-wave generation

Having reviewed the applications and target metrics in section 2, we now discuss how photonics technology is capable of realizing the mm-wave functionalities. We start by summarizing the main photonics building blocks and then present an overview of the techniques and approaches commonly used to generate mm-waves. Even though mm-wave functionalities are typically implemented using fiber-optic approaches, this overview provides a necessary background

for discussing the implementation of these functionalities on SOI-based PICs.

3.1. Photonic building blocks

The main building blocks found in photonics-based mm-wave links are listed and briefly discussed below:

Source: the optical source in a mm-wave link is a laser that typically operates in the telecom window with a wavelength of around 1550 nm. The laser can be continuous wave or pulsed through mode locking (ML). The laser can be fiber-based or a laser diode (LD) coupled to a fiber [65, 66].

Modulator: this component transfers the electric mm-wave signal onto the optical carrier wave. The modulator can be placed outside the laser cavity, i.e. external modulation of CW laser light or the mm-wave signal can be applied directly to the laser, i.e. direct modulation. The optical modulator may serve different purposes in mm-wave optical systems, both for mm-wave upconversion (i.e. when driven with a sinusoidal signal) and for modulation with data in telecommunications applications.

Transmission: this functionality is achieved with optical fibers that can transmit optical signals carrying mm-waves with far lower loss, cost and weight than electronic cables.

Filter: this component is required for various signal-processing tasks in a mm-wave photonic system. Filters are typically either feedback-type filters, such as Fabry–Perot (FP) and ring resonators, or feedforward-type filters, such as asymmetric Mach–Zehnder interferometers (MZIs). One can also employ whispering-gallery-mode (WGM) -based filters, whereby the ring resonator is replaced with a sphere that is evanescently coupled with a tapered fiber [67–69]. These components provide lower footprints than ring resonators and higher loaded Q-factors but also suffer from higher-order mode coupling and vibrational instabilities.

Detector: this component retrieves the mm-wave signal from the optical carrier. The main detector technology used in microwave photonic links is the PIN PD, which consists of a junction diode where an intrinsic absorbing layer is placed between p-doped and n-doped layers. Under reverse bias, this PD converts light into a photocurrent [70], or more precisely, the envelope of an optical wave will be transferred into the electrical domain. Fiber-based PDs are typically vertically illuminated PIN PDs (VPIN) and their potential for use in microwave photonic links has been extensively studied, as light can easily be coupled to a PD. The electrical bandwidth, responsivity and linearity are the main characteristics for mm-wave applications. Nevertheless, there is a trade-off between the responsivity and the bandwidth. The bandwidth can be improved by optimizing the width of the active absorption region and the saturation velocity in the semiconductor material [70]. A resonant-cavity-enhanced PD can be used to optimize the bandwidth efficiency, by creating multiple reflections inside the PD [71]. To tackle bandwidth–responsivity trade-offs, one can employ vertically illuminated uni-travelling-carrier PDs (UTC-PDs), where the layer stack causes the photoresponse to only be determined by the electron transport, as opposed to regular PIN PDs, where both electron and low-velocity-hole dynamics determine the photoresponse [72]. Finally, one can also employ avalanche PDs since they provide higher responsivity as compared to PIN devices due to their higher internal gain [73], but nevertheless, they suffer from the gain–bandwidth trade-off in these structures.

3.2. Generating mm-waves through photonic approaches

3.2.1. Heterodyning of two CW lasers. The basic concept of the generation of optical signals using optical heterodyning is shown in figure 2(a). Two laser sources, with an optical output frequency difference equal to the desired frequency of the mm-wave signal, are combined in a waveguide or fiber. The optical signal is then, if necessary, transmitted through an optical fiber, and a PD transfers the envelope of the beat signal in the electrical domain, thus generating a mm-wave signal [74, 75]. This technique does not require a mm-wave source or a modulator. Optical heterodyning enables the generation of mm-wave signals with ultra-wide tuning range, and was already reported as early as 1955 [76]. In practice, the tunable range of frequencies is typically limited by the PD's bandwidth.

This approach has one major drawback: the random frequency and phase fluctuations of the lasers will appear in the frequency and phase of the generated mm-wave signal [75]. As such, heterodyning requires stabilization techniques for the generated mm-wave signal. One such technique is shown in figure 2(b), where an optical-injection-locking system is depicted [75]. The system consists of a master laser that is directly modulated by a radio-frequency (RF) signal, two slave lasers, and a PD. The output of the master laser, which is a comb of optical frequencies with a spacing corresponding to the RF modulation frequency, is injected into the slave lasers. The free-running wavelengths of the two slave lasers are selected to be close to the sidebands, e.g. the +second order and −second order, as indicated in figure 2(b), and can lock to the injected wavelengths, thereby stabilizing the mm-wave frequency to the RF modulator. This technique was, for example, used to generate a 35 GHz mm-wave signal with a 10 Hz linewidth [77], and to generate a tunable signal from 10 GHz to 110 GHz [78]. Such systems may offer additional advantages to telecommunications networks, since with the addition of slave lasers tuned to other spectral lines of the comb, additional coherent mm-wave signals can be created or additional functions such as optical downconversion of mm-wave signals can be achieved [79].

In another approach to lock the phase of two lasers, one uses an optical phase-locked loop (OPLL). As shown in figure 2(c), an OPLL system consists of two LDs, a PD and an RF phase detector consisting of an RF mixer, RF amplifier and RF loop filter. The two LDs each have a different optical frequency, thus creating a beat signal when combined at the PD. This beat signal is converted to a mm wave by the PD with a frequency equal to the optical frequency difference of the LDs. The mm wave is sent to a phase detector that measures the phase difference between the mm-wave signal and a reference RF signal. The difference signal is then used to control the frequency of (one of) the LDs, e.g. by varying the injection current. A short

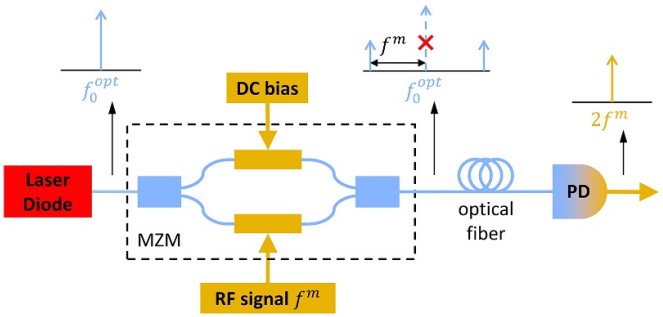

Figure 3. System schematic of microwave and mm-wave signal generation using an external modulation technique [80] (picture reworked, with permission, from the IEEE Photonics Society Newsletter, © 2012).

feedback-loop length increases the bandwidth of the locked frequencies [80], which is a clear rationale for integrating this system in a small area such as a PIC, as part of a system-in-package approach [81].

Finally, the use of a dual-wavelength source is another technique for generating stable mm-wave signals. This approach has several advantages as compared to optical injection locking and OPLL techniques. Not only are the two wavelengths generated from the same cavity instead of two separate free-running lasers [75], but also the RF reference source can be eliminated and only a single laser is required instead of two. An example configuration of such a dual-wavelength laser is shown in figure 2(d) [75, 82]. Two ultra-narrow-band fiber Bragg gratings are used in a laser cavity to select the modes. The generation of microwave signals at 18.68 GHz and 6.95 GHz and a mm-wave signal at 40.95 GHz, with a linewidth below 80 kHz and stability of around 1 MHz was reported [82]. The same functionality is demonstrated by a dual-longitudinal-mode microchip laser, where 102 GHz signal generation, with a linewidth of 430 Hz, was achieved [83].

3.2.2. External modulation. Instead of direct modulation of the laser source as used with the optical-injection-locking approach, an external modulator can also be used to generate the optical sidebands used for mm-wave generation. We refer to the system depicted in figure 3, where only one laser source, an optical modulator, typically a Mach–Zehnder modulator (MZM), and a PD are used [80].

An oscillating RF driving signal is applied to the external modulator to create higher-order optical sidebands. The carrier and unwanted sidebands can be suppressed, e.g. by biasing the MZM at its minimum-transmission point [84], and the resulting optical beat signal is converted to a mm wave using a PD. This approach has the advantage that no optical frequency control is required, since frequency and phase fluctuations do not affect the beat signal at the PD and as such, stable and low-phase-noise mm-wave signals can be generated. Moreover, since the high-frequency mm-wave signals are generated from a lower-frequency driving signal, relatively low-bandwidth optical modulators can be used to generate mm waves. For example, the generation of a 36 GHz signal using an 18 GHz RF driving signal has been reported in [84]. In another example, the quadrupling of a 15 GHz RF driving signal to generate a 60 GHz signalusing an imbalanced MZ filter was achieved in [85].

3.2.3. Comb generation with consecutive line filtering. The comb generation with line filtering approach is an extension of the external modulation technique discussed above, though often based on pure phase modulation rather than an MZM for higher efficiencies in comb generation. An RF driving signal is frequency multiplied in the optical domain by generating a wide comb of optical frequencies, and filtering the comb lines with a spacing corresponding to the target mm-wave frequency. Several multiplication factors have been reported so far. For example, using a tunable FP filter, 54 GHz, 90 GHz and 126 GHz signal generation has been reported [86]. In [87], a $LiNbO_3$ intensity modulator and a Bragg grating filter were used to achieve frequency quadrupling of tunable RF driving signals from 8 GHz to 12.5 GHz, thus generating frequencies from 32 GHz to 50 GHz. Since the odd-order harmonics were suppressed by the MZM bias, and a filter was used to suppress the carrier, the need for tunable optical components was eliminated. The optical filter can be eliminated using a dual−parallel MZM configuration whereby each MZM arm has an MZM as well. This has been demonstrated in [3], where frequency quadrupling was used to generate 40 GHz and 72 GHz signals. Simulations show that this approach can be extended to frequency sextupling [88] and octupling [89]. Finally, one can also employ cascaded MZMs as a flexible way to achieve frequency quadrupling, sextupling and octupling [90]. In general, such high multiplication factors are of great interest since modulators with lower bandwidths, and consequently RF driving signals with lower frequencies can be used.

3.2.4. Mode-locked lasers (MLLs). MLLs are lasers that have an optical output of spectrally equidistant comb lines, whose phases are locked in such a way that the frequency comb generates a pulsed output, where the repetition rate of the pulses is equal to the frequency difference between two adjacent comb lines. As a result, MLLs coupled to a PD have the potential to generate mm-wave signals when the pulse repetition rate is in this frequency regime [91].

The signal quality of the generated mm-wave signals depends on the properties of the MLLs and in particular, whether one uses the active or passive ML technique. For example, passive-mode locking can be achieved using saturable absorbers and does not require a reference source or an external modulator [92]. This greatly simplifies the system, but the generated mm waves also typically contain more phase noise than when active mode locking with a low-phase-noise driving RF signal is employed. Microwave signal generation at 15 GHz was achieved using an active MLL, based on a distributed feedback (DFB) indium phosphide (InP) laser and an integrated passive extended cavity [93]. To avoid the use of high-frequency driving signals and high-bandwidth

modulators in these actively MLLs, a (rational) harmonic ML technique can be used. Signal generation at 22.08 GHz from a 5.52 GHz modulator driving signal was achieved [91] in a fiber-based MLL. Alternatively, frequency multiplication in actively MLLs has also been proposed to increase the repetition rate [94].

3.2.5. Opto-electronic and coupled-opto-electronic oscillators (OEOs and COEOs). An effective approach for generating ultra-stable, low-phase-noise mm-wave signals is to use an OEO [95]. The OEO does not require an external RF source, and produces microwave or mm-wave signals, which are more stable than those derived from OPLLs and injection-locking techniques [96]. An example schematic of an OEO is shown in figure 4(a) [97]. This OEO uses a ring configuration, where the light from a CW laser is externally modulated, sent through a high-Q delay line, and detected by a PD, where the envelope of the beat-signal is demodulated back into the electrical domain. This electrical signal is then filtered and amplified, after which it drives the modulator. When the open-loop gain is higher than one, oscillation is achieved at an RF frequency that corresponds to a harmonic of the loop length which is selected by the filter. In this way, highly stable mm-wave signals can be generated, such as the 75 GHz mm-wave signals in [96].

One important parameter that impacts the signal quality or phase noise of the generated mm-waves is the fiber length in the OEO [99]. While lengthening the fiber will result in a reduction of the noise, it will also cause an increased number of harmonics, with a small free spectral range (FSR) between these modes. As a consequence, an increasingly narrow band filter is required for suppression of the unwanted modes. This issue can be addressed by implementing an optical filter, such as employing multiple fiber loops in the OEO configuration. For instance, using a triple-loop OEO and an yttrium iron garnet (YIG) filter, microwave signal generation with center frequencies between 6 GHz and 12 GHz was demonstrated in [100].

The COEO simultaneously generates short optical pulses at its optical output, and high-quality mm-wave signals at its electrical output [98]. The COEO working principle is similar to an OEO, in which laser light in an electro–optical feedback loop generates mm-wave signals. However, unlike the OEO in figure 4(a), the COEO configuration also contains an optical feedback loop with an optical amplifier, which is used to generate optical pulses. Figure 4(b) depicts a COEO with feedback towards an MZM that modulates loop gain; a 10 GHz microwave signal was generated with this configuration [98, 101, 102]. The feedback can also be directly routed towards an SOA, but the small modulation bandwidth of the SOA limits the output frequency to less than 1 GHz [102].

4. Si photonics as a platform for mm-wave generation

Having discussed the main photonic building blocks and device topologies that enable photonics-based mm-wave generation, we now delve into the opportunities to enable this functionality on PICs. We start by summarizing photonics integration technologies that realize the main photonics building blocks on a PIC and then discuss how well the different MPW material platforms are suited to each component. As explained in the introduction, the MPW material platforms provide the highest level of fabrication maturity in terms of cost, yield, reproducibility and standardization, which is crucial in the commercialization of photonics-based mm-wave devices. Finally, we provide a rationale for using Si or hybrid Si as the ultimate platform to generate mm waves and give some examples of mm-wave generation on this platform.

4.1. Realizing mm-wave functionality on a PIC: required integration technologies for the main photonic building blocks

The building blocks found in optical-fiber-based mm-wave links are not very different from those needed in PICs. The integrated photonics technologies needed to realize their functions are discussed below:

Source: an on-chip laser is realized by placing a semiconductor optical amplifier (SOA) in a resonant cavity, where the SOA is a multiple-quantum well (MQW) structure fabricated with a III–V material such as InP [26, 103]. As with LDs, these components have the potential to achieve fast modulation and thus be employed in mm-wave devices [104], but their performance is ultimately limited by their modulation bandwidth. This bandwidth depends on factors such as differential gain, optical power inside the cavity, photon lifetime, and the gain-compression factor [26]. As such, in most mm-wave links, the focus is on realizing a stable integrated CW laser source, with a tunable wavelength and a high output power, while leaving the fast modulation for the modulator part [13, 105]. Monolithically integrated lasers have been shown to achieve a tuning range of up to 74.3 nm at around 1550 nm, but they have a relatively low off-chip power of around a couple of mW and a relatively wide linewidth of 360 kHz [106]. A wider tuning range of 96 nm has been achieved at around 1600 nm by combining three lasers whose active sections have slightly different emission wavelengths, but their off-chip output power is limited to 0.14 mW [107]. A hybrid III–V/Si laser configuration containing long low-loss Bragg gratings improves the lasing stability and on-chip powers of up to 37 mW and a low linewidth of 1 kHz was demonstrated, although it had little wavelength tunability [108]. Finally, a hybrid III–V silicon nitride (SiN) laser achieved a record on-chip power of 117 mW, a tuning range of 120 nm and an ultralow linewidth of 320 Hz [109].

Modulator: PIC-based phase modulators can be realized in a wide range of different materials and are mostly used in an MZM configuration. For example, a Ti:LiNbO3 MZM using velocity-matched contacts showed a large electrical 3 dB bandwidth of 70 GHz with 5.1 V half-wave voltage [110]. An example of electro-optic modulation in GaAs can be found in [111], where a 1 cm-long traveling-wave MZM, with a half-wave voltage of 13 V and a 3dB electrical bandwidth of 50 GHz, is realized. Organic nonlinear materials can also be employed, as demonstrated by the MZM modulator with

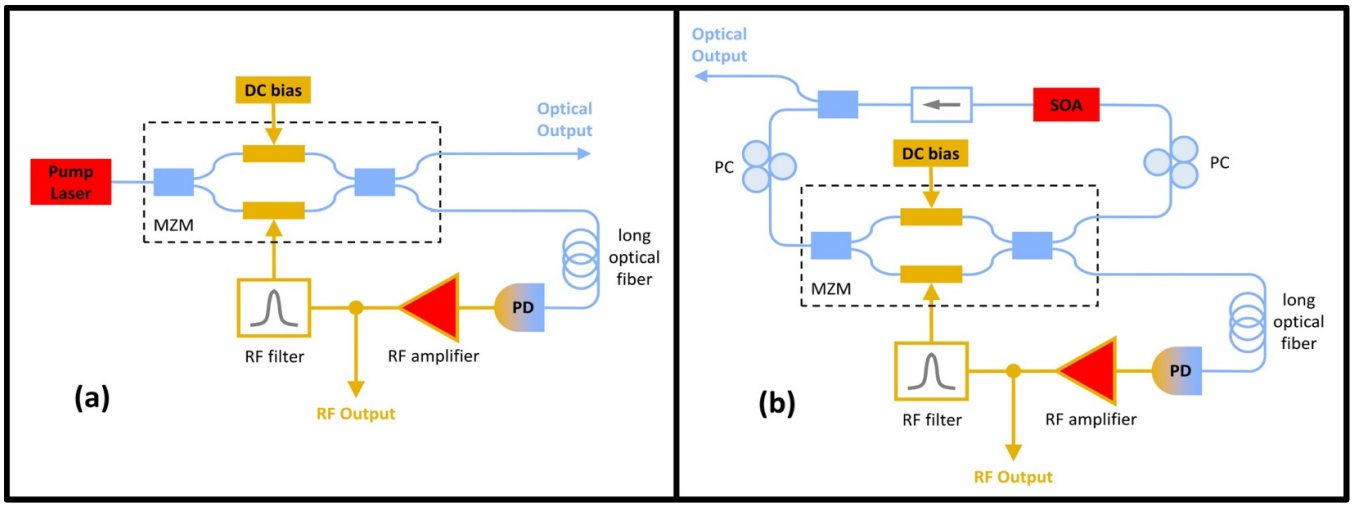

Figure 4. (a) Microwave and mm-wave signal generation using an OEO approach (adapted with permission from [97]; © The Optical Society). (b) Microwave and mm-wave signal generation using a COEO approach (© 2000 IEEE. Reprinted, with permission, from [98]).

a 40 GHz bandwidth and a 10 V driving voltage reported in [112]. An even higher bandwidth of 110 GHz for a polymer-based modulator was achieved in [113]. Apart from phase modulators, intensity modulators such as electro-absorption modulators (EAMs) can be employed as well [26]. These components are typically reversely biased MQW-based SOAs and rely on the quantum-confined Stark effect [26]. This greatly benefits the integration of EAMs with semiconductor lasers, considering the high coupling efficiency between SOAs and EAMs. An EAM integrated with a DFB laser, with a modulation bandwidth of more than 40 GHz was shown in [114]. The strong electro-optic response of such devices further enables efficient modulation over short interaction lengths, and consequently keeps the EAM capacitance low, resulting in higher bandwidths. A relatively short 50 μm MQW EAM with a bandwidth of 50 GHz and a 3 V driving voltage was reported in [115]. A traveling-wave approach can also be employed, e.g. in [116], a 40 GHz EAM was realized with small-signal modulation sensitivities down to 0.65 V^{-1}.

Transmission: while fibers will never be fully eliminated from mm-wave devices (not in the least, considering they have to communicate with fiber-optic networks), when they are employed as delay lines, low-loss integrated waveguides can be a good alternative. Although the optical propagation losses of integrated waveguides are several orders of magnitude higher than their fiber-based counterparts, their integration results in extremely small footprints. Delay lines 3 m long and resulting delays of over 10 ns have been realized on a 21 cm^2 large SiN chip [117], while a 1.46 m-long waveguide with a resulting delay of 17.2 ns and a total chip footprint of just 6.6 mm^2 has been realized on SOI [118]. Combining the low-loss chip with SOAs through hybrid or heterogeneous integration can further alleviate the losses in passive waveguides.

Filter: as compared to their fiber-based counterparts, PICs dramatically extend the filter capabilities of photonic devices. One key advantage of PICs is that they can realize existing configurations such as MZ or ring-resonator filters in a much smaller space, as is demonstrated by integrated add–drop microring resonators (MRRs) that filter out a target frequency or enable de-multiplexing for separation of optical carriers with a 60 GHz difference in frequency [119–121]. Micro-heaters were implemented to control both the extinction ratio (ER) and the quality factor. Another key advantage of PIC-based systems is that they will considerably improve the robustness of the filter system. As explained in the previous section, fiber-based WGM filters, for example, rely on evanescent coupling between high-Q resonators and tapered fibers; integrating this functionality on a PIC will make the filter much more stable against vibration. This not only improves reproducibility, but it also facilitates cascading the filter with other resonators to create new functionalities. For example, a novel optical bandpass filter has been demonstrated based on a Si microring-MZI structure [122], as shown in figure 5. The bandpass characteristic is realized by combining the drop-port transmission spectra of two identical MRRs in an MZI structure. Thermal control is used in both MRRs and the straight section of the MZI to control the bandwidth-tuning range and the wavelength-tuning range to achieve a good ER value. A bandwidth tuning range of 57 to 110 GHz and a wavelength tuning range of 1550 to 1554 nm were reported.

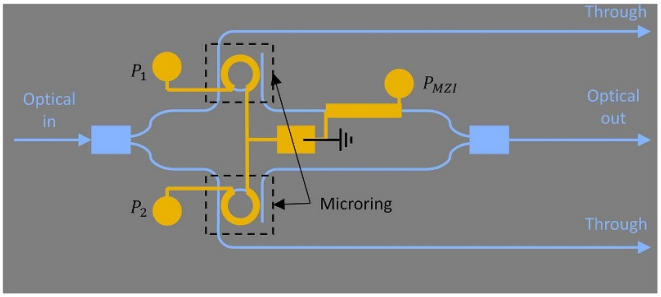

Figure 5. Schematic of the integrated optical bandpass filter (adapted with permission from [122] © The Optical Society): two identical add–drop MRRs with micro-heaters are inserted into the two arms of an MZI structure (one arm has a micro-heater as well).

Table 1. Qualitative overview of the strengths and weaknesses of the main integration PIC platforms, taken from [127, 129]. NA = not available; + = possible; ++ = good; +++ = very good; SoC = system on a chip; SiP = system in a package.

	InP	Silica/SiN	Silicon	Hybrid silicon
Lasers	+++	NA	NA	+++
PDs	+++	NA	++	+++
Modulators	++	NA	+	++
Passive devices	+	+++	++	++
Wafer level packaging	NA	+++	+++	++
Electronic SoC and SiP integration	NA	+++	+++	++

Detector: integrated detectors are PDs illuminated from the side with a waveguide and typically consist of an MQW stack or heterogeneously integrated materials such as Ge or InP. Although the layer stack of the PD is often determined by the foundry's fabrication process, one can nevertheless optimize the PD performance by a careful design of the PD top-layout. For example, one can increase the PD size to improve the responsivity or optoelectronic conversion efficiency and achieve better power-handling capabilities, but this will also negatively impact the attainable bandwidth, as discussed in [123]. To circumvent this issue, one can, for example, place the PDs in parallel rather than relying on a single PD. This strategy has yielded bandwidths of up to 27.5 GHz for PD structures realized in a commercial PIC foundry [124]. Another important parameter to consider is the reverse bias for which the PD yields an optimized performance; low reverse-bias voltages are important to lower the power consumption and improve compatibility with electronic circuitry [125, 126]. More information on all these metrics will be provided in section 5, where the integrated PDs are discussed in more detail.

A wide range of material platforms exists to realize the components used in a mm-wave photonic system. However, the most mature photonic-integration platforms thatare offered by commercial foundries at this point, and have standardized fabrication processes are silica or SiN, InP, and SOI or Si photonics [127]. Each of these platforms has its respective advantages and disadvantages, as can be seen from the qualitative overview of the pros and cons of the various PIC platforms shown in table 1. We also add the hybrid Si platform for reference, which will be discussed further on in this paper [128].

From table 1, it is clear that the silica-based integration platform, where the waveguide core consists of doped silica and with undoped silica as the cladding, only offers passive functionality such as routing, switching, and filtering. It offers the lowest propagation losses of all platforms and it has the same index as optical fiber, which can minimize coupling losses from fiber to chip. Nevertheless, it also has the largest footprint as compared to the other platforms and it lacks the main active components required in a mm-wave photonic link. The same applies to SiN, where the waveguide consists of SiN material embedded in a silicon dioxide cladding [129]. However, SiN components have a smaller chip footprint than their silica-based counterparts and thus provide more passive functionality in a smaller space.

The InP-based integration platform, on the other hand, offers active components such as lasers, high-speed modulators, and detectors on a chip, and up to a few hundred components can be integrated into one PIC [130]. Although the InP-based integration platform seems to be the platform of choice for implementation of a mm-wave photonic link from a functional point of view, the fabrication and packaging infrastructure is relatively immature, as compared to, for example, the CMOS industry, and this might be a bottleneck for ubiquitous real-world implementation [131]. As such, the SOI platform, which is compatible with CMOS technology and offers most of the functionalities of the InP-based platform, such as photodetection and modulation, can provide, in theory, the lowest cost and highest volume fabrication of integrated photonics-based mm-wave devices [127]. The SOI platform is also compatible with system-on-chip (SoC) and system-in-package (SiP) technologies. The only drawback is that the SOI platform lacks efficient integrated laser sources and as a consequence, for all the applications where a laser is required, the active regions need to be bonded on the PIC separately or heterogeneously grown.

4.2. The case for hybrid Si integration for mm-wave generation

One of the pioneering foundries offering semi-commercial SOI photonics technology is the imec platform [132, 133]. Since it is widely accessible through MPW runs, and since similar MPW services are offered by other commercial SOI foundries, it serves as a good benchmark for our discussion. Using this platform, modulators and PDs with bandwidths of up to 50 GHz are available [134], while other platforms and implementations provide even larger PD bandwidths of up to 120 GHz [135–137]. This means that efficient optical-to-electronic conversion can be achieved over a large part of the mm wave band. If we go beyond the 3-dB bandwidth and compromise on conversion efficiency, even larger mm-wave frequencies can be generated. While the availability of modulators with tens of gigahertz of bandwidth enables efficient microwave signal generation, the higher frequencies in the mm-wave regime can be generated through techniques such as frequency multiplication, as discussed previously. Although the InP platform still has superior electro-optic functionality in terms of bandwidth and modulation depth as compared to SOI, SOI does offer monolithic integration with high-speed electronics, e.g. through co-integration on a bipolar CMOS (BiCMOS) platform [138, 139]. This co-integration also offers distinct advantages over co-packaging approaches in the mm-wave regime, such as higher attainable speeds and better energy consumption [140]. Finally, passive components such as high-Q filters and low-loss delay lines that are crucial for many mm-wave applications can be achieved on chip [9], as they benefit from the low propagation losses in Si and, perhaps, SiN [9, 127, 141]. As such, when comparing all the mature integration platforms, it is clear that the SOI platform

for mm-wave generation should certainly be considered for future systems, hence the reason for this review.

As explained previously, the major drawback is that the SOI platform does not contain monolithically integrated lasers. One can employ the nonlinear optical Raman effect in crystalline Si to create a CW Si laser or even use monolithic integration of III–V quantum dots but the practical value is impeded by either the requirement for optical pumping [12, 142] or the immaturity of the fabrication process [143, 144]. As such, light emission in the SOI platform needs to be achieved through heterogeneous integration or hybrid approaches. The latter typically refers to wafer-bonding of the III–V circuitry with an SOI chip, with both material platforms linked through grating couplers, as exemplified by Luxtera [145]. This approach, however, increases packaging costs, and does not scale well if multiple light sources are required [146, 147]. These devices also suffer from low power efficiency due to coupling losses [148]. As such, heterogeneous integration is therefore a better approach, whereby an InP-based epitaxial layer is bonded to a fully processed SOI wafer and then further processed [128, 149]. This allows for lithographic alignment of the lasers to the Si waveguides and thus multiple light sources can be integrated. Moreover, III–V-based modulators and PDs can be similarly integrated on Si, bringing the strengths of InP-based actives, such as high electronic bandwidth and efficient electro-optic modulation, to the SOI photonics platform. Finally, heterogeneous integration of InP functionality with the SOI platform is not only maturing rapidly [128, 150–155] and being geared up for commercial implementation [156, 157], but it is also becoming increasingly CMOS compatible [158].

Apart from III–V materials, one can also combine the SOI platform with germanium (Ge), since it not only has a lower bandgap energy of 0.65 eV but can also be grown on Si, despite a small lattice mismatch of 4% [123, 159–170]. There are two approaches to integrating Ge with SOI. One way is to use bulk Ge or a Ge_xSi_{1-x} alloy, matched to a Si substrate through a layer with a gradually increasing proportion of Si in Ge_xSi_{1-x} [171]. This offers the possibility of tuning the bandgap from the one found in bulk Si to the one of bulk Ge [172]. A second way is to make a strained superlattice of pure Si and Ge_xSi_{1-x} alloy. This will induce strain in the Ge_xSi_{1-x} alloy, which will lead to a decrease in the bandgap energy compared, to bulk Ge_xSi_{1-x} [163, 170]. It must be noted that these Ge_xSi_{1-x} alloys have an indirect bandgap, which means that they can only be used for photodetection. Nevertheless, such PDs have been shown to have a large responsivity and, as such, have been realized using the aforementioned approaches, in SOI platforms offered by semi-commercial foundries through their mature MPW services [134, 173, 174].

4.3. A review of mm-wave generation using SOI

Having established the (hybrid) SOI platform as a very promising technology for mm-wave applications, we will now discuss a few implementations of mm-wave generation on this platform.

4.3.1. Modulators for comb generation. This approach is depicted in figure 6(a) and boils down to frequency multiplication of a microwave driving signal to generate mm waves, as explained in more detail for the fiber-based systems in section 3.2.3. This approach is fully compatible with the abovementioned commercial Si photonics platforms and existing packaging approaches. Depending on the target frequency, this can lead to overall more efficient system performance, as was theoretically shown by [131, 175].

Further optimizations of this topology have been proposed for the SOI platform. An example is the configuration shown in figure 6(b), which can achieve frequency multiplication factors of 8 and 24 [176]. The proposed PIC consists of four MZMs, placed in parallel with each other. This design eliminates the need for a filter to suppress unwanted harmonics. Another proposed configuration is shown in figure 6(c) and consists of two pairs of cascaded MZMs, embedded in a larger MZI structure [177]. By proper biasing, only the odd integer multiples of four, i.e. ±4, ±12, ±20, etc, are excited, leading to a filterless design for octupling.

Although these more complex designs seem promising in terms of optical performance, this does not necessarily mean that these proposed configurations can be used in real-world applications. Indeed, in ubiquitous mm-wave 5G networks, for example, the energy efficiency of mm-wave generation has to be considered. And as the simulations in [11] have shown, the driving electronics are the efficiency bottleneck, especially for MZMs, thus making multi-MZM-based configurations unattractive. To increase the modulator energy efficiency, one can employ ring resonators, as reported in [179], where a Si ring resonator was able to generate five uniform comb lines spaced at 10 GHz. However, two driver tones of 10 GHz and 20 GHz were required and the laser needed to be actively locked to the ring resonance. The ring modulator approach is also plagued by lower bandwidth and higher nonlinearity, as will be explained in more detail in section 6.

Instead of relying on frequency multiplication, mm-wave generation can also be achieved by heterodyning two lasers, as explained for the fiber-based system in section 3.2.1. An example of such a broadband microwave synthesizer is presented in [180], where mm-wave generation of 90 GHz signals is demonstrated in a fully integrated III–V/Si platform. The PIC integrates two tunable lasers with individual phase modulators, a directional coupler and a fast PD. To decrease the linewidth and thus increase the stability of these lasers, high-Q ring cavities can be employed. Mm-wave signal generation between 1 GHz and 112 GHz was demonstrated with the structure shown in figure 6(d) from [178], and has a configuration similar to that in [180]. The lasers have a tuning range of 42 nm and an intrinsic linewidth of less than 150 kHz.

4.3.2. Hybrid Si MLLs. As explained in section 3.2.4, MLLs can also be employed for mm-wave signal generation and have already been realized in the InP platform. For example, a 100 GHz MLL with timing jitter of 2.5 ps (when integrated from 20 kHz to 100 MHz) has been realized in [181], while even lower timing jitter values down to 1 ps have been reported

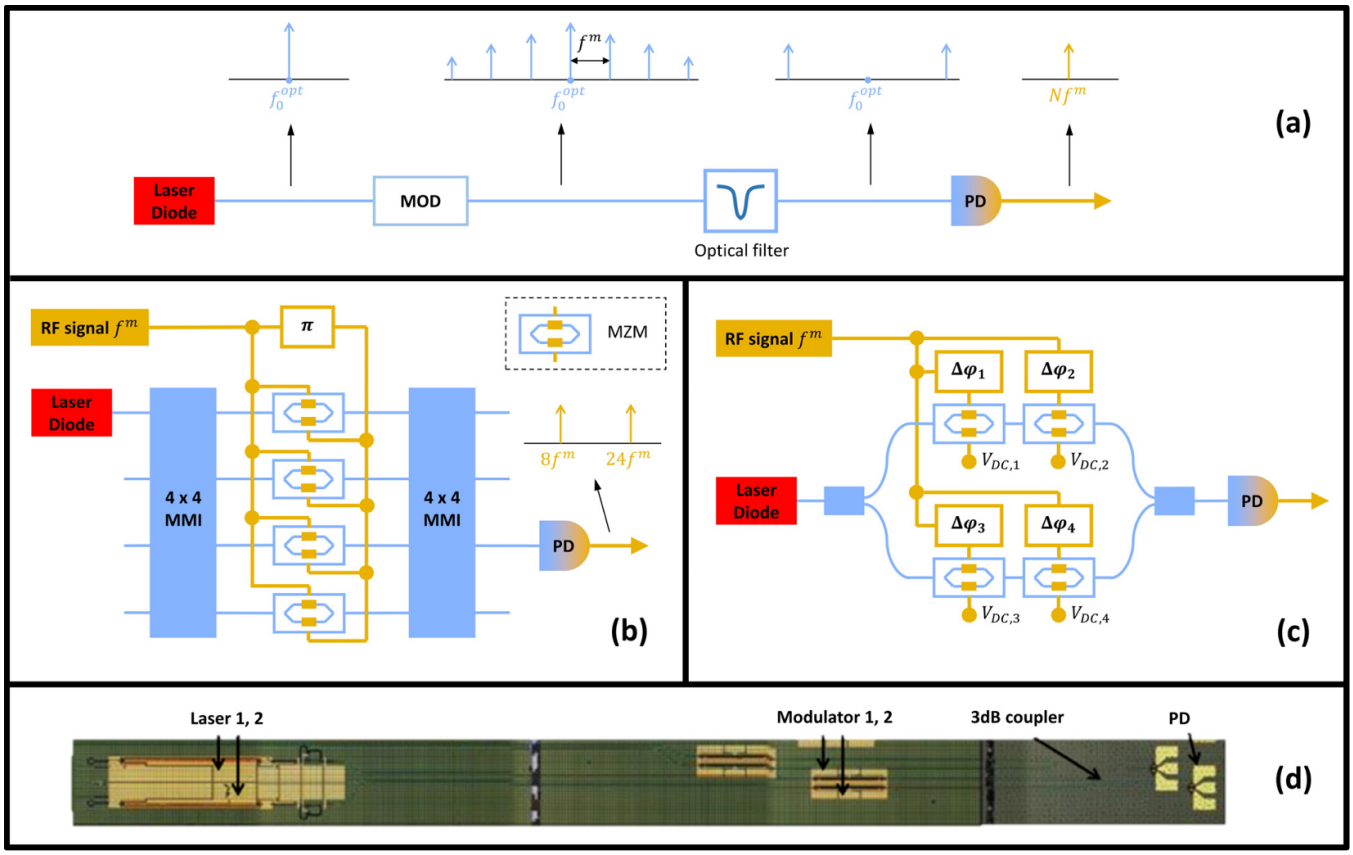

Figure 6. (a) Schematic of mm-wave signal generation using a modulator (MOD), driven by an RF oscillator. All the components, except the laser, can be monolithically integrated onto an SOI PIC. (b) Schematic of frequency 8-tupling and frequency 24-tupling circuit, including four parallel MZMs (adapted with permission from [176] © The Optical Society). (c) Schematic of a frequency octo tupler, using cascaded MZM structures placed in each arm of a an MZI (reprinted from [177], © 2016, with permission from Elsevier). (d) Microscope image of a fully integrated photonic microwave-frequency synthesizer (reprinted with permission from [178] © The Optical Society).

for a 40 GHz MLL (integrated from 10 kHz to 1 GHz) in [182]. Using heterogeneous integration, not only can one implement this functionality on SOI, but the low-loss Si waveguides will also improve the noise characteristics of the MLLs when employed as an external cavity [183], as compared to using all-InP devices. Several heterogeneously integrated MLLs have been realized so far, such as FP and ring MLLs that operate at around 40 GHz and 30 GHz, respectively [184, 185]. Stable colliding-pulse ML operation of the hybrid Si MLL shown in figure 7 has been demonstrated in [186, 187], with a repetition rate of 18 GHz.

Another implementation using an extended ring cavity was reported in [187] and operates at around 20 GHz. The unidirectional operation of such ring MLLs was hypothesized and proven theoretically, based on experimental microwave photonic isolators [188, 189]. Longer cavities can be used to decrease the optical and RF line widths, but will also decrease the operating frequency. For example, an active MLL with a 9 cm-long cavity that operates at 930 MHz was reported in [190]. Another realization of this device showed 1 GHz operation [191]. However, using harmonic ML, a long cavity can be 'forced' to operate at higher frequencies and this will increase the stability while decreasing timing jitter. In [192], an MLL with a 4 cm-long ring cavity was reported, with 20 GHz operation achieved at the 10th harmonic.

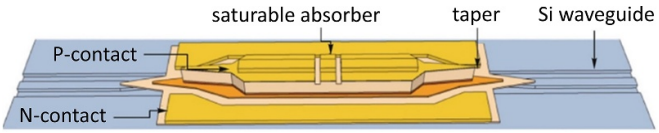

Figure 7. Schematic of a colliding-pulse MLL on a hybrid III–V/Si platform (reprinted by permission from Springer Nature Customer Service Centre GmbH: Springer Frontiers of Optoelectronics [187] © 2014).

4.3.3. Opto-electronic and COEOs. OEOs and COEOs based on fiber-optic configurations are among the lowest-noise sources of microwave and mm-wave generation and so there have been efforts to integrate at least part of such a system into SOI. In [193], a 10 GHz OEO was demonstrated, mostly integrated into a commercial 130 nm SOI CMOS photonic platform [194], except for an SOA and a long optical fiber. A picture of the PIC is shown in figure 8. Phase noise of -112 dBc Hz^{-1} at 10 kHz offset was reported.

More recent work also integrated the high-Q element into the PIC using a Si disk, although the electronics were off-chip, the same as the laser. Tunable microwave generation from 3 GHz to 7 GHz was achieved, with phase noise of -80 dBc Hz^{-1} at a 10 kHz offset and a 5.4 GHz carrier frequency [195]. Finally, using heterogeneous integration, a COEO was realized, operating at 20 GHz and having a 14 kHz RF linewidth [196]. Although only the MLL component was integrated, this does stress the benefits of bringing the active components, such as the laser and/or SOA, onto the SOI PIC for a fully integrated (C)OEO.

4.4. SOI-based antenna arrays

Although antennas do not themselves contribute to mm-wave generation, they are nevertheless crucial to the distribution of mm-wave signals, e.g. in the wireless applications discussed in section 2.1.3. As was discussed in section 2.2.1, at these high frequencies and high data rates, beam-forming and beam-steering become increasingly important for efficient wireless mm-wave transmission, as these methods enable the radiation levels of the antennas to be effectively lowered [28]. It is here that PICs can play a crucial role as well. Indeed, these PICs allow the realization of compact optical phased-array antennas (OPAAs) that not only enables the formation of an arbitrary beam shape but are also capable of steering a beam towards a moving target in real time without the need for mechanical components [197, 198]. OPAAs rely on splitting the optical signal into N channels, changing the time delay in each channel and routing the N delayed signals to an antenna array, in which each antenna can be either an optical grating or a PD connected to a metal antenna for optical or mm-wave beam-steering/beam-forming, respectively [199–201]. Because of the tunable time delays between channels, the transmitted signals interfere and form a tunable beam shape in the far field [202]. These OPAAs can also be used for efficiently receiving optical and mm-wave signals of an arbitrary beam shape, although for receiving mm waves, each PD–antenna structure is replaced with an antenna connected to a high-speed modulator [203, 204]. A large number of antennas is required to ensure high beam quality and maximal beam-forming/beam-steering flexibility [205].

Achieving a tunable, or 'true' time delay as well as many individual on-chip antennas are thus the main challenges for the operation of OPAAs and the SOI platform has been shown to be an excellent candidate to enable these functionalities on a PIC. Indeed, OPAAs with hundreds and even thousands of antennas have been demonstrated on the SOI platform, but they only achieved phase shifting of the carrier optical wave rather than true time-delay functionality over a wide frequency range [202, 205, 206]. True time delay has been realized, however, with ring resonators having a tunable coupling section or switchable waveguide delay lines but the number of antennas remains limited to 16 [203, 207–209]. As such, current research is focused on making the tuning elements more energy-efficient and compact [203, 210].

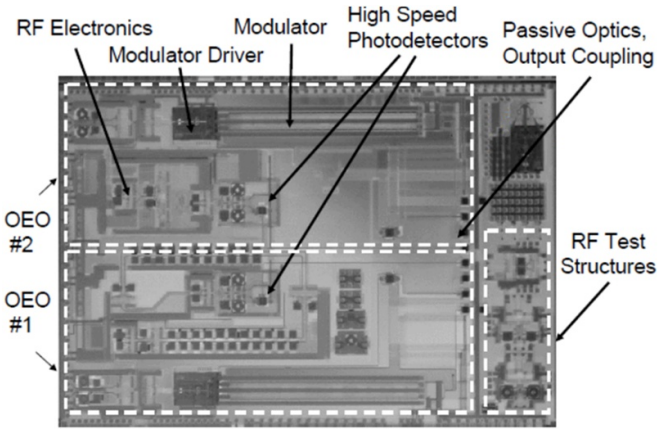

Figure 8. Microscope picture of the Si photonic PIC, containing two side-by-side OEO circuits on a 5×8 mm^2 die (© 2007 IEEE. Reprinted, with permission, from [193]).

Nevertheless, it is clear that the (hybrid) SOI platform not only has tremendous potential to enable mm-wave generation but also wireless mm-wave distribution.

5. High-power PDs

In the previous section, we have given a general overview of the photonic technologies needed for mm-wave generation, both in optical-fiber-based systems in section 3 and (hybrid) SOI PICs in section 4, and discussed some devices that have been realized so far. In this section, we will focus on one of the key components of the mm-wave link: the PD. In particular, we will discuss the important PD parameters and the operation of PDs in mm-wave links in more detail. Considering that approaches for improving integrated PD performance have been extensively studied by several groups [123, 159–162, 211], we will also provide an overview of these in this section.

5.1. Important metrics of a PD in a mm-wave system

PD performance is typically characterized by responsivity, dynamic range, bandwidth (and its trade-off with the bias voltage), and noise. These metrics will be discussed in detail in the following sections.

5.1.1. Responsivity. The responsivity, $\Re$, is defined as the ratio between the photo-current and the incoming optical power [212]. Most high-speed PDs have an $\Re$ in the range from 0.5 to 1.1 A W^{-1} [126, 159, 213–215]. However, avalanche effects can deliver extremely high $\Re$ values, due to their internal multiplication [216][3]. It is desirable to maximize the $\Re$ of PDs, as this makes the entire system more efficient, and allows it to operate at lower optical power, while maintaining a high output power for the mm-wave signal. This renders the

[3] This is not to be confused with a quantum efficiency of more than 1.

mm-wave link less power-consuming than when a PD with a lower $\Re$ is employed and it also increases the signal-to-noise ratio in the link, as explained later on.

Currently, the responsivity of state-of-the-art Ge-on-SOI PDs has reached a value of 1.19 A W^{-1} at 1550 nm [125], while InP-based PDs, integrated with Si-on-diamond waveguides, have been demonstrated with responsivities of up to 1.07 A W^{-1} at 1550 nm [211].

5.1.2. Dynamic range. When operating PDs at higher powers, the PD responsivity, $\Re$, becomes dependent on the optical power, or more precisely, the relation between the optical power and the photo-current becomes non-linear [217]. The causes of these non-linearities have been extensively studied in the literature [218–221], and these studies have shown that although there are many causes, the space–charge effect is the dominating contribution to the nonlinearities arising from PDs operating at low biases. The space–charge effect stems from the electric field due to the generated carriers, which has a direction opposite to that of the biasing field and reduces the drift velocity of the carriers [222].

PD non-linearity will result in the presence of higher harmonics in the generated mm-wave when the PD is illuminated with an optical beating signal containing a pure RF tone [223]. The generation of even harmonics will only be an issue for multi-octave systems,[4] while the odd harmonics will also affect single-octave systems; the generation of these harmonics not only results in a compression of the output RF power but when the nonlinearly generated spurious signals above the noise level from one frequency band end up in another frequency band, they create crosstalk between data channels [212]. The dynamic range of the PD, i.e. the optical power range for which the impact of nonlinearities is limited, is then quantified by either the compression-free dynamic-range (CDR) or the spurious-free dynamic range (SFDR). The power for which the signal is distinguishable from the noise level defines the lower limit for both the SFDR and the CDR. The upper limit of the SFDR is simply the optical power for which the upper harmonics become distinguishable from the noise. The SFDR is often defined for the n^{th} harmonic, i.e. SFDRn, where the second or third harmonic is the most used, i.e. SFDR2 or SFDR3, respectively. For the CDR, on the other hand, the upper limit is the optical power for which the mm-wave power generated is compressed by a certain amount from the linear slope. Commonly used compression factors are the 1 dB and 3 dB points. Instead of using the CDR, one can also rely on the 'saturation current' which is defined as the photo-current at which the mm-wave output power is compressed by 1 dB [224].

At this point, large signal 1 dB compression currents of up to 60 mA at 1 GHz have been reported for Ge-based PDs [160] and 61 mA at 10 GHz for InP-based PDs [211].

[4] Where the highest utilized frequency is more than twice of the lowest frequency.

5.1.3. Electrical bandwidth and the voltage bias vs. bandwidth trade-off. The bandwidth is commonly defined as the range of frequencies available, before the mm-wave signal power is compressed by 3 dB, i.e. $f_{3\text{dB}}$, or 1 dB, i.e. $f_{1\text{dB}}$, as compared to the DC signal. The bandwidth is usually limited by two physical effects, namely the transit time and the RC time.

On one hand, the motion of carriers across the PD is a limiting factor for the bandwidth; due to the finite speed of the carriers, the generated carriers are only extracted by the electric circuit after a certain time, i.e. the transit time. For top-illuminated PIN photo-diodes, this is the limiting factor, as reducing the thickness shortens the transit time, but also reduces the absorption length, and, by extension, reduces the responsivity [225]. On the other hand, the RC time constant is also dependent on the diode dimensions; for example, increasing the diode length of waveguide PDs (WPDs) improves their responsivity but also increases the electrical capacitance and thus the RC-time constant, which imposes a limit on how fast the diode can operate. Therefore, the bandwidth of a diode can often be considered to be RC- or transit-limited [123], depending on the design. It is clear that a trade-off often needs to be made between the responsivity and the bandwidth, and to compare different designs of PDs, the bandwidth–efficiency product is regularly used. This will be discussed in more detail later on in section 5.3.

Hybrid Si PDs based on Ge or InP have similar performance; the bandwidths of Ge-based PDs can be expected to be up to 70 GHz for small signals [166] and up to 67 GHz for InP-based PDs [226].

5.1.4. Noise. When considering noise in PDs, it is relevant to look at both the PD itself and the receiver electronics that read out the current generated in the PD. Shot noise is inherent to PDs, whereas thermal noise is unavoidable in the receiver electronics [227]. Both these noise terms are white-noise sources and distribute their power evenly in the frequency domain. Another noise type to consider in the receiver electronics is flicker noise, which has a $1/f$ dependence in the frequency domain and is thus most pronounced at lower frequencies. However, it is worth noting that when non-linearities are present in the system, this noise type will broaden the linewidth of single-frequency signals modulated onto the optical carrier through the mixing effect [228].

The most direct and empirical measure of the noise in a receiver system is given by the noise equivalent power (NEP). This quantity is defined as the power, normalized to the square root of the bandwidth, for which the input signal is equal to the noise power present in the system [229]. This quantity is independent of the signal power and can only be found by measuring the noise in the system, in the absence of an input. However, this is not entirely true, since shot noise depends on the average current flowing in the PD and thus on the average optical input power present; this is not an issue if the system is thermal-noise-limited. NEP is essential in sensing applications to determine the resolution and lower limit for which it is possible to determine the given physical quantity being measured [230].

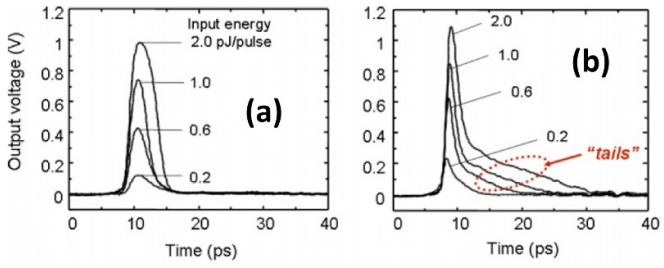

Figure 9. The impulse response of (a) a UTC-PD and (b) a PIN PD. Reprinted with permission from [245] © John Wiley and Sons.

Another noise metric that is of great importance, especially in communication systems, is the SNR, since this can be translated directly into a bit error rate (BER) [231]. The SNR is defined as being the signal power divided by the sum of all noise power contributions [232]. Typically, this quantity includes relative intensity noise, which is noise generated in the light source of the communication system. In direct relation to SNR is the noise factor, *F*. This quantity describes the degradation of the SNR caused by one or more amplifier stages of a system, when the input is thermal-noise limited [233]. When amplifying stages are cascaded, it enables the calculation of the output SNR through Friis's formula for noise[5] [234], when the gain values of the different stages are also known.

5.2. Typical experimental characterization methods for PDs

As a PD has many different parameters that have to be measured to fully characterize it, a setup capable of generating various optical inputs is required. It has to be able to deliver sufficient power to reach saturation in the PD while maintaining linearity, and besides, the generation of a stable mm-wave signal is required. For the optical signal to be as linear as possible, a common technique is to heterodyne two single-frequency lasers, creating a beat frequency of a single (mm-wave) frequency. One such setup can be seen in figure 1 of [235]. The setup consists of two single-frequency phase-locked lasers [236] that are superimposed on each other and followed by a variable attenuator, to allow for easy control of the optical power. This setup is only limited by the maximum output power of the lasers and produces pure sinusoidal and tunable beat RF-tones, allowing for measurements of the common parameters of interest [237].

An alternative setup, sometimes used to characterize the spectral response of a PD, uses short-pulsed lasers. Performing a Fourier transform on the transient response results in a measurement of the bandwidth [218]. Such a setup was developed and compared to the heterodyne technique in [238] and gave comparable results within the range of reproducibility. For the setup to be capable of measuring the SFDR, two or more gigahertz-range signals are required, such that the frequency of the harmonic can be placed in the frequency band of the PD. A more thorough treatment of these techniques can be found in [239].

Finally, to characterize PD saturation, one can rely on two common approaches: pulsed-laser saturation and CW-laser saturation [240]. For CW-laser saturation characterization, one can employ either 'large-signal compression,' where the test signal is a CW laser modulated with a single mm-wave frequency and having a modulation depth close to one or 'small signal' that uses modulation depths below 0.05 [241]. It has been observed that for higher frequencies, the saturation current decreases due to the space-charge effect that increases the carrier-transit time [218, 224].

5.3. Approaches to improve the PD performance

As previously mentioned, there is a trade-off between achieving high responsivity/large dynamic range and high bandwidth. Several approaches are being investigated to address this trade-off, and we briefly discuss four of these techniques, specifically: increasing the PD size, the UTC PD, the velocity-matched PD (VMPD), and the traveling-wave PD (TWPD). Although some of these approaches have not yet been implemented in the current SOI PIC platforms, we believe they will greatly benefit the performance of SOI-based PDs when these technologies are standardized by the SOI foundries.

5.3.1. PD size: the power/responsivity vs. bandwidth trade-off. One of the trade-offs in the geometrical design of a PD is between high power and high bandwidth. Intuitively, a larger PD will be harder to saturate or drive into the nonlinear regime and thus it will respond better to higher optical input powers, as compared to smaller ones. However, it will also negatively affect the bandwidth, due to the larger RC time constant. This is indeed the case and expressions for both bandwidth and saturation powers can be found in [242].

Another trade-off is between obtaining high responsivity and high bandwidth. To achieve the shortest possible transit time and, by extension, increase the bandwidth, the PD can be made thinner in the direction of extraction. For conventional VPINs, this results in a reduction of the responsivity, as less light is absorbed and an increase in the RC-time-constant is also seen [243]. To overcome the reduction in responsivity, different designs, other than the VPIN, have been developed. The WPD, which extracts carriers perpendicular to the propagative direction of the light, is one of these designs. The WPD permits the use of larger absorption lengths while maintaining the shortened transit length, allowing higher bandwidth with high responsivity [164, 165]. However, as this increases in the RC time constant, the desired length of the WPD is as short as possible. One way to shorten the WPD length without compromising the responsivity is by introducing a distributed Bragg grating, as was done in [244]. This makes the light pass through the detector twice, rendering it more efficient.

[5] This formula is different from Friis' transmission equation for antennas [400].

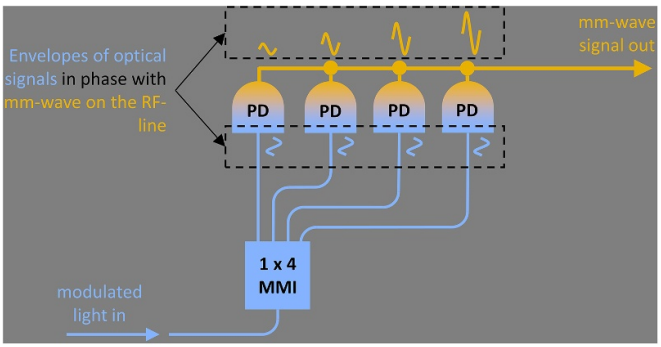

Figure 10. A depiction and the working principle of the VMPD from [250] (© 2000 IEEE. Reprinted, with permission, from [250]).

5.3.2. Uni-traveling-carrier PDs (UTC-PDs). In 1997, Ishibashi *et al* [72] proposed a new layer stack for PDs to improve the speed and power-handling capabilities as compared to regular PIN PDs. The proposed layer structure was shown to suppress the current created by slow holes and enhance the current created by fast electrons by overshooting their velocities. The absorption layer is located in the p-doped region, which is different from a regular PIN PD, where it is located in the intrinsic region. A small potential gradient in the p-doped layer enhances the transfer of electrons into the intrinsic region, which is referred to as the carrier-collecting region. In this region, electrons are accelerated and overshoot their velocity. Figure 9 shows how this approach removes the tail of the PD impulse response by the suppression of holes and thereby increases the bandwidth.

The space-charge effect is also reduced, because positive charges in the form of holes do not build up in the depletion region. This leads to better high-power performance.

Several modifications have been reported, and those are typically known as modified UTC-PDs (MUTC-PDs). Examples of MUTC-PDs can be found in [246, 247]. Up until now, several UTC-PDs have been presented and they are the state-of-the-art approach for making fast and high-power single PDs, both in heterogeneous III–V integration [248] and SiGe [123, 169].

5.3.3. TWPDs and VMPDs. Given a certain type of WPD layer stack, it is possible to optimize the power handling vs. speed capabilities by a smart geometrical top-view layout. The trade-off between small diodes with a short RC time constant and larger diodes with high power-handling capabilities can be circumvented by matching the velocity of the generated mm-wave signal to the group velocity of the optical signal. In this way, the current generated throughout the PD will add up in phase and thus eliminate the RC limitation whilst retaining a large interaction length and thus large responsivity.

In the case of a TWPD, this is done by matching the velocity of the optical field propagating in the WPD and the velocity of the induced mm-wave signal in the electrical transmission line, parallel to the waveguide [249]. VMPDs are quite similar, but instead of having a single-section WPD, the VMPD consists of several discrete PDs, connected electrically by a transmission line [242]. This discretization allows optimization of the optical waveguide, electrical transmission line and PDs independently. With this type of arrangement, it is even possible to distribute the input light evenly among the different PDs, by feeding them in parallel as depicted in figure 10 [250], where modulated light is evenly distributed over four waveguides and delayed to make sure that the generated mm waves are in phase on the RF line.

Since the VMPD and TWPD are geometrical approaches to the top-view layout, i.e. the circuit design, while the UTC-PD is an optimization of the lateral layer structure and thus the fabrication process itself, it is possible to combine these into a hybrid approach [251]. Current SiGe based VMPDs can handle output powers of 7 dBm at 15 GHz [252] and 5.3 dBm at 40 GHz [253].

5.4. State-of-the-art Si-based PDs in terms of their key metrics

This section gives a graphical overview of state-of-the-art Si PDs that can be found in the literature. A comparison of hybrid III–V/Si- and SiGe-based approaches is explicitly visible in all plots.

First of all, we plot the map of the large-signal 1-dB compression current versus bandwidth in figure 11(a). This quantity reveals power handling capabilities, linearity and speed. In general, the performance of the hybrid III–V/Si PDs is better than that of SiGe for this metric. It is also worth noting that the intuitive trend of a decreasing compression current with increasing frequency is observed.

In figure 11(b), we look at how much RF power can possibly an be extracted from a PD at different frequencies. The plot shows the maximum RF output power available at given frequencies for different PDs. Hybrid III–V/Si-based PDs also outperform SiGe ones using this metric. In addition to Si-based PDs, a map of non-Si-based PDs has been included from [258] and added to the plot. It is clear that in terms of power-generating performance, there is a gap of about 15 dB that needs to be bridged for Si-based PDs, when compared to their non-Si-based counterparts.

Finally, in figures 11(c) and (d), we plot the bandwidth and maximum RF output power as functions of the reverse-bias voltage at which these metrics were achieved. Low-voltage-level operation around or below 1 V is key for low-power CMOS designs [259], and the PD reverse-bias voltage must therefore be taken into account when power consumption is a metric. It can be seen from these plots that (1) high-power operation is typically achieved at larger reverse-bias voltages for the III–V/Si-based PDs, while for the SiGe PDs there is no clear trend and (2) that the bandwidth appears to increase with decreasing bias voltage for both III–V/Si and SiGe PDs. The latter can be explained by the fact that in the literature corresponding to figures 11(c) and (d), the bias conditions were already optimized for low-voltage operation, i.e. higher bandwidths are feasible at larger reverse-bias voltages but for these points, the large signal performance was not characterized.

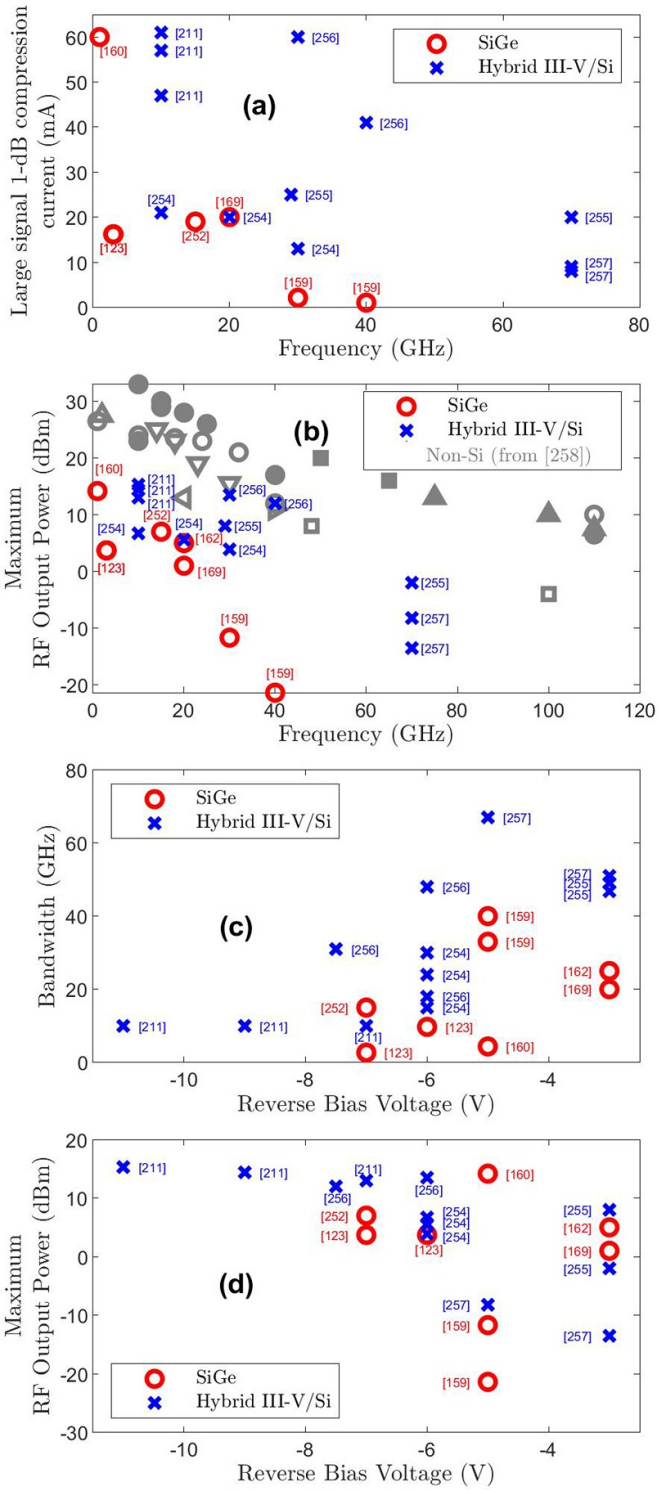

Figure 11. PD performance maps, where for the SiGe PDs we include WG-UTC [159], WG-PIN [160], V-UTC [123, 169] and VMPD [162, 252], while for the hybrid III–V/Si PDs we include WG-MUTC [211, 254–256] and WG-PIN [257]. (a) Map of large signal-compression currents for the Si-based PDs. (b) Maximum RF power achieved by PDs versus frequency. A mapping of non-Si-based PDs has been included from [258] (gray markers). Reverse bias voltage versus (c) bandwidth and (d) maximum RF output power.

Once more, we see that III–V/Si outperforms SiGe in terms of bandwidth and output RF power.

6. Linear high-speed modulators

It is not only the PD but also the modulator performance that dictates the overall performance of a mm-wave photonic system and thus a thorough understanding of modulator types and their capabilities is relevant. As such, just as we discussed PDs in detail in section 5, we will focus on modulators for mm-wave generation in this section. In particular, we start by explaining how modulation is achieved in (hybrid) SOI platforms and then discuss the important modulator parameters in mm-wave links. While we specifically focussed on bandwidth, output power and bias voltage trade-offs for the case of the PDs in section 5, in this section, we will instead pay special attention to the modulator linearity. We also briefly discuss the potential of utilizing plasmonic effects and lithium niobate ($LiNbO_3$) or graphene's optical properties to improve SOI modulators, rather than relying on InP or SiGe-based heterogeneous integration.

6.1. Optical modulation in Si

Si modulators rely on phase shifting through dynamic manipulation of the refractive index. Although many physical processes exist that can offer this functionality, only the plasma-dispersion effect is useful for mm-wave applications. Indeed, the thermal effect is too slow for mm-wave operation [260], the non-linear Franz–Keldysh effect (FKE) is two to three orders of magnitude weaker than the plasma dispersion effect at wavelengths around 1550 nm [261], and due to the centrosymmetry of Si crystals, the Pockels effect is non-existent in standard SOI waveguides. The plasma-dispersion effect is a carrier-driven change of both the absorption coefficient and the refractive index. The change in optical response is described by the Drude model [261, 262]:

$$\Delta n = -\frac{e^2\lambda^2}{8\pi^2 c^2 \in_0 n}\left(\frac{\Delta N_e}{m_e^*} + \frac{\Delta N_h}{m_h^*}\right) \tag{1a}$$

$$\Delta\alpha = \frac{e^3\lambda^2}{4\pi^2 c^3 \in_0 n}\left(\frac{\Delta N_e}{(m_e^*)^2\mu_e} + \frac{\Delta N_h}{(m_h^*)^2\mu_h}\right). \tag{1b}$$

These equations describe the changes to the refractive index, Δn, and the absorption coefficient, $\Delta\alpha$, as a function of carrier density, N. The subscripts e and h denote electrons and holes, respectively, while m^* denotes the conductive effective masses of the free carriers. Since modulation can be achieved by both a positive and negative change in refractive index, the plasma-dispersion effect can be utilized by carrier injection, accumulation, or depletion, with the latter not only being the most promising for high-speed operation but also more compatible with CMOS technology, due to simpler fabrication [263–265].

For the modulator to be practical, the phase-shifted light needs to be transformed into intensity-modulated light, such that the PD can demodulate the processed signal back into the electronic domain. To do so, the modulator is either placed in an MZI or resonant structures such as microrings, as shown

schematically in figures 12(a)–(c). In MZI-based modulators (MZMs), the phase difference between the MZI arms cause interference and thus a change in intensity at the output port(s), while in ring-based modulators, the resonance frequency shifts caused by phase changes generate an intensity-modulated signal at the drop and through ports. Depending on the bias conditions, one can optimize the modulation efficiency. The most efficient modulation for MZMs happens at their quadrature bias, while for ring modulators, it occurs when the center wavelength is biased close to ring resonance. It is clear from the current-swing plots in figure 12(b)–(d) that ring modulators offer superior modulation efficiency as compared to MZMs, but this comes at the cost of having lower bandwidth (for the ring modulator configuration depicted in figure 12(c)) [266].

While these devices can be fully integrated into SOI platforms, one can also rely on EAMs in InP or SiGe through heterogeneous integration, as mentioned earlier. Indeed, these EAMs benefit from the strong electro-absorption effect in these materials, either arising from the quantum-confined Stark-effect (QCSE) in MQWs or the FKE [152, 267, 268]. This change in absorption can function as direct intensity modulation, thus making the realization of very compact modulators possible [269, 270] without the need for a long phase modulator in an MZI or ring configuration.

6.2. Modulator performance

6.2.1. Overview. Although various parameters are required to characterize the performance of a modulator, the most common ones are bandwidth, modulation efficiency or driving voltage, footprint and linearity. However, trade-offs often need to be made for these performance metrics. For example, for the realization of highly linear mm-wave links, the driving voltage and footprint are not directly relevant. Nevertheless, in any practical mm-wave system, fabrication complexity, power efficiency and footprint, among others, should be considered along with linearity. Insight regarding the relation between classical figures of merit and microwave system performance can be found, for example, in [271, 272], while an overview of the qualitative strengths and weaknesses of the modulator types discussed above is given in table 2. However, there are some important notes that accompany table 2. Firstly, a driving voltage below 1 V allows for direct CMOS driving, depending on the technology node, as explained in [273]. Secondly, ER and losses in the device lead to a lower SNR, which is closely coupled to linearity performance, as elaborated below. Thirdly, ring resonators with a high Q-value are limited in operation frequency due to photon lifetime, rather than RC time constants or carrier dynamics. This can be circumvented, for instance, by using the dual-injection method of the FLAME ring modulator introduced in [274] or by using the FSR coupling as described in [275]. Finally, fabrication complexity should be considered along with the required number of driving signals, considering that electrical probing and wiring become complex and expensive at mm-wave frequencies.

6.2.2. Improving the modulator bandwidth. To switch our focus back to the performance of the SOI modulator itself, an important metric is the speed or bandwidth. For optical modulators, the bandwidth is typically defined as the RF frequency at which the modulation index is reduced by half or drops by 3 dB, as compared to low frequencies [263, 277–279]. It should be stressed that the modulation index is defined in the *optical* domain, i.e. the induced phase change (for phase modulators) or change in optical power transmission (for amplitude modulators). This means that for the electrical domain, the 3 dB roll-off of the modulator's modulation index corresponds to a 6 dB drop in RF power when the optical signal is demodulated back to the RF domain through a PD [263, 279].

As explained previously, the carrier-depletion mechanism, in which a reversely biased PN diode region inside the waveguide depletes it of carriers and thus induces a phase change, will yield the highest bandwidths [280]. Nevertheless, the speed will still be affected by the depletion capacitance of the PN junction, the RC constant of the electrodes and, in the case of traveling-wave modulators, the mm-wave loss in the RF line as well as the velocity matching between the mm-wave and the optical wave [263, 280]. Many different techniques have been developed to improve the bandwidth of depletion-based modulators—a thorough review is provided in [263, 280, 281]—but generally, they rely on an optimized doping profile, an optimized design of the travelling-wave electrode and its cross-section, or an appropriate RF-matching circuit to prevent RF reflections—or a combination of these. For example, a depletion-based Si modulator has achieved a bandwidth of up to 60 GHz at a bias voltage of −8 V [282]—the key in this design is to lower the mm-wave propagation losses in the TW electrode by removing part of the Si substrate. However, the latter does complicate the fabrication process and thus it is advantageous to employ more CMOS-compatible Si modulator cross-sections, but these devices are limited to speeds below 50 GHz, for both MZM and ring-based configurations [264, 265, 281, 283–288].

Instead of using the carrier-depletion effect, one can also employ the QCSE or FKE in SiGe or III–V/Si heterostructures for the development of SOI-based EAMs. As explained earlier, while these modulators have a strong nonlinear response, they not only require lower driving voltages and attain higher bandwidths than the carrier-depletion type of modulator but they also typically have a smaller chip footprint [268, 289]. Bandwidths of up to 67 GHz for III–V/Si hybrid EAMs and exceeding 65 GHz for SiGe EAMs have been reported [152, 268].

6.2.3. Improving the modulator efficiency. Apart from modulator bandwidth, efficiency is also an important performance metric. For the plasma-dispersion effect, we can see from the Drude model equations that increased modulation efficiency can be achieved either through the optimization of doping levels or a reduction in the effective conductive mass of the free carriers. The first approach has been explored in, for example, [290–292], achieving either improved modulation efficiency

Table 2. A qualitative comparison of modulator types and methods for improvement. The numbers posted are approximate, to quantify the orders of magnitude of the relative performance between the different types. The table is adjusted to fit the scope of this paper and most of the statements originate from [276].

Design	Advantages	Challenges
MZI	Easy tuning	Large footprint (10^{4-5} μm^2) Inefficient High power consumption
Ring/disk	Small footprint (10^2 μm^2) Highly efficient	Low optical bandwidth (0.1 nm) Needs dynamic fine tuning Very sensitive to fabrication tolerance
Slow light	Enhanced modulation efficiency Compatible with MZI	Large optical loss Low optical bandwidth (1 nm) Sensitive to fabrication tolerance
Material	**Advantages**	**Challenges**
GeSi	Reduced footprint of Ring/MZI Broad optical bandwidth (∼20 nm)	Large optical loss (>5 dB), Temperature sensitive Increased complexity of fabrication
Hybrid III–V	Highly efficient Very short Tunable optical parameters	Insertion loss (>5 dB), Increased complexity of fabrication
Plasmonic	Very high bandwidth (>150 GHz) Extremely efficient (<25 fJ) Small footprint (10^2 μm^2)	Small footprint Immature fabrication Highly nonlinear

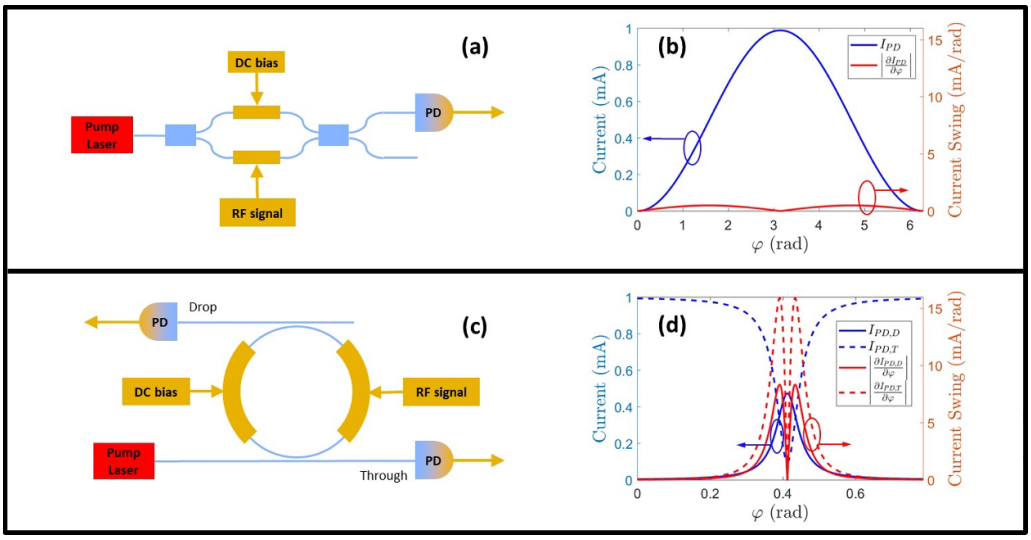

Figure 12. The generic working principles of the two modulator designs typically used in Si photonics: (a), (b) the MZM and its response while in (c), (d) the ring modulator and its response are depicted. (b), (d) The blue lines correspond to the current generated in the PD as the phase of one of the phase shifters is varied. The red lines correspond to the sensitivity of the modulator towards a phase change and are indicative of the modulation efficiency. For the ring modulator, the full and dashed lines correspond to the responses at the drop and through ports, respectively. The parameter values shown are meant for illustrative purposes and will vary for specific modulator implementations.

or improved linearity. The effective conductive mass has successfully been lowered by introducing Ge in the Si waveguide, as this applies a strain to the Si due to the lattice-constant mismatch, consequently lowering the effective conductive mass through changes in the band structure [293]. Another available approach in the SOI platform is in terms of layout optimization, namely by introducing slow-light structures into the phase shifters. Here, periodic structures are operated in an off-Bragg condition, resulting in 'slow' light with a high group refractive index. This ensures an enhanced interaction time with the modulating medium, regardless of the electro-optic effect in use, and allows the creation of sub-100 μm carrier-depletion Si MZMs [294].

6.2.4. Improving the modulator linearity. Apart from modulator efficiency, modulator linearity is another performance metric that requires attention in this review. Indeed, with microwave and mm-wave photonics, a shift is made from the digital signals of telecom and datacom to analog signals where linearity is a key performance indicator. The non-linearities that negatively impact modulator linearity can be seen as duplicates of the source signal at integers of the driving frequencies. Multiples of one signal are called higher harmonics, while mixtures formed from several sources are called intermodulation distortions (IMDs). For the non-linearities to become significant, the input mm-wave power has to be increased, as they generally respond to input power as an exponent of the harmonic or inter-modulation order—this is different from the PD nonlinearities, i.e. saturation, where high optical powers will excite PD nonlinearities. The parameters commonly used to quantify linearity are the third-order output-intercept point (OIP3), defined as the extrapolated point where the third-order distortion (IMD3) is equal to the carrier in power, and the SFDR that quantifies the usable dynamic range from the point where the carrier signal crosses the noise floor until an IMD or higher harmonic crosses the noise floor. In this review, we only consider the SFDR related to the IMD3, as the fifth- and higher-order IMDs are negligible, while even higher harmonics can be suppressed with a bandpass filter for microwave and mm-wave applications. Hence, in the following, the SFDR is presented as a measure of linearity, as the SFDR depends on noise bandwidth to the power of two-thirds for third-order distortions. Mathematically, the SFDR is defined, if we have a noise floor of N_0, as:

$$\mathrm{SFDR} = \frac{2}{3}(OIP3 - N_0)$$

and an example is given below, in figure 15(b).

The cause of these nonlinearities is often the nonlinear behavior of the physical mechanism behind the modulation itself. For example, the plasma-dispersion effect based on carrier injection is non-linear. Specifically, at 1550 nm, the index change is found to vary with $\Delta N_\mathrm{h}{}^{0.8}$ and $\Delta N_\mathrm{e}{}^{1.05}$, where ΔN_h and ΔN_e are the hole and electron density changes, respectively [261, 262]—although depletion-mode carrier injection has been found to result in a higher SFDR, compared to injection mode [296]. The electro-absorption in Si is not only weak but it is also non-linear, due to both the curvature of the band structure and the non-linear nature of the QCSE [289]. As well as the non-linear nature of the underlying modulation mechanisms, the transfer function of the modulator structure should be considered. An MZI modulator converts a phase shift to intensity modulation through interference, therefore it converts a sinusoidal response to a continuous phaseshift. For the ring resonator, the transfer function shows peaks at resonance wavelengths, where the sharpness is determined by geometry and waveguide loss. The transfer functions of both designs

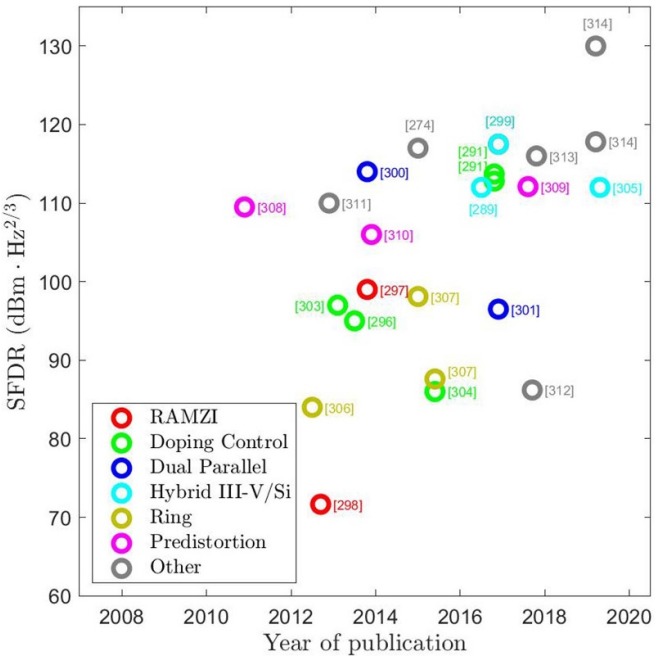

Figure 13. Highest SFDRs achieved for various linearization schemes. Some of the methods are compatible with any modulator type, while others are specific to a certain design. References used are for RAMZI [297–299], doping control [291, 296, 303, 304], dual-parallel [300, 301], hybrid III–V/Si [289, 299, 305], ring [306, 307], predistortion [308–310], and other [274, 311–314].

are shown in figures 12(b)–(d). The combined non-linearities of the modulator limit the linear performance, particularly for analog applications, and thus linearity is a vital parameter for modulators used in microwave and mm-wave photonics.

As such, efforts to linearize SOI modulators are crucial to enable integrated photonics-based mm-wave technology and overviews of such efforts are shown in figure 13. One approach to decreasing modulator non-linearities relies on an appropriate modulator configuration. One example is the ring-assisted MZI (RAMZI) structure, depicted in figure 14(a), that relies on cancellation of the opposing non-linear responses that are inherent to MZI and ring resonators; SFDRs of up to 99 dB $Hz^{2/3}$ at 10 GHz have been achieved [297–299]. Other design approaches attempt to cancel out the IMD3, such as the dual-parallel-MZIs that achieve SFDRs of up to 114 dB $Hz^{2/3}$ at 10 GHz [300–302] depicted in figure 14(b), and the FLAME configuration mentioned earlier that attains SFDRs of up to 120 dB $Hz^{2/3}$ at 10 GHz [274], depicted in figure 14(c).

Beyond the design of the modulator, the linearity can be improved by material composition or doping control. For doping optimization, both the position of the doping profile and the thickness of the depleted zone can be tuned, which, based on the overlap with the optical field, determine the refractive index change. Generally, the logic regarding linearity is to decrease the integration width of the overlap between the optical field distribution and the depletion region, thereby giving the modulated signal fewer non-linear components, as was demonstrated in [291]—here, an SFDR of 118 dB $Hz^{2/3}$ was attained at 10 GHz. With heterogeneous Si III–V approaches, the non-linearity of the modulator is the sum of the inherent non-linearities of the modulator design and several non-linear electro-optic effects present in the III–V composition. Since the relevant non-linear effects have different signs, it is possible to cancel them out to achieve linear operation, for example, by tuning the doping level of each material, as was done in [289], where a hybrid III–V/Si-based MZI achieved an SFDR of 112 dB $Hz^{2/3}$ at 10 GHz. This linear performance can be further improved when a heterogeneously integrated modulator is combined with the aforementioned design approaches, as demonstrated by a hybrid III–V/Si RAMZI configuration achieving SFDR values of 117.5 dB $Hz^{2/3}$ at 10 GHz [299].

Finally, an approach for linearizing a modulator is to either pre-emphasize the mm-wave signal driving the modulator or to post-compensate the output signal [308, 315–318]. For pre-distortion circuits (PDCs), the non-linear response of a Schottky barrier diode can be utilized, as it is the opposite of the MZI's inherent non-linearity. By tuning the bias, the transfer function can be tuned to match the desired IMD, in most cases, IMD3. Efforts have been made using single [308], dual [310], and cascaded Schottky-diode-based PDCs, whereby SFDRs of 112.1 dB $Hz^{2/3}$ at 2 GHz were attained [309]. The improvement in the SFDR is on the order of 10 dB, and this method could be combined with other linearizing schemes for better overall performance. Moreover, these Schottky diodes operate well into the low THz regime, and thus they are capable of processing mm-waves with very high frequencies. However, such PDCs introduce higher complexity to the overall system.

Post-compensation is generally done digitally and, hence, imposes the need for an analog-to-digital converter (ADC) and digital signal processing [319]. In the mm-wave regime, ADCs are both extremely costly and power consuming [315], and as such, post-compensation can only be a viable solution when the mm-wave is downconverted—either optically or electronically—to an intermediate frequency (IF) where ADCs are more cost-effective, as demonstrated in [319].

As a concluding remark, one should recognize that SFDR is closely coupled to SNR_{max}, in the sense that they are equal for a truly linear device. Due to this logic, several considerations regarding the 'conventional' performance parameters of modulators are highly relevant for linearity as well. Lowering V_π and the noise figure, while increasing the input power handling and the transmission, improves linearity.

6.2.5. Measuring modulator linearity. Experimental measurements of linearity are not trivial and there are pitfalls to be aware of. To measure the non-linearities in a controlled way, the modulator is driven by two closely spaced driving frequencies—a method called two-tone measurement. A generic setup for two-tone measurement is shown in figure 15(a)

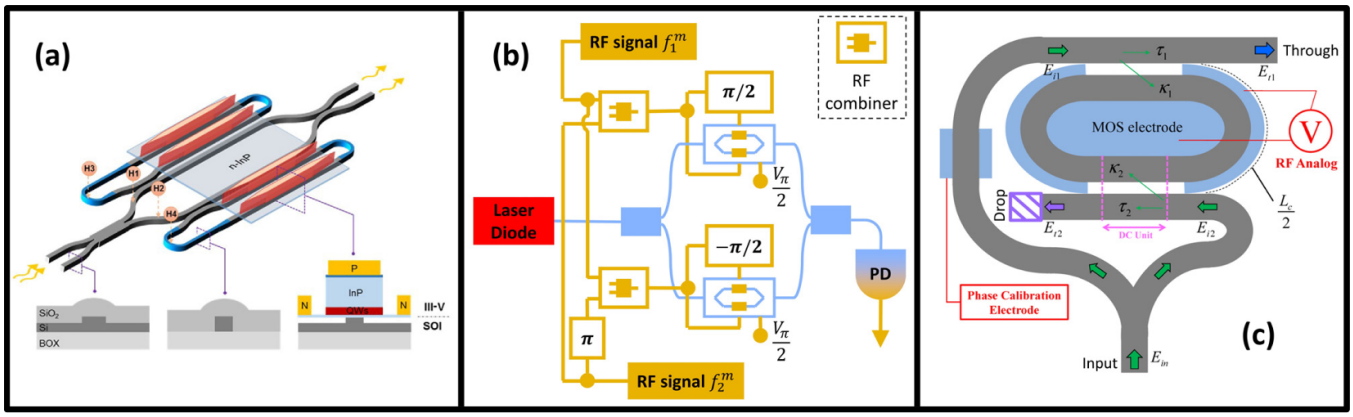

Figure 14. Different linearization schemes based on a specific design of the modulator configuration, (a) RAMZI (reprinted with permission from [299] © The Optical Society), (b) dual-parallel-MZI (adapted with permission from [300] © The Optical Society) and (c) FLAME (reprinted with permission from [274] © The Optical Society).

and the output of such experiments will determine the power of each non-linear component arising in the modulator, of which an example is given in figure 15(b). As a rule of thumb, all systems create IMD, and it is, therefore, important to consider the non-linearity of the test system on its own.

As explained earlier, the main parameter used to quantify modulator linearity is the SFDR. When comparing the SFDR performance of devices tested on different systems, a few measures should be taken to ensure a correct comparison. A lot of these discrepancies originate from the fact that there is no agreed standard for SFDR measurements. The details to consider regarding SFDR values are the following:

- *Center frequency*: Two-tone experiments must be carried out at a center frequency and with a given spacing. Since nonlinearities are generally more pronounced at higher frequencies, the SFDR will decrease with frequency, but in a non-trivial device-specific way. Hence, the reported SFDR values should be accompanied by a center-frequency specification.
- *Noise floor*: The noise floor of a given measurement setup is not truly flat over the given frequency and power range. This will affect any comparison between studies, as some authors base SFDR measurements on a flat standard-value noise floor, while others measure the noise floor at a given output power and frequency.
- *Slope*: The theory of IMD dictates the slope of the measured signals. This introduces the possibility of two approaches: either a line with the expected slope is fitted to the data points or a line is fitted to the linear part of the data, with the slope as a variable. In some cases, the lines are extrapolated from very few data points, which decreases the accuracy of the extracted SFDR value.
- It should be further noted that for highly linear systems, the fifth-order SFDR component could become the dominant term, due to the steeper slope and linearization efforts towards IMD3.

6.3. The $LiNbO_3$-on-insulator (LNOI) platform and heterogeneous integration with SOI

Apart from modulators fabricated using the SOI platform, integrated $LiNbO_3$-based modulators have become a hot research topic in recent years due to the excellent properties of this material, such as its strong electro-optic Pockels effect that enables energy-efficient and fast switching of the refractive index, and its transparency over a wide wavelength range from visible to mid-infrared wavelengths. Currently, $LiNbO_3$ dominates the market for stand-alone optical modulators [26], and so it is an obvious candidate for integration into a PIC platform. The LNOI platform is a promising technology for $LiNbO_3$-based PICs, in which a thin $LiNbO_3$ film is bonded to a Si or $LiNbO_3$ wafer (coated with a silica buffer layer) through ion-slicing [320]. While these wafers are already commercially available, there is still no standardized process to realize PIC building blocks, although the dry etching process is a promising approach for the fabrication of low-loss integrated $LiNbO_3$ components [321]. Another promising approach—and one that is in line with the context of this review—is the hybrid $LiNbO_3$/Si platform. Here, a $LiNbO_3$ membrane is bonded to a patterned SOI wafer and can be employed in combination with Si waveguides, with or without further processing [322, 323]. Although this bonding process complicates the fabrication of these chips and is not yet at the level of fabrication maturity of the hybrid III–V/Si platform, the hybrid $LiNbO_3$/Si platform is becoming more and more feasible commercially, due to recent developments [307, 321, 324–326].

As such, modulators integrated into these platforms have tremendous potential to compete with the other approaches such as hybrid III–V/Si. A recent example that demonstrates this is a $LiNbO_3$/Si modulator that uses a combination of silicon and $LiNbO_3$ waveguides that are coupled through adiabatic tapers [322]. This device operates at up to 70 GHz, has an SFDR of 99.6 dB $Hz^{2/3}$ at 1 GHz and exhibits a relatively low voltage-length product of 2.2 V cm. A similar result is obtained when this modulator has an on-chip termination

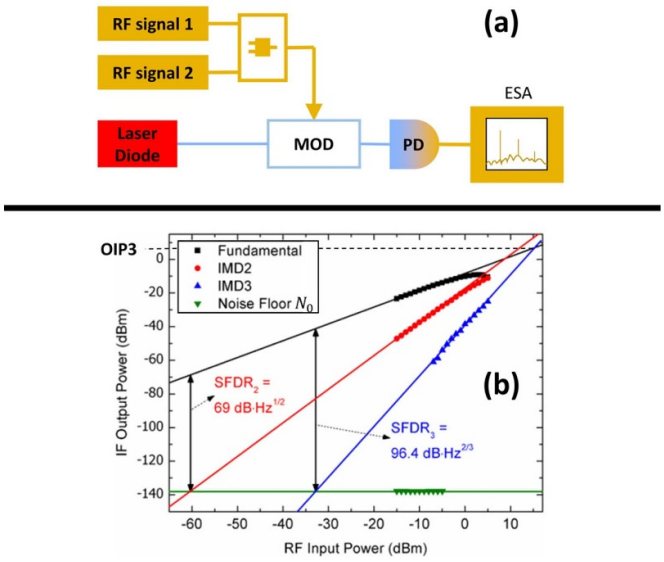

Figure 15. (a) A generic setup for two-tone measurement of an optical modulator. Consideration must be made regarding the nonlinearity of the driving sources and the measurement system as a whole. (b) An example of a two-tone measurement, measured at a center frequency of 26 GHz (reprinted with permission from [295] © The Optical Society).

resistor [327]. Another modulator realized using the hybrid $LiNbO_3$/Si platform exhibited even higher bandwidths of 106 GHz or more, while not requiring etching of the $LiNbO_3$ layer, but it also had a voltage-length product three times larger, at 6.7 V cm [323, 328]. A similar bandwidth of 100 GHz and beyond but a smaller voltage-length product of 2.2 V cm was achieved in an LNOI-based modulator [329]. Modulation has been demonstrated beyond its 3 dB bandwidth, at up to 500 GHz, in an LNOI modulator, where the waveguide and electrode geometries have been optimized for modal overlap and phase matching [330]. Finally, an LNOI modulator based on a Michelson interferometer configuration (a modulator containing reflectors, thus increasing the interaction length between the mm waves and optical waves) achieved an extremely low voltage-length product of 1.6 V cm, as demonstrated in [331], although it had a low bandwidth of 12 GHz due to the velocity mismatch. It is clear from these developments that further improvements to the waveguide and/or the CPW electrode design in either the LNOI or $LiNbO_3$/Si platforms could further boost the bandwidth and energy efficiency of these integrated $LiNbO_3$-based modulators [326].

6.4. Heterogeneous integration with graphene and plasmonics

Apart from hybrid integration with III–V materials or $LiNbO_3$, two other approaches are being explored to achieve ultra-high-speed operation up to 300 GHz, namely, combining SOI modulators with noble metals to benefit from the plasmonic effects, or enhancing the SOI functionality with graphene.

Plasmonic effects in noble metals [272, 332–334] show the potential for very fast modulation, beyond 100 GHz, and ultralow energy consumption, below 50 fJ bit^{-1}. For example, in [335], a 170 GHz modulator was realized, for which the driving energy was reported to be 25 fJ bit^{-1} [336]. However, the modulation effects were non-linear, due to the non-linear relation between the interaction strength and the electric field enhancement. For example, aplasmonic enhancement by a factor of 30 of the electric field led to an increased third-order interaction by nearly four orders of magnitude [272]. As can be seen from figure 13, the initial results for the linearity of plasmonic Si modulators were not competitive with other approaches, as an SFDR of only 86.2 dB Hz$^{2/3}$ at 1 GHz was achieved [312].

Graphene, on the other hand, has recently been promoted as a very promising material for future modulators, partly due to its extremely high electron and hole mobility. Utilizing graphene in photonics has been an active area of research for several years and has resulted in actual realizations [337, 338]. Although graphene-based modulation has only been experimentally demonstrated up to 30 GHz and 35 GHz [339, 340] due to the electronic-band structure of graphene, there is reason to believe that faster and more linear devices based on graphene can be realized [341]. Indeed, a numerical study of hybrid graphene/Si modulators showed that these devices have the potential to achieve SFDR values of up to 130 dB Hz$^{2/3}$ [314]. However, at the moment, graphene-based modulators remain niche due to their relatively complex fabrication.

7. THz generation

While the previous discussions were limited to mm-wave frequencies of up to 300 GHz, the band in the electromagnetic spectrum with a frequency range from 0.3 THz to 10 THz, known as the THz regime, is also relevant for this overview. Indeed, the THz band is a natural extension of the mm-wave range and has many applications, including spectroscopy, short-range communication, remote earth sensing, security sensing, nondestructive evaluation and medical diagnosis [342–346]. Although there has been significant technological progress in this field over recent decades, and despite the latest promising technological breakthroughs [347], these applications have not been fully exploited yet, due to the immature state of THz technology, i.e. the lack of compact, low-power-consuming sources, PDs and photomixers (PMs) [348–350]. Since a technology gap exists between the well-developed areas of electronics and photonics, this frequency region is also known as the 'THz gap,' which accounts for a large amount of currently little-used spectrum.

Since THz frequencies border mm-wave frequencies, it is interesting to see how far photonics-based mm-wave technology can be extended towards or into the THz regime and therefore, a review of the technology and approaches to generate these high frequency signals is provided in this section. We first discuss the four main approaches or current

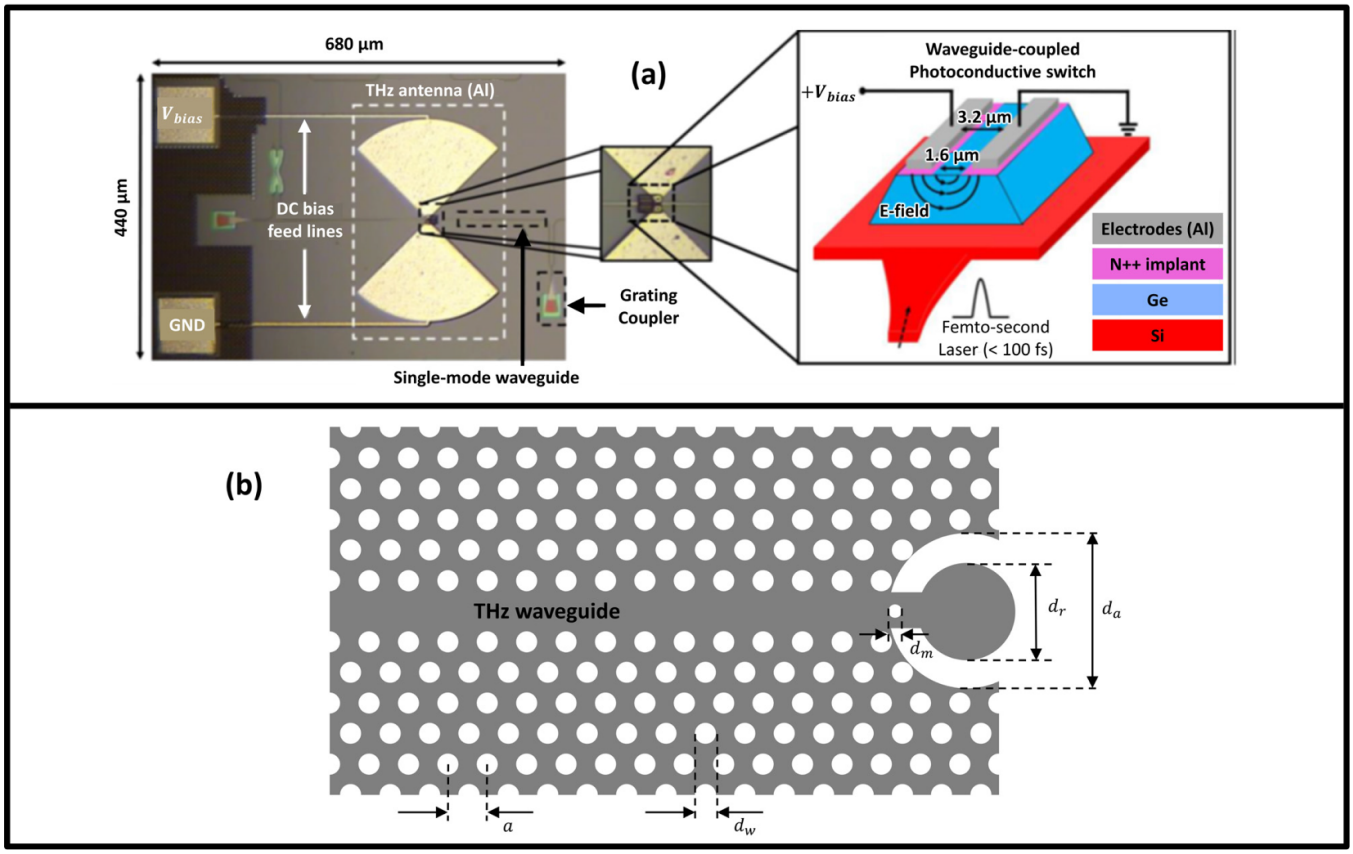

Figure 16. (a) Microscope image of a Ge PCA, integrated into an SOI platform and coupled to a Si optical waveguide and a schematic view of the waveguide-coupled PCA. Picture taken from [381] (reprinted with permission from Chen *et al*, © 2016). (b) Picture of the dielectric resonator antenna characterized in [382] (adapted with permission © The Optical Society). Some relevant parameters are $a = 240$ μm, $d_w = 144$ μm, $d_m = 100$ μm, $d_r = 642$ μm and $d_a = 1016$ μm. The Si slab itself is thick.

techniques that enable >100 GHz generation. We then explore the opportunities to use Si photonics for mm-wave generation beyond the typical bandwidth of SOI-based PDs, i.e. the frequencies beyond 100 GHz and into the THz region. In particular, we will discuss the heterogeneous integration of quantum-cascade lasers on Si, the use and design of PDs beyond 100 GHz, the use of PMs and the use of Si/Ge-based photoconductive antennas (PCAs).

7.1. Current methods of THz generation

The approaches to developing THz sources can be divided into roughly four groups. The first approach is based on an extension of mm-wave technology, i.e. frequency multiplication of a signal from a mm-wave oscillator [351]. The second method relies on the same optical heterodyning technique as described in section 3.2.1, i.e. the beating signal or envelope of two infrared lasers is transferred into the THz domain through ultrahigh-speed PDs or PMs [352]. The third approach is employing the novel THz quantum-cascade laser (QCL) whose operation is based on intersubband transitions in the conduction band of GaAs/AlGaAs quantum-well heterostructures [353] or the valence band of SiGe/Ge quantum-well heterostructures [354]. Finally, the fourth approach is either based on the hot-phonon effect as was demonstrated in an AlGaAs/InGaAs layer stack [355] or population inversion/stimulated THz emission in Si doped by group-V donors [356]. However, due to their complexity, these approaches are mainly restricted to laboratory research.

7.2. Si photonics for THz generation

7.2.1. QCL sources on Si. As pointed out before, efficient electrically pumped Si THz lasers have not been demonstrated yet [357], but through the heterogeneous integration of III–V materials, this functionality can be realized in the SOI platform [358, 359], for example, by employing QCLs. This is the most direct approach for generating THz optical signals based on SOI technology and has several advantages: firstly, the emission wavelength primarily depends on the quantum-well thickness, and thus allows the generation of light in a wavelength range unrelated to the material's energy bandgap. The radiation frequency is determined by the energy spacing of the lasing sub-bands, which in principle allows operation at arbitrarily long wavelengths [360]. Secondly, the cascade process makes it is feasible to generate multiple photons per electron and thus makes it possible to have high-power lasers [361].

In [362, 363], InP-based QCLs were realized, bonded to Si, to generate THz radiation. Another type of QCL is based

on intra-cavity difference-frequency generation (DFG) in the mid-infrared and such QCLs have been used as THz sources at room temperature. The output power and tunability of such DFG-based QCLs have been improved remarkably in recent years, following the implementation of the Cherenkov waveguide scheme [364]. A 4.2 mm cavity length Cherenkov THz DFG-QCL, grown on a 660 μm-thick native InP substrate, was transfer-printed [365, 366] on a 1 mm thick Si substrate. A frequency tuning range from 1.3 THz to 4.3 THz was demonstrated. With peak output powers of up to 270 μW, the mid-IR-to-THz conversion efficiencies far exceeded the performance of devices with similar dimensions that are fabricated on a semi-insulating InP substrate.

Other works, with III–V QCLs heterogeneously integrated on Si using integrating gratings for distributed-feedback operation—although strictly in the mid-infrared, and further away from the mm-wave regime—show the potential for high-power operation at 200 mW and the versatility of integration on Si [367, 368].

7.2.2. High speed PDs. Most current PDs operate at the lower frequencies in the THz band, i.e. 0.1 THz to 0.5 THz. For example, report of the first Si metal–semiconductor–metal PDs (MSM PDs) stated that a bandwidth of 110 GHz was achieved at short wavelengths of around 400 nm, but that the bandwidth dropped to 40 GHz when operated at longer wavelengths of around 800 nm [369]. To solve this issue, an MSM PD on an SOI substrate with a scaled top Si thin layer was designed and fabricated, achieving a bandwidth of up to 140 GHz [370]. Furthermore, the response speed of this PD was independent of the wavelength, albeit limited to the Si bandgap.

Nevertheless, to have these PDs operate at telecom wavelengths rather than in the visible spectrum, Ge-based compounds need to be used. For example, a Ge PD that was grown at the end of a Si waveguide and operated at a wavelength of around 1550 nm, was demonstrated to have a bandwidth of 120 GHz [137, 371]. Output power of -28 dBm at 200 GHz was achieved using a SiGe PIN PD [372]. Also, a compact SOI-based optically driven mm-wave radiator was reported to generate 180 GHz radiation, using 8 SiGe PDs having a 25 GHz bandwidth, where a multi-port driven travelling-wave antenna design was chosen to boost the output power [373].

Rather than generating THz waves, one can also employ the SOI platform as a THz detector. For example, an integrated bow-tie coupling antenna realized in a commercial 130 nm CMOS technology, was reported to detect THz waves of around 300 GHz at room temperature and was used for THz imaging [374]. It is clear that mm wave and THz components greatly benefit from photonic integrated SOI technology.

7.2.3. PMs and THz antennas. One promising approach for achieving CW THz sources at room temperature is photomixing in ultrafast photoconductive semiconductor materials, which is possible due to their ultrashort carrier lifetime [375–377]. However, the efficiency of photon-to-current conversion is low, which limits the output power of CW THz PMs to the microwatt level [378, 379].

A THz beat note can be generated by the optoelectronic mixture of two laser signals whose optical frequencies are separated by the target THz frequency. Alternatively, by illuminating the PM or PCA with picosecond or sub-picosecond optical pulses, broadband THz radiation can be generated. Bulk InGaAs and GaAs are two common and promising materials for building ultrafast PCAs [380]. Another demonstration is illustrated in figure 16(a), from the report of a Ge-based optical waveguide, integrated into an SOI platform and coupled to a THz PCA, and emitting THz pulses with a bandwidth of 1.5 THz [381].

In the context of THz antennas, it should be noted that there is growing research into the recently developed all-dielectric THz antennas implemented on Si [382–385]; in figure 16(b), we depict the antenna from [382] that operates at a frequency of 325 GHz. Although these antennas do not have photomixing capabilities, this is nevertheless an important development, considering that superior passive functionality for THz waves—in terms of ultra-low waveguiding, splitting and high-Q filtering—has been realized in Si as well, specifically, using Si 'photonic' crystals operating in the THz regime [384, 386–388]. This means that in the future, Si photonics platforms have much potential to offer THz building blocks (in addition to the photonic components already offered) that will enable all-THz analog signal processing to some degree, thus placing all the THz and photonic functionality for optically generating and processing THz waves into a single chip.

7.2.4. Other Si photonics-based approaches for THz generation. Apart from Si, other materials can be utilized for THz generation. Firstly, one can employ semiconducting nanowires for THz emission. While bulk Ge and Si only exhibit weak THz emission because they are indirect-gap semiconductors [389, 390], indirect-gap semiconducting nanowires have larger transient currents and can be used to improve the power of THz radiation. For example, the power of the THz radiation from nanostructured Ge wafers is comparable to that from an n-GaAs wafer [390]. This is a potentially cheap and simple path to improve THz emission efficiency, by properly designing nanostructures on semiconductor surfaces.

Secondly, the impurity-doped Ge and Si THz lasers described in [351] were studied both theoretically and experimentally. These different doping types can increase the THz emission efficiency, thereby leading to another way to improve the THz radiation based on Si photonics.

Finally, as reported in [391], graphene-based PDs integrated into Si photonic structures have outstanding advantages, such as high responsivity over a broad spectral range and fast operation. Indeed, a recent study shows that graphene-covered Si WPDs, which rely on the strong coupling between the waveguide mode and the graphene plasmons, could potentially have responsivities exceeding 200 A W^{-1} and bandwidths beyond 500 GHz [392]. As such, the hybrid SOI/graphene platform

opens up new opportunities to improve the performance of PDs that are designed to operate at THz frequencies.

8. Outlook and perspectives

Overall, it is clear that for photonics-based mm-wave technologies, there is a shift from fiber-based systems towards PICs, as the latter enable more complex and reliable functionality in a much smaller footprint and at a lower cost, while optimizing the energy consumption. Combined with the fact that optical fibers are finding their way into more and more short-haul links due to the increasing bandwidth requirements [393, 394], these PIC-based mm-wave components will play a key role in telecommunication networks and increasingly obsolete the all-electronic chips. The same applies to sensing and imaging applications, where electromagnetic waves in the mm-wave and THz bands enable more sensitive detection than in other frequency bands.

While both sources and filters are key elements in mm-wave links [13], special attention needs to be paid to integrated PDs and modulators, as they interface the photonic and electronic domains. Indeed, the sources do not require mm-wave electronic signals (unless direct modulation is involved), and neither do the integrated filters that process the signals entirely in the optical domain—only DC electronic signals are required for tuning/biasing the lasers/filters. The PDs and modulators, on the other hand, need to perform efficient optical-to-electrical and electrical-to-optical conversions, respectively, at mm-wave frequencies. Although materials with a strong electro-optic response, such as $LiNbO_3$, or a III–V material, such as InP, are superior for this purpose, SOI-based PDs/-modulators and $LiNbO_3$ or InP PDs/modulators heterogeneously integrated into SOI platforms will have the most potential to be implemented in photonics-based mm-wave circuits. This is because the SOI platform not only benefits from mature fabrication processes and excellent co-integration with electronic devices, it also offers the lowest chip footprint and has excellent passive functionality. Moreover, many strategies for optimizing electro-optic performance do not rely on optimizing the layer stack itself, but rather the building block 'topology,' such as travelling-wave approaches, where an array of PDs is connected by an RF-line or where a modulator is placed in a ring resonator. These solutions are virtually independent of the fabrication process and thus many SOI foundries are capable of fabricating these devices.

When considering the target metrics discussed in section 2.2, we thus believe that in the short term, photonics-based mm-wave applications will rely heavily on SOI chips realized with the building blocks offered by mature SOI foundries and tackle the lower mm-wave frequencies up to around 50 GHz that target both the current and some future telecommunications links. For higher frequencies of up to 100 GHz that are key for radar and more advanced mobile networks, we predict that hybrid III–V/Si or $LiNbO_3$/Si circuits will play a more important role at the very least, considering that the heterogeneous integration of III–V materials and $LiNbO_3$ on Si continues to mature rapidly in terms of reproducibility and compatibility with CMOS processes. Meeting bandwidth requirements of up to 14 GHz should thus not be an issue for these devices, however, depending on the application, when a trade-off needs to be made with other metrics such as linearity and efficiency, it will affect the modulator design. In addition, while the frequency stability requirements can already be met with fiber-based mm-wave systems, the consistent improvement in PIC foundry building blocks implies that similar or sufficient performance is achievable on PICs as well [395–397]. Moreover, in terms of signal-power requirements, while the photonically generated mm-wave powers are still below 100 mW, even for hybrid III–V/Si-based PDs [398], there is intensive research towards on-chip parallelization and beam-forming networks to make the power consumption more efficient and thus lower the power requirements for individual PDs [28, 399]. Finally, since these PICs already enable most of the mm-wave functionality in chip footprints measuring tens of mm^2, we predict that these devices will find their way into densely integrated systems and mobile applications.

In the long term, when new topologies such as graphene-on-Si or hybrid Si–plasmonic devices have become more mature, use of the high-frequency bands at up to 200 GHz will become feasible, thus realizing photonics-based radar, imaging and sensing applications (see section 2.2.1). As Si has already been proven to enable low-loss THz waveguiding, filtering and all-dielectric antenna radiation, and as heterogeneously integrated THz sources/PMs continue to improve in performance, the hybrid SOI platform will also open up exciting new opportunities for THz-based applications.

Acknowledgment

This work was supported by Det Frie Forskningsråd AUFF (Starting Grant Lektor Martijn Heck)and Det Frie Forskningsråd MH micro-NIST.

ORCID iDs

Iterio Degli-Eredi https://orcid.org/0000-0001-9576-9979
Simon Rommel https://orcid.org/0000-0001-8279-8180
Martijn J R Heck https://orcid.org/0000-0003-4201-4614

References

[1] Muthu K E, Raja A S and Shanmugapriya G 2017 Frequency 16-tupled optical millimeter wave generation using dual cascaded MZMs and 2.5 Gbps RoF transmission *Optik* **140** 338–46
[2] Alavi S E, Soltanian M R K, Amiri I S, Khalily M, Supa'at A S M and Ahmad H 2016 Towards 5G: a photonic based millimeter wave signal generation for applying in 5G access Fronthaul *Sci. Rep.* **6** 19891
[3] Lin C-T, Shih P-T, Chen J, Xue W-Q, Peng P-C and Chi S 2008 Optical millimeter-wave signal generation using frequency quadrupling technique and no optical filtering *IEEE Photonics Technol. Lett.* **20** 1027–9
[4] Wiberg A, Perez-Millan P, Andres M V and Hedekvist P O 2006 Microwave-photonic frequency multiplication

utilizing optical four-wave mixing and fiber Bragg gratings *J. Lightwave Technol.* **24** 329–34
[5] Gao L, Liu W, Chen X and Yao J 2013 Photonic-assisted microwave frequency multiplication with a tunable multiplication factor *Opt. Lett.* **38** 4487–90
[6] Chen H, Xu Z, Fu H, Zhang S, Wu C, Wu H, Xu H and Cai Z 2015 Switchable and tunable microwave frequency multiplication based on a dual-passband microwave photonic filter *Opt. Express* **23** 9835–43
[7] Gao Y, Wen A, Jiang W, Liang D, Liu W and Xiang S 2015 Photonic microwave generation with frequency octupling based on a DP-QPSK modulator *IEEE Photonics Technol. Lett.* **27** 2260–3
[8] Long Y, Zhou L and Wang J 2016 Photonic-assisted microwave signal multiplication and modulation using a silicon Mach–Zehnder modulator *Sci. Rep.* **6** 1–6
[9] Marpaung D, Roeloffzen C, Heideman R, Leinse A, Sales S and Capmany J 2013 Integrated microwave photonics *Laser Photonics Rev.* **7** 506–38
[10] Ghosh A, Thomas T A, Cudak M C, Ratasuk R, Moorut P, Vook F W, Rappaport T S, MacCartney G R, Sun S and Nie S 2014 Millimeter-wave enhanced local area systems: a high-data-rate approach for future wireless networks *IEEE J. Sel. Areas Commun.* **32** 1152–63
[11] Mohammadhosseini H and Heck M J R 2017 Silicon photonics to improve the energy-efficiency of millimeter wave communication systems *Int. Topical Meeting on Microwave Photonics* (*Beijing, China*) (http://doi.org/10.1109/MWP.2017.8168654)
[12] Jalali B and Fathpour S 2006 Silicon photonics *J. Lightwave Technol.* **24** 4600–15
[13] Marpaung D, Yao J and Capmany J 2019 Integrated microwave photonics *Nat. Photon.* **13** 80–90
[14] Miller S E 1969 Integrated optics: an introduction *Bell Syst. Tech. J.* **48** 2059–69
[15] Kogelnik H 1975 An introduction to integrated optics *IEEE Trans. Microw. Theory Tech.* **MTT-23** 2–16
[16] Wu M-C and Lin R-B 2005 Multiple project wafers for medium-volume IC production *IEEE Int. Symp. on Circuits and Systems* (*Kobe, Japan*) (http://doi.org/10.1109/ISCAS.2005.1465688)
[17] Kish F A *et al* 2011 Current status of large-scale InP photonic integrated circuits *IEEE J. Sel. Top. Quantum Electron.* **17** 1470–89
[18] Rickman A 2014 The commercialization of silicon photonics *Nat. Photon.* **8** 579–82
[19] imec 2019 (https://www.imec-int.com/en/silicon-photonic-ICs-prototyping)
[20] Wang J and Long Y 2018 On-chip silicon photonic signaling and processing: a review *Sci. Bull.* **63** 1267–310
[21] Liu J, Beals M, Pomerene A, Bernardis S, Sun R, Cheng J, Kimerling L C and Michel J 2008 Waveguide-integrated, ultralow-energy GeSi electro-absorption modulators *Nat. Photon.* **2** 433–7
[22] Marshall O, Hsu M, Wang Z, Kunert B, Koos C and Van Thourhout D 2018 Heterogeneous integration on silicon photonics *Proc. IEEE* **106** 2258–69
[23] Tanaka S, Jeong S-H, Sekiguchi S, Kurahashi T, Tanaka Y and Morito K 2012 High-output-power, single-wavelength silicon hybrid laser using precise flip-chip bonding technology *Opt. Express* **20** 28057–69
[24] Xie W, Komljenovic T, Huang J, Tran M, Davenport M, Torres A, Pintus P and Bowers J 2019 Heterogeneous silicon photonics sensing for autonomous cars *Opt. Express* **27** 3642–63
[25] Smulders P 2002 Exploiting the 60 GHz band for local wireless multimedia access: prospects and future directions *IEEE Commun. Mag.* **40** 140–7
[26] Seeds A J and Williams K J 2006 Microwave photonics *J. Lightwave Technol.* **24** 4628–41
[27] Wells J 2009 Faster than fiber: the future of multi-G/s wireless *IEEE Microw. Mag.* **10** 104–12
[28] Xiao M *et al* 2017 Millimeter wave communications for future mobile networks *IEEE J. Sel. Areas Commun.* **35** 1909–35
[29] Rommel S, Cavalcante L C P, Quintero A G, Mishra A K, Vegas Olmos J J and Tafur Monroy I 2016 W-band photonic-wireless link with a Schottky diode envelope detector and bend insensitive fiber *Opt. Express* **24** 11312–22
[30] Ghelfi P *et al* 2014 A fully photonics-based coherent radar system *Nature* **507** 341–5
[31] Nagatsuma T, Hisatake S and Nguyen Pham H H 2016 Photonics for millimeter-wave and terahertz sensing and measurement *IEICE Trans. Electron.* **E99.C** 173–80
[32] Knöchel R, Damm C and Lyons W G 2017 Microwave sensors in your life [from the Guest Editors' desk] *IEEE Microw. Mag.* **18** 24–25
[33] Hussain Naqvi A and Lim S 2018 Review of recent phased arrays for millimeter-wave wireless communication *Sensors* **18** 1–31
[34] Cavalcante L, Rommel S, Rodriguez S, Olmos J J V and Tanfur Monroy I 2016 On the capacity of radio-over-fiber links at the W-band *Opt. Quantum Electron.* **48** 1–10
[35] Andrews J G, Buzzi S, Choi W, Hanly S V, Lozano A, Soong A C K and Zhang J C 2014 What will 5G be? *IEEE J. Sel. Areas Commun.* **32** 1065–82
[36] Rappaport T S, Sun S, Mayzus R, Zhao H, Azar Y, Wang K, Wong G N, Schulz J K, Samimi M and Gutierrez F 2013 Millimeter wave mobile communications for 5G cellular: it will work! *IEEE Access* **1** 335–49
[37] Rommel S, Rodríguez S, Chorchos Ł, Grakhova E P, Sultanov A K, Turkiewicz J P, Vegas Olmos J J and Tafur Monroy I 2016 Outdoor W-band hybrid photonic wireless link based on an optical SFP+ module *IEEE Photonics Technol. Lett.* **28** 2303–6
[38] Boccardi F, Heath R W, Lozano A, Marzetta T L and Popovski P 2014 Five disruptive technology directions for 5G *IEEE Commun. Mag.* **52** 74–80
[39] IEEE 802.11ad 2012 Enhancements for very high throughput in the 60 GHz band (part 11, amendment 3) (http://doi.org/10.1109/IEEESTD.2012.6392842)
[40] Feng W, Wang Y, Lin D, Ge N, Lu J and Li S 2017 When mmWave communications meet network densification: A scalable interference coordination perspective *IEEE J. Sel. Areas Commun.* **35** 1459–71
[41] Chih-Lin I, Rowell C, Han S, Xu Z, Li G and Pan Z 2014 Toward green and soft: a 5G perspective *IEEE Commun. Mag.* **52** 66–73
[42] Rodríguez S, Rommel S, Vegas OImos J J and Tafur Monroy I 2017 Reconfigurable radio access unit to dynamically distribute W-band signals in 5G wireless access networks *Opt. Switch. Network.* **24** 21–24
[43] Konstantinou D, Bressner T A H, Rommel S, Johannsen U, Johansson M N, Ivashina M V, Smolders A B and Tafur Monroy I 2020 5G RAN architecture based on analog radio-over-fiber fronthaul over UDWDM-PON and phased array fed reflector antennas *Opt. Commun.* **454** 1–10
[44] Rommel S, Perez-Galacho D, Fabrega J M, Muñoz R, Sales S and Tafur Monroy I 2019 High-capacity 5G fronthaul networks based on optical space division multiplexing *IEEE Trans. Broadcast.* **65** 434–43
[45] Appleby R and Anderton R N 2007 Millimeter-wave and submillimeter-wave imaging for security and surveillance *Proc. IEEE* **95** 1683–90

[46] Zankl D, Schuster S, Feger R and Stelzer A 2017 What a blast!: a massive MIMO radar system for monitoring the surface in steel industry blast furnaces *IEEE Microw. Mag.* **18** 52–69
[47] Hasch J, Topak E, Schnabel R, Zwick T, Weigel R and Waldschmidt C 2012 Millimeter-wave technology for automotive radar sensors in the 77 GHz frequency band *IEEE Trans. Microw. Theory Tech.* **60** 845–60
[48] Zhang F, Guo Q, Wang Z, Zhou P, Zhang G, Sun J and Pan S 2017 Photonics-based broadband radar for high-resolution and real-time inverse synthetic aperture imaging *Opt. Express* **25** 16274–81
[49] Usichenko T I, Edinger H, Gizhko V V, Lehmann C, Wendt M and Feyerherd F 2006 Low-intensity electromagnetic millimeter waves for pain therapy *Evidence-Based Complement. Altern. Med.* **3** 201–7
[50] Mattsson M-O and Simkó M 2019 Emerging medical applications based on non-ionizing electromagnetic fields from 0 Hz to 10 THz *Med. Devices Evidence Res.* **12** 347–68
[51] Mattsson M-O, Zeni O and Simkó M 2018 Is there a biological basis for therapeutic applications of millimetre waves and THz waves? *J. Infrared Millim. Terahertz Waves* **39** 863–78
[52] Elbamby M S, Perfecto C, Bennis M and Doppler K 2018 Edge computing meets millimeter-wave enabled VR: paving the way to cutting the cord *2018 IEEE Wireless Communications and Networking Conf. (WCNC)* (*Barcelona, Spain*) (http://doi.org/10.1109/WCNC.2018.8377419)
[53] Bekkali A, Kobayashi T, Nishimura K, Shibagaki N, Kashima K and Sato Y 2018 Millimeter-wave-based fiber-wireless bridge system for 8K UHD video streaming and gigabit ethernet data connectivity *J. Lightwave Technol.* **36** 3988–98
[54] Matsusaki Y, Yamagishi F, Yamasato A, Nakagawa T, Okabe S and Iai N 2020 Development of UHDTV wireless camera transmitter using millimeter-wave band *2020 IEEE Radio and Wireless Symp. (RWS)* (*San Antonio, TX*) (http://doi.org/10.1109/RWS45077.2020.9050101)
[55] Webber J, Kamoda H, Kukutsu N and Kumagai T 2015 Millimeter-wave wireless communication in a data center cabinet with adaptive control of propagation *2015 21st Asia-Pacific Conf. on Communications (APCC)* (*Kyoto, Japan*) (http://doi.org/10.1109/APCC.2015.7412524)
[56] Zeman K, Stusek M, Pokorny J, Masek P, Hosek J, Andreev S, Dvorak P and Josth R 2017 Emerging 5G applications over mmwave: hands-on assessment of WiGig radios *2017 40th Int. Conf. on Telecommunications and Signal Processing (TSP)* (*Barcelona, Spain*) (http://doi.org/10.1109/TSP.2017.8075942)
[57] Chorchos Ł, Rommel S, Turkiewicz J P, Tafur Monroy I and Vegas Olmos J J 2017 Reconfigurable radio access unit for DWDM to W-band wireless conversion *IEEE Photonics Technol. Lett.* **29** 489–92
[58] Ramírez R P, Rommel S, Vegas Olmos J J and Tafur Monroy I 2017 Optically generated single side-band radio-over-fiber transmission of 60Gbit/s over 50m at W-band *Optical Fiber Communication Conf. 2017* (*Los Angeles, CA*)
[59] SM.1045-1, Rec. ITU-R 1997 *Frequency tolerance of transmitters*
[60] Kanno A, Dat P T, Kuri T, Hosako I, Kawanishi T, Yoshida Y and Kitayama K 2014 Evaluation of frequency fluctuation in fiber-wireless link with direct IQ downconverter *2014 The European Conf. on Optical Communication (ECOC)* (*Cannes, France*) (http://doi.org/10.1109/ECOC.2014.6963972)
[61] Törnevik C 2017 Impact of EMF limits on 5G network roll-out *ITU-T Workshop on 5G, EMF & Health* (*Warsaw, Poland*)
[62] Lewicki F 2017 Impact of 5G technology on human exposure *ITU-T Workshop on 5G, EMF & Health* (*Warsaw, Poland*)
[63] Stohr A, Weib M, Malcoci A, Steffan A G, Trommer D, Umbach A and Jager D 2007 Wideband photonic millimeter-wave synthesizer using a high-power pin waveguide photodiode *2007 European Microwave Conf.* (*Munich, Germany*) (http://doi.org/10.1109/EUMC.2007.4405259)
[64] Zwick T, Boes F, Göttel B, Bhutani A and Pauli M 2017 Pea-sized mmW transceivers: QFN-based packaging concepts for millimeter-wave transceivers *IEEE Microw. Mag.* **18** 79–89
[65] Zervas M N and Codemard C A 2014 High power fiber lasers: a review *IEEE J. Sel. Top. Quantum Electron.* **20** 0904123
[66] Newport 2020 (www.newport.com/p/LD-1550-21B)
[67] Volyanskiy K, Salzenstein P, Tavernier H, Pogurmirskiy M, Chembo Y K and Larger L 2010 Compact optoelectronic microwave oscillators using ultra-high Q whispering gallery mode disk-resonators and phase modulation *Opt. Express* **18** 22358–63
[68] Savchenkov A A, Ilchenko V S, Liang W, Eliyahu D, Matsko A B, Seidel D and Maleki L 2010 Voltage-controlled photonic oscillator *Opt. Lett.* **35** 1572–4
[69] Rasoloniaina A, Huet V, Nguyên T K N, Le Cren E, Mortier M, Michely L, Dumeige Y and Féron P 2014 Controling the coupling properties of active ultrahigh-Q WGM microcavities from undercoupling to selective amplification *Sci. Rep.* **4** 1–7
[70] Iezekiel S 2009 *Microwave Photonics: Devices and Applications* (Chichester: Wiley) pp 21–6
[71] Selim Ünlü M and Strite S 1995 Resonant cavity enhanced photonic devices *J. Appl. Phys.* **78** 607–39
[72] Ishibashi T, Shimizu N, Kodama S, Ito H, Nagatsuma T and Furuta T 1997 Uni-traveling-carrier photodiodes *OSA Trends in Optics and Photonics Series on Ultrafast Electronics and Optoelectronics* (http://doi.org/10.1364/UEO.1997.UC3)
[73] Cohen-Jonathan C, Giraudet L, Bonzo A and Praseuth J P 1997 Waveguide AlInAs/GaAlInAs avalanche photodiode with a gain-bandwidth product over 160 GHz *Electron. Lett.* **33** 1492–3
[74] Baylón-Fuentes A, Hernández-Nava P, Zaldívar-Huerta I E, Rodríguez-Asomoza J, García-Juárez A and Aguayo-Rodríguez G 2011 Microwave signal generation based on optical heterodyne and its application in optical telecommunication system *CONIELECOMP 2011, 21st Int. Conf. on Electrical Communications and Computers* (*San Andres Cholula, Mexico*) (http://doi.org/10.1109/CONIELECOMP.2011.5749336)
[75] Yao. J 2009 Microwave photonics *J. Lightwave Technol.* **27** 314–35
[76] Forrester A T, Gudmundsen R A and Johnson P O 1955 Photoelectric mixing of incoherent light *Phys. Rev.* **99** 1691–700
[77] Goldberg L, Yurek A M, Taylor H F and Weller J F 1985 35 GHZ microwave signal generation with an injection-locked laser diode *Electron. Lett.* **21** 814–5
[78] Fukushima S, Silva C F C, Muramoto Y and Seeds A J 2003 Optoelectronic millimeter-wave synthesis using an optical frequency comb generator, optically injection locked lasers, and a unitraveling-carrier photodiode *J. Lightwave Technol.* **21** 3043
[79] Morales A, Konstantinou D, Rommel S, Raddo T R, Johannsen U, Okonkwo C and Tafur Monroy I 2019 Bidirectional K-band photonic/wireless link for 5G

communications *2019 44th Int. Conf. on Infrared, Millimeter, and Terahertz Waves (IRMMW-THz)* (*Paris, France*) (http://doi.org/10.1109/IRMMW-THz.2019.8874031)
[80] Yao J 2012 A tutorial on microwave photonics *IEEE Photonics Soc. Newsl.* **26** 5–12
[81] Ristic S, Bhardwaj A, Rodwell M J, Coldren L A and Johansson L A 2010 An optical phase-locked loop photonic integrated circuit *J. Lightwave Technol.* **28** 526–38
[82] Chen X, Deng Z and Yao J 2006 Photonic generation of microwave signal using a dual-wavelength single-longitudinal-mode fiber ring laser *IEEE Trans. Microw. Theory Tech.* **54** 804–9
[83] Hyodo M, Tani M, Matsuura S, Onodera N and Sakai K 1996 Generation of millimetre-wave radiation using a dual-longitudinal-mode microchip laser *Electron. Lett.* **32** 1589–91
[84] O'Reilly J J, Lane P M, Heidemann R and Hofstetter R 1992 Optical generation of very narrow linewidth millimetre wave signals *Electron. Lett.* **28** 2309–11
[85] O'Reilly J J and Lane P M 1994 Fibre-supported optical generation and delivery of 60 GHz signals *Electron. Lett.* **30** 1329–30
[86] Shen P, Gomes N J, Davies P A, Shillue W P, Huggard P G and Ellison B N 2003 High-purity mm-wave photonic local oscillator generation and delivery *MWP 2003 Proc. Int. Topical Meeting on Microwave Photonics* (*Budapest, Hungary*) (http://doi.org/10.1109/MWP.2003.1422862)
[87] Qi G, Yao J, Seregelyi J, Paquet S and Belisle C 2005 Generation and distribution of a wide-band continuously tunable mm-wave signal with an optical external modulation technique *IEEE Trans. Microw. Theory Tech.* **53** 3090–7
[88] Shi P, Yu S, Li Z, Song J, Shen J, Qiao Y and Gu W 2010 A novel frequency sextupling scheme for optical mm-wave generation utilizing an integrated dual-parallel Mach-Zehnder modulator *Opt. Commun.* **283** 3667–72
[89] Ma J, Xin X, Yu J, Yu C, Wang K, Huang H and Rao L 2008 Optical millimeter wave generated by octupling the frequency of the local oscillator *J. Opt. Network.* **7** 837–45
[90] Li W and Yao J 2010 Investigation of photonically assisted microwave frequency multiplication based on external modulation *IEEE Trans. Microw. Theory Tech.* **58** 3259–68
[91] Deng Z and Yao J 2006 Photonic generation of microwave signal using a rational harmonic mode-locked fiber ring laser *IEEE Trans. Microw. Theory Tech.* **54** 763–7
[92] Derickson D J, Helkey R J, Mar A, Wasserbauer J G, Wey Y G and Bowers J E 1992 Microwave and millimeter wave signal generation using mode-locked semiconductor lasers with intra-waveguide saturable absorbers *1992 IEEE MTT-S Microwave Symp. Digest* (http://doi.org/10.1109/MWSYM.1992.188095)
[93] Bordonalli A C, Cai B, Seeds A J and Williams P J 1996 Generation of microwave signals by active mode locking in a gain bandwidth restricted laser structure *IEEE Photonics Technol. Lett.* **8** 151–3
[94] Onodera N, Lowery A J, Zhai L, Ahmed Z and Tucker R S 1993 Frequency multiplication in actively mode-locked semiconductor lasers *Appl. Phys. Lett.* **62** 1329–31
[95] Yao X S and Maleki L 1996 Optoelectronic microwave oscillator *J. Opt. Soc. Am.* B **13** 1725–35
[96] Yao X S and Maleki L 1996 Optoelectronic oscillator for photonic systems *IEEE J. Quantum. Electron.* **32** 1141–9
[97] Yao X S and Maleki L 1996 Converting light into spectrally pure microwave oscillation *Opt. Lett.* **21** 483–5
[98] Yao X S, Davis L and Maleki L 2000 Coupled optoelectronic oscillators for generating both RF signal and optical pulses *J. Lightwave Technol.* **18** 73–8
[99] Yao X S, Maleki L and Eliyahu D 2004 Progress in the opto-electronic oscillator—a ten year anniversary review *2004 IEEE MTT-S Int. Microwave Symp. Digest (IEEE Cat. No.04CH37535)* (*Fort Worth, TX, United States*) (http://doi.org/10.1109/MWSYM.2004.1335872)
[100] Eliyahu D and Maleki L 2003 Low phase noise and spurious level in multi-loop opto-electronic oscillators *Proc. IEEE Int. Frequency Control Symp. and PDA Exhibition Jointly with the 17th European Frequency and Time Forum* (*Tampa, FL*) (http://doi.org/10.1109/FREQ.2003.1275126)
[101] Yao X S and Maleki L 1997 Dual microwave and optical oscillator *Opt. Lett.* **22** 1867–9
[102] Yao X S, Maleki L and Davis L 1998 Coupled opto-electronic oscillators *Proc. 1998 IEEE Int. Frequency Control Symp. (Cat. No. 98CH36165)* (*Pasadena, CA*) (http://doi.org/10.1109/FREQ.1998.717951)
[103] van der Ziel J P, Dingle R, Miller R C, Wiegmann W and Nordland Jr W A 1975 Laser oscillation from quantum states in very thin GaAs-Al0.2Ga0.8As multilayer structures *Appl. Phys. Lett.* **26** 463–5
[104] Ikegami T and Suematsu Y 1967 Resonance-like characteristics of the direct modulation of a junction laser *Proc. IEEE* **55** 122–3
[105] Pollock C R and Lipson M 2003 Waveguide modulators *Integrated Photonics* vol II 2nd edn (Berlin: Springer) (http://doi.org/10.1007/978-1-4757-5522-0_12)
[106] Latkowski S, Hänsel A, Bhattacharya N, de Vries T, Augustin L, Williams K, Smit M and Bente E 2015 Novel widely tunable monolithically integrated laser source *IEEE Photonics J.* **7** 1503709
[107] Lemaître F, Latkowski S, Fortin C, Lagay N, Pajković R, Smalbrugge E, Decobert J, Ambrosius H and Williams K 2018 96 nm extended range laser source using selective area growth *2018 European Conf. on Optical Communication (ECOC)* (*Rome, Italy*) (http://doi.org/10.1109/ECOC.2018.8535218)
[108] Huang D, Tran M A, Guo J, Peters J, Komljenovic T, Malik A, Morton P A and Bowers J E 2019 High-power sub-kHz linewidth lasers fully integrated on silicon *Optica* **6** 745–52
[109] Epping J P, Oldenbeuving R M, Geskus D, Visscher I, Grootjans R, Roeloffzen C G H and Heideman R G 2020 High power integrated laser for microwave photonics *2020 Optical Fiber Communications Conf. and Exhibition (OFC)* (*San Diego, CA*) (http://doi.org/10.1364/OFC.2020.Th2A.2)
[110] Noguchi K, Mitomi O and Miyazawa H 1998 Millimeter-wave Ti:$LiNbO_3$ optical modulators *J. Lightwave Technol.* **16** 615–9
[111] Walker R G 1995 Electro-optic modulation at mm-wave frequencies in GaAs/AIGaAs guided wave devices *LEOS '95. IEEE Lasers and Electro-Optics Society 1995 8th Annual Meeting. Conf. Proc.* (*San Francisco, CA*) (http://doi.org/10.1109/LEOS.1995.484535)
[112] Teng C C 1992 Traveling-wave polymeric optical intensity modulator with more than 40 GHz of 3-dB electrical bandwidth *Appl. Phys. Lett.* **60** 1538–40
[113] Chen D and Fetterman H R 1997 Demonstration of 110 GHz electro-optic polymer modulators *Appl. Phys. Lett.* **70** 3335–7
[114] Kawanishi H, Yamauchi Y, Mineo N, Shibuya Y, Mural H, Yamada K and Wada H 2001 EAM-Integrated DFB laser modules with more than 40-GHz bandwidth *IEEE Photonics Technol. Lett.* **13** 954–6

[115] Ido T, Tanaka S, Suzuki M, Koizumi M, Sano H and Inoue H 1996 Ultra-high-speed multiple-quantum-well electro-absorption optical modulators with integrated waveguides *J. Lightwave Technol.* **14** 2026–34

[116] Li G L, Pappert S A, Sun C K, Chang W S C and Yu P K L 2001 Wide bandwidth traveling-wave InGaAsP/InP electroabsorption modulator for millimeter wave applications *2001 IEEE MTT-S Int. Microwave Sympsoium Digest (Cat. No. 01CH37157)* (*Phoenix, AZ*) (http://doi.org/10.1109/MWSYM.2001.966839)

[117] Huffman T, Davenport M, Belt M, Bowers J E and Blumenthal D J 2017 Ultra-low loss large area waveguide coils for integrated optical gyroscopes *IEEE Photonics Technol. Lett.* **29** 185–8

[118] Moralis-Pegios M, Mourgias-Alexandris G, Terzenidis N, Cherchi M, Harjanne M, Aalto T, Miliou A, Pleros N and Vyrsokinos K 2018 On-chip SOI delay line bank for optical buffers and time slot interchangers *IEEE Photonics Technol. Lett.* **30** 31–34

[119] Chrostowski L and Hochberg M 2015 *Silicon Photonics Design: From Devices to Systems* (Cambridge: Cambridge University Press) (http://doi.org/10.1017/CBO9781316084168)

[120] Bogaerts W, De Heyn P, Van Vaerenbergh T, De Vos K, Selvaraja S K, Claes T, Dumon P, Bienstman P, Van Thourhout D and Baets R 2012 Laser & photonics reviews *Silicon Microring Resonators* **6** 47–73

[121] Aamer M 2013 Development of an integrated silicon photonic transceiver for access networks *Thesis* (http://doi.org/10.4995/Thesis/10251/31649)

[122] Ding Y, Pu M, Liu L, Xu J, Peucheret C, Zhang X, Huang D and Ou H 2011 Bandwidth and wavelength-tunable optical bandpass filter based on silicon microring-MZI structure *Opt. Express* **19** 6462–70

[123] Li C, Xue C, Liu Z, Cong H, Cheng B, Hu Z, Guo X and Liu W 2016 High-responsivity vertical-illumination Si/Ge uni-traveling-carrier photodiodes based on silicon-on-insulator substrate *Sci. Rep.* **6** 22743

[124] Bogaert L, Van Gasse K, Spuesens T, Torfs G, Bauwelinck J and Roelkens G 2018 Silicon photonics traveling wave photodiode with integrated star coupler for high-linearity mm-wave applications *Opt. Express* **26** 34753–65

[125] Benedikovic D *et al* 2019 25 Gbps low-voltage hetero-structured silicon-germanium waveguide pin photodetectors for monolithic on-chip nanophotonic architectures *Photonics Res.* **7** 437–44

[126] Ahn D, Hong C-Y, Liu J, Giziewicz W, Beals M, Kimerling L C, Michel J, Chen J and Kärtner F X 2007 High performance, waveguide integrated Ge photodetectors *Opt. Express* **15** 3916–21

[127] Heck M J R, Bauters J F, Davenport M L, Spencer D T and Bowers J E 2014 Ultra-low loss waveguide platform and its integration with silicon photonics *Laser Photon. Rev.* **8** 667–86

[128] Heck M J R, Bauters J F, Davenport M L, Doylend J K, Siddharth J, Kurczveil G, Srinivasan S, Tang Y and Bowers J E 2013 Hybrid silicon photonic integrated circuit technology *IEEE J. Sel. Top. Quantum Electron.* **19** 6100117

[129] Wörhoff K, Heideman R G, Leinse A and Hoekman M 2015 TriPleX: a versatile dielectric photonic platform *Adv. Opt. Technol.* **4** 189–207

[130] Smit M, van der Tol J and Hill M 2012 Moore's law in photonics *Laser Photonics Rev.* **6** 1–13

[131] Mohammadhosseini H and Heck M J R 2016 Silicon photonics for millimeter-wave generation: an energy-efficiency analysis *18th European Conf. on Integrated Optics (ECIO) 2016* (*Warsaw, Poland*)

[132] Lim A E-J, Song J, Fang Q, Li C, Tu X, Duan N, Chen K K, Tern R P-C and Liow T-Y 2014 Review of silicon photonics foundry efforts *IEEE J. Sel. Top. Quantum Electron.* **20** 8300112

[133] Rahim A *et al* 2019 Open-access silicon photonics platforms in Europe *IEEE J. Sel. Top. Quantum Electron.* **25** 8200818

[134] imec. Technologies (https://europractice-ic.com/mpw-prototyping/siphotonics/imec/) (February 2020)

[135] Novack A *et al* 2013 Germanium photodetector with 60 GHz bandwidth using inductive gain peaking *Opt. Express* **21** 28387–93

[136] Liu J 2014 Monolithically integrated Ge-on-Si active photonics *Photonics* **1** 162–97

[137] Vivien L, Polzer A, Marris-Morini D, Osmond J, Hartmann J M, Crozat P, Cassan E, Kopp C, Zimmermann H and Fédéli M 2012 Zero-bias 40 Gbit/s germanium waveguide photodetector on silicon *Opt. Express* **20** 1096–101

[138] Zimmermann L, Knoll D, Kroh M, Lischke S, Petousi D, Winzer G and Yamamoto Y 2015 BiCMOS silicon photonics platform *Optical Fiber Communication Conf.* (http://doi.org/10.1364/OFC.2015.Th4E.5)

[139] Zimmermann L 2016 Monolithic electronic-photonic co-integration in photonic BiCMOS *ECOC 2016; 42nd European Conf. on Optical Communication* (*Dusseldorf, Germany*)

[140] Smit M, Williams K and van der Tol J 2019 Past, present, and future of InP-based photonic integration *APL Photonics* **4** 1–10

[141] Bauters J F, Davenport M L, Heck M J R, Doylend J K, Chen A, Fang A W and Bowers J E 2013 Silicon on ultra-low-loss waveguide photonic integration platform *Opt. Express* **21** 544–55

[142] Rong H, Jones R, Liu A, Cohen O, Hak D, Fang A and Paniccia M 2005 A continuous-wave Raman silicon laser *Nature* **433** 725–8

[143] Chen S *et al* 2016 Electrically pumped continuous-wave III–V quantum dot lasers on silicon *Nat. Photon.* **10** 307–11

[144] Liu A Y, Zhang C, Norman J, Snyder A, Lubyshev D, Fastenau J M, Liu A W K, Gossard A C and Bowers J E 2014 High performance continuous wave 1.3 μm quantum dot lasers on silicon *Appl. Phys. Lett.* **104** 041104

[145] Gunn. C 2006 CMOS photonics for high-speed interconnects *IEEE Micro* **26** 58–66

[146] Zhou Z, Yin B and Michel J 2015 On-chip light sources for silicon photonics *Light Sci. Appl.* **4** e358

[147] Willner A E 2019 *Optical Fiber Telecommunications VII* (New York: Academic Press) pp 162–3

[148] Roelkens G, Liu L, Liang D, Jones R, Fang A, Koch B and Bowers J 2010 III-V/silicon photonics for on-chip and inter-chip optical interconnects *Laser Photon. Rev.* **4** 751–79

[149] Heck M J R, Chen H-W, Fang A W, Koch B R, Liang D, Park H, Sysak M N and Bowers J E 2011 Hybrid silicon photonics for optical interconnects *IEEE J. Sel. Top. Quantum Electron.* **17** 333–46

[150] Chen H-W, Kuo Y-H and Bowers J E 2008 A hybrid silicon–AlGaInAs phase modulator *IEEE Photonics Technol. Lett.* **20** 1920–2

[151] Chen H-W, Peters J D and Bowers J E 2011 Forty Gb/s hybrid silicon Mach-Zehnder modulator with low chirp *Opt. Express* **19** 1455–60

[152] Tang Y, Peters J D and Bowers J E 2012 Over 67 GHz bandwidth hybrid silicon electroabsorption modulator

with asymmetric segmented electrode for 1.3 μm transmission *Opt. Express* **20** 11529–35
[153] Han J-H, Boeuf F, Fujikata J, Takahashi S, Takagi S and Takenaka M 2017 Efficient low-loss InGaAsP/Si hybrid MOS optical modulator *Nat. Photon.* **11** 486–90
[154] Hiraki T, Aihara T, Hasebe K, Takeda K, Fujii T, Kakitsuka T, Tsuchizawa T, Fukuda H and Matsuo S 2017 Heterogeneously integrated III–V/Si MOS capacitor Mach–Zehnder modulator *Nat. Photon.* **11** 482–5
[155] Witzens J 2017 Silicon photonics: modulators make efficiency leap *Nat. Photon.* **11** 459–62
[156] Bowers. J E 2016 Heterogeneous III-V/Si photonic integration *Conf. on Lasers and Electro-Optics* (*San Jose, CA*) (http://doi.org/10.1364/CLEO_SI.2016.SM1G.1)
[157] LioniX International 2017 LXI & HHI intensify collaboration of their PIC platforms (https://photonics.lionix-international.com/lxi-hhi-intensify-collaboration-of-their-pic-platforms/)
[158] Szelag B *et al* 2019 Hybrid III–V/silicon technology for laser integration on a 200-mm fully CMOS-compatible silicon photonics platform *IEEE J. Sel. Top. Quantum Electron.* **25** 8201210
[159] Piels M and Bowers J E 2014 40 GHz Si/Ge uni-traveling carrier waveguide photodiode *J. Lightwave Technol.* **32** 3502–8
[160] Ramaswamy A, Piels M, Nunoya N, Yin T and Bowers J E 2010 High power silicon-germanium photodiodes for microwave photonic applications *IEEE Trans. Microw. Theory Tech.* **58** 3336–43
[161] Luo X, Song J, Tu X, Fang Q, Jia L, Huang Y, Liow T-Y, Yu M and Lo G-Q 2014 Silicon-based traveling-wave photodetector array (Si-TWPDA) with parallel optical feeding *Opt. Express* **22** 20020–6
[162] Chang C-M, Sinsky J H, Dong P, de Valicourt G and Chen Y-K 2015 Dual-illuminated parallel-fed traveling wave germanium photodetectors *Optical Fiber Communication Conf. 2015* (*Los Angeles, CA*) (http://doi.org/10.1364/OFC.2015.W3A.5)
[163] Temkin H, Pearsall T P, Bean J C, Logan R A and Luryi S 1986 Ge_xSi_{1-x} strained-layer superlattice waveguide photodetectors operating near 1.3 μm *Appl. Phys. Lett.* **48** 963–5
[164] Chen H *et al* 2016 −1 V bias 67 GHz bandwidth Si-contacted germanium waveguide p-i-n photodetector for optical links at 56 Gbps and beyond *Opt. Express* **24** 4622–31
[165] Yin T, Cohen R, Morse M M, Sarid G, Chetrit Y, Rubin D and Paniccia M J 2007 31 GHz Ge n-i-p waveguide photodetectors on silicon-on-Insulator substrate *Opt. Express* **15** 13965–71
[166] Lischke S, Knoll D, Mai C, Zimmermann L, Peczek A, Kroh M, Trusch A, Krune E, Voigt K and Mai A 2015 High bandwidth, high responsivity waveguide-coupled germanium p-i-n photodiode *Opt. Express* **23** 27213–20
[167] DeRose C T, Trotter D C, Zortman W A, Starbuck A L, Fisher M, Watts M R and Davids P S 2011 Ultra compact 45 GHz CMOS compatible germanium waveguide photodiode with low dark current *Opt. Express* **19** 24897–904
[168] Ang K-W, Zhu S, Yu M, Lo G-Q and Kwong D-L 2008 High-performance waveguided Ge-on-SOI metal-semiconductor-metal photodetectors with novel silicon–carbon (Si:C) Schottky barrier enhancement layer *IEEE Photonics Technol. Lett.* **20** 754–6
[169] Piels M and Bowers J E 2012 Si/Ge uni-traveling carrier photodetector *Opt. Express* **20** 7488–95
[170] Bean J C 1985 Strained-layer epitaxy of germanium-silicon alloys *Science* **230** 127–31
[171] Qiu W, Ma -L-L, Wang H-T, Liang -R-R, Zhao Y-C and Zhou Y-S 2018 Experimental analyses on multiscale structural and mechanical properties of e-Si/GeSi/C-Si materials *Appl. Sci.* **8** 1–13
[172] Haddara Y M, Ashburn P and Bagnall D M 2017 Silicon-germanium: properties, growth and applications *Springer Handbook of Electronic and Photonic Materials*, ed S Kasap and P Capper (Berlin: Springer) (http://doi.org/10.1007/978-3-319-48933-9_22)
[173] Europractice 2020 Si-photonics foundries and technologies (https://europractice-ic.com/mpw-prototyping/siphotonics/)
[174] Liu A Y and Bowers J 2018 Photonic integration with epitaxial III–V on silicon *IEEE J. Sel. Top. Quantum Electron.* **24** 6000412
[175] Heck M J R and Mohammadhosseini H 2017 Energy-efficient millimeter-wave generation using silicon photonics *Proc. SPIE* **10108** 101080O
[176] Hasan M, Guemri R, Maldonado-Basilio R, Lucarz F, de Bougrenet de la Tocnaye J-L and Hall T 2014 Theoretical analysis and modeling of a photonic integrated circuit for frequency 8-tupled and 24-tupled millimeter wave signal generation *Opt. Lett.* **39** 6950–3
[177] Hasan M and Hall T J 2016 A photonic frequency octo-tupler with reduced RF drive power and extended spurious sideband suppression *Opt. Laser Technol.* **81** 115–21
[178] Hulme J, Kennedy M J, Chao R-L, Liang L, Komljenovic T, Shi J-W, Szafraniec B, Baney D and Bowers J E 2017 Fully integrated microwave frequency synthesizer on heterogeneous silicon-III/V *Opt. Express* **25** 2422–31
[179] Demirtzioglou I, Lacava C, Bottrill K R H, Thomson D J, Reed G T, Richardson D J and Petropoulos P 2018 Frequency comb generation in a silicon ring resonator modulator *Opt. Express* **26** 790–6
[180] Hulme J C, Shi J-W, Kennedy M J, Komljenovic T, Szafraniec B, Baney D and Bowers J E 2016 Fully integrated heterodyne microwave generation on heterogeneous silicon-III/V *2016 IEEE Int. Topical Meeting on Microwave Photonics (MWP)* (*Long Beach, CA, USA*) (http://doi.org/10.1109/MWP.2016.7791274)
[181] Rosales R, Merghem K, Martinez A, Accard A, Lelarge F and Ramdane A 2011 High repetition rate two-section InAs/InP quantum-dash passively mode locked lasers *IPRM 2011-23rd Int. Conf. on Indium Phosphide and Related Materials* (*Berlin, Germany*)
[182] Fiol G, Kleinert M, Arsenijević D and Bimberg D 2011 1.3 μm range 40 GHz quantum-dot mode-locked laser under external continuous wave light injection or optical feedback *Semicond. Sci. Technol.* **26** 014006
[183] Roelkens G *et al* 2015 III-V-on-silicon photonic devices for optical communication and sensing *Photonics* **2** 969–1004
[184] Koch B R, Fang A W, Cohen O and Bowers J E 2007 Mode-locked silicon evanescent lasers *Opt. Express* **15** 11225–33
[185] Fang A W, Koch B R, Gan K-G, Park H, Jones R, Cohen O, Paniccia M J, Blumenthal D J and Bowers J E 2008 A racetrack mode-locked silicon evanescent laser *Opt. Express* **16** 1393–8
[186] Davenport M L, Kurczveil G, Heck M J R and Bowers J E 2012 A hybrid silicon colliding pulse mode-locked laser with integrated passive waveguide section *IEEE Photonics Conf. 2012* (*Burlingame, CA*) (http://doi.org/10.1109/IPCon.2012.6358873)
[187] Srinivasan S, Davenport M, Heck M J R, Hutchinson J, Norberg E, Fish G and Bowers J E 2014 Low phase noise hybrid silicon mode-locked lasers *Front. Optoelectron.* **7** 265–76
[188] Heck M J R, Srinivasan S, Davenport M L and Bowers J E 2015 Integrated microwave photonic isolators: theory, experimental realization and application in a

unidirectional ring mode-locked laser diode *Photonics* **2** 957–68
[189] Nielsen L, Bente E A J M, den Haan E and Heck M J R 2018 Theoretical and experimental investigation of unidirectionality in an integrated semiconductor ring mode-locked laser with two saturable absorbers *IEEE J. Quantum. Electron.* **54** 2000810
[190] Heck M J R, Davenport M L, Park H, Blumenthal D J and Bowers J E 2010 Ultra-long cavity hybrid silicon mode-locked laser diode operating at 930 MHz *2010 Conf. on Optical Fiber Communication (OFC/NFOEC), collocated National Fiber Optic Engineers Conf.* (*San Diego, CA*) (http://doi.org/10.1364/OFC.2010.OMI5)
[191] Van Gasse K, Wang Z, Moskalenko V, Latkowski S, Kuyken B, Bente E and Roelkens G 2016 Passively mode-locked III–V-on-silicon laser with 1 GHz repetition rate *2016 Int. Semiconductor Laser Conf. (ISLC)* (*Kobe, Japan*)
[192] Srinivasan S, Arrighi A, Heck M J R, Hutchinson J, Norberg E, Fish G and Bowers J E 2014 Harmonically mode-locked hybrid silicon laser with intra-cavity filter to suppress supermode noise *IEEE J. Sel. Top. Quantum Electron.* **20** 1100208
[193] Gunn C, Guckenberger D, Pinguet T, Gunn D, Eliyahu D, Mansoorian B, van Blerkom D A and Salminen O 2007 A low phase noise 10GHz optoelectronic RF oscillator implemented using CMOS photonics *2007 IEEE Int. Solid-State Circuits Conf.. Digest of Technical Papers* (*San Francisco, CA*) (http://doi.org/10.1109/ISSCC.2007.373548)
[194] Analui B, Guckenberger D, Kucharski D and Narasimha A 2006 A fully integrated 20-Gb/s optoelectronic transceiver implemented in a standard 0.13-μm CMOS SOI technology *IEEE J. Solid-State Circuits* **41** 2945–55
[195] Zhang W and Yao J 2017 A silicon photonic integrated frequency-tunable optoelectronic oscillator *2017 Int. Topical Meeting on Microwave Photonics (MWP)* (*Beijing, China*) (http://doi.org/10.1109/MWP.2017.8168643)
[196] Srinivasan S, Spencer D T, Heck M J R, Norberg E, Fish G, Theogarajan L and Bowers J E 2013 Microwave generation using an integrated hybrid silicon mode-locked laser in a coupled optoelectronic oscillator configuration *CLEO: 2013* (*San Jose, CA*) (http://doi.org/10.1364/CLEO_SI.2013.CTu2G.2)
[197] Hutchison D N, Sun J, Doylend J K, Kumar R, Heck J, Kim W, Phare C T, Feshali A and Rong H 2016 High-resolution aliasing-free optical beam steering *Optica* **3** 887–90
[198] Dostart N, Zhang B, Khilo A, Brand M, Al Qubaisi K, Onural D, Feldkhun D, Wagner K H and Popović M A 2020 Serpentine optical phased arrays for scalable integrated photonic LIDAR beam steering *Optica* **7** 726–32
[199] Chung S, Abediasl H and Hashemi H 2018 A monolithically integrated large-scale optical phased array in silicon-on-insulator CMOS *IEEE J. Solid-State Circuits* **53** 275–96
[200] Ross D D, Konkol M R, Shi S and Prather D 2017 Photodiode-integrated UWB phased array antennas *2017 IEEE Photonics Conf. (IPC)* (*Orlando, FL*) (http://doi.org/10.1109/IPCon.2017.8116026)
[201] Duan M and Ma J 2019 Optical true time delay unit with wide range and high resolution for phased array beamforming *Photonic Netw. Commun.* **38** 89–97
[202] Poulton C V, Byrd M J, Russo P, Timurdogan E, Khandaker M, Vermeulen D and Watts M R 2019 Long-range LiDAR and free-space data communication with high-performance optical phased arrays *IEEE J. Sel. Top. Quantum Electron.* **25** 7700108
[203] Han S, Ji S, Kang I, Kim S C and You C 2019 Millimeter wave beamforming receivers using a Si-based OBFN for 5Gwireless communication systems *Opt. Commun.* **430** 83–97
[204] Fatemi R, Abiri B, Khachaturian A and Hajimiri A 2018 High sensitivity active flat optics optical phased array receiver with a two-dimensional aperture *Opt. Express* **26** 29983–99
[205] Sun J, Timurdogan E, Yaacobi A, Hosseini E S and Watts M R 2013 Large-scale nanophotonic phased array *Nature* **493** 195–9
[206] Zhao C, Peng C and Hu W 2017 Blueprint for large-scale silicon optical phased array using electro-optical micro-ring pixels *Sci. Rep.* **7** 17727-1–12
[207] Zheng P, Wang C, Xu X, Li J, Lin D, Hu G, Zhang R, Yun B and Cui Y 2019 A seven bit silicon optical true time delay line for Ka-band phased array antenna *IEEE Photonics J.* **11** 5501809
[208] Xiang C, Davenport M L, Khurgin J B, Morton P A and Bowers J E 2018 Low-loss continuously tunable optical true time delay based on Si_3N_4 ring resonators *IEEE J. Sel. Top. Quantum Electron.* **24** 5900109
[209] Choo G, Madsen C K, Palermo S and Entesari K 2018 Automatic monitor-based tuning of an RF silicon photonic 1×4 asymmetric binary tree true-time-delay beamforming network *J. Lightwave Technol.* **36** 5263–75
[210] Kang G *et al* 2019 Silicon-based optical phased array using electro-optic p-i-n phase shifters *IEEE Photonics Technol. Lett.* **31** 1685–8
[211] Xie X *et al* 2016 High-power heterogeneously integrated waveguide-coupled photodiodes on silicon-on-diamond *2016 IEEE Int. Topical Meeting on Microwave Photonics (MWP)* (*Long Beach, CA*) (http://doi.org/10.1109/MWP.2016.7791321)
[212] Urick V J Jr , Mckinney J D and Williams K J 2015 *Fundamentals of Microwave Photonics* (New York: Wiley) vol 1 pp 39–52
[213] Michel J, Liu J and Kimerling L C 2010 High-performance Ge-on-Si photodetectors *Nat. Photon.* **4** 527–34
[214] Rouvalis E, Müller P, Fedderwitz S, Trommer D, Stephan J, Steffan A G and Unterbörsch G 2014 A high-power and high-linearity 50 GHz waveguide photodiode module *Optical Fiber Communication Conf.* (*San Francisco, CA*) (http://doi.org/10.1364/OFC.2014.M2G.1)
[215] Feng D *et al* 2009 High-speed Ge photodetector monolithically integrated with large cross-section silicon-on-insulator waveguide *Appl. Phys. Lett.* **95** 261105
[216] Campbell J C 2007 Recent advances in telecommunications avalanche photodiodes *J. Lightwave Technol.* **25** 109–21
[217] Williams K J 1994 Microwave nonlinearities in photodiodes *Dissertation* Vols (University of Maryland College Park) pp 4538
[218] Williams K J, Esman R D and Dagenais M 1996 Nonlinearities in pin microwave photodetectors *J. Lightwave Technol.* **14** 84–96
[219] Hu Y, Marks B S, Menyuk C R, Urick V J and Williams K J 2014 Modeling sources of nonlinearity in a simple p-i-n photodetector *J. Lightwave Technol.* **32** 3710–20
[220] Piels M, Ramaswamy A and Bowers J E 2013 Nonlinear modeling of waveguide photodetectors *Opt. Express* **21** 15634–44
[221] Dentan M and de Cremoux B 1990 Numerical simulation of the nonlinear response of a p-i-n photodiode under high illumination *J. Lightwave Technol.* **8** 1137–44
[222] Williams K J, Esman R D and Dagenais M 1994 Effects of high space-charge fields on the response of microwave photodetectors *IEEE Photonics Technol. Lett.* **6** 639–41

[223] Hastings A S, Draa M and Williams K 2011 Quantifying current-dependant quantum efficiency photodiode nonlinearities *2011 Int. Topical Meeting on Microwave Photonics Jointly Held with the 2011 Asia-Pacific Microwave Photonics Conf.* (*Singapore, Singapore*) (http://doi.org/10.1109/MWP.2011.6088759)

[224] Beling A, Xie X and Campbell J C 2016 High-power, high-linearity photodiodes *Optica* **3** 328–38

[225] Malyshev S and Chizh A 2004 State of the art high-speed photodetectors for microwave photonics application *15th Int. Conf. on Microwaves, Radar and Wireless Communications (IEEE Cat. No.04EX824)* (*Warsaw, Poland*) (http://doi.org/10.1109/MIKON.2004.1358469)

[226] Shen L, Jiao Y, Yao W, Cao Z, van Engelen J P, Roelkens G, Smit M K and van der Tol J J G M 2016 High-bandwidth uni-traveling carrier waveguide photodetector on an InP-membrane-on-silicon platform *Opt. Express* **24** 8290–301

[227] Pettai R 1984 *Noise in Receiving Systems* (New York: Wiley) pp 10–11, 17–39

[228] Rubiola E 2008 *Phase Noise and Frequency Stability in Oscillators* (Cambridge: Cambridge University Press) (http://doi.org/10.1017/CBO9780511812798)

[229] Richards P L 1994 Bolometers for infrared and millimeter waves *J. Appl. Phys.* **76** 1–24

[230] Lsoshima T, Isojima Y, Hakomori K, Kikuchi K, Nagai K and Nakagawa H 1995 Ultrahigh sensitivity single-photon detector using a Si avalanche photodiode for the measurement of ultraweak biochemiluminescence *Rev. Sci. Instrum.* **66** 2922–6

[231] Marcuse D 1990 Derivation of analytical expressions for the bit-error probability in lightwave systems with optical amplifiers *J. Lightwave Technol.* **8** 1816–23

[232] Busch K W and Busch M A 2018 Light polarization and signal processing in chiroptical instrumentation *Chiral Analysis (Second Edition), Advances in Spectroscopy, Chromatography and Emerging Methods* (Amsterdam: Elsevier) pp 73–151

[233] Rouphael T J 2014 Noise in wireless receiver systems *Wireless Receiver Architectures and Design - Antennas, RF, Synthesizers, Mixed Signal, and Digital Signal Processing* (New York: Academic) pp 105–78

[234] Friis H T 1944 Noise figures of radio receivers *Proc. IRE* **32** 419–22

[235] Williams K J, Goldberg L, Esman R D, Weller J F and Dagenais M 1989 6-34 GHz offset phase-locking of Nd:YAG 1319 nm nonplanar ring lasers *Electron. Lett.* **25** 1242–3

[236] Yogesh Prasad K R, Srinivas T and Ramana D V 2015 Design and demonstration of hardware efficient OPLL for generation of stable microwave signals by optical heterodyning *J. Opt.* **44** 103–18

[237] Tulchinsky D A, Hastings A S and Williams K J 2016 Characteristics and performance of offset phase locked single frequency heterodyned laser systems *Rev. Sci. Instrum.* **87** 053107-1–15

[238] Hawkins R T, Jones M D, Pepper S H and Goll J H 1991 Comparison of fast photodetector response measurements by optical heterodyne and pulse response techniques *J. Lightwave Technol.* **9** 1289–94

[239] Draa M N, Hastings A S and Williams K J 2011 Comparison of photodiode non-linearity measurement systems *Opt. Express* **19** 12635–45

[240] Liu P-L, Williams K J, Frankel M Y and Esman R D 1999 Saturation characteristics of fast photodetectors *IEEE Trans. Microw. Theory Tech.* **47** 1297–303

[241] Williams K J and Esman R D 1998 Large-signal compression measurements in high-current pin photodiodes with +11 to +20 dBm output microwave power *Int. Topical Meeting on Microwave Photonics. Technical Digest (including High Speed Photonics Components Workshop)* (*Princeton, NJ*) (http://doi.org/10.1109/MWP.1998.745659)

[242] Lin L Y, Wu M C, Itoh T, Vang T A, Muller R E, Sivco D L and Cho A Y 1997 High-power high-speed photodetectors-design, analysis, and experimental demonstration *IEEE Trans. Microw. Theory Tech.* **45** 1320–31

[243] Iezekiel S 2009 *Microwave Photonics: Devices and Applications* (New York: Wiley) pp 22–3, 69, 92–4

[244] Li G *et al* 2012 S-compatible germanium *Opt. Express* **20** 26345–50

[245] Nagatsuma T, Ito H and Ishibashi T 2009 High-power RF photodiodes and their applications *Laser Photonics Rev.* **3** 123–37

[246] Pan H, Li Z, Beling A and Campbell J C 2009 Measurement and modeling of high-linearity modified uni-traveling carrier photodiode with highly-doped absorber *Opt. Express* **17** 20221–6

[247] Xie X, Zhou Q, Li K, Shen Y, Li Q, Yang Z, Beling A and Campbell J C 2014 Improved power conversion efficiency in high-performance photodiodes by flip-chip bonding on diamond *Optica* **1** 429–35

[248] Xie X, Zhou Q, Norberg E, Jacob-Mitos M, Chen Y, Yang Z, Ramaswamy A, Fish G, Campbell J C and Beling A 2016 High-power and high-speed heterogeneously integrated waveguide-coupled photodiodes on silicon-on-insulator *J. Lightwave Technol.* **34** 73–78

[249] Giboney K S, Rodwell M J W and Bowers J E 1992 Traveling-wave photodetectors *IEEE Photonics Technol. Lett.* **4** 1363–5

[250] Murthy S, Jung T, Chau T, Wu M C, Sivco D L and Cho A Y 2000 A novel monolithic distributed traveling-wave photodetector with parallel optical feed *IEEE Photonics Technol. Lett.* **12** 681–3

[251] Hirota Y, Hirono T, Ishibashi T and Ito H 2001 Traveling-wave photodetector for 1.55 μm wavelength fabricated with unitraveling-carrier photodiodes *Appl. Phys. Lett.* **78** 3767–9

[252] Sun K, Costanzo R, Tzu T-C, Yu Q, Bowers S M and Beling A 2018 Ge-on-Si waveguide photodiode array for high-power applications *2018 IEEE Photonics Conf. (IPC)* (*Reston, VA*) (http://doi.org/10.1109/IPCon.2018.8527107)

[253] Chang C-M, Sinsky J H, Dong P, de Valicourt G and Chen Y-K 2015 High-power dual-fed traveling wave photodetector circuits in silicon photonics *Opt. Express* **23** 22857–66

[254] Beling A, Cross A S, Piels M, Peters J, Zhou Q, Bowers J E and Campbell J C 2013 InP-based waveguide photodiodes heterogeneously integrated on silicon-on-insulator for photonic microwave generation *Opt. Express* **21** 25901–6

[255] Wang Y, Wang Z, Yu Q, Xie X, Posavitz T, Jacob-Mitos M, Ramaswamy A, Norberg E J, Fish G A and Beling A 2018 High-power photodiodes with 65 GHz bandwidth heterogeneously integrated onto silicon-on-insulator nano-waveguides *IEEE J. Sel. Top. Quantum Electron.* **24** 6000206

[256] Xie X, Zhou Q, Norberg E, Jacob-Mitos M, Chen Y, Ramaswamy A, Fish G, Bowers J E, Campbell J and Beling A 2015 Heterogeneously integrated waveguide-coupled photodiodes on SOI with 12 dBm output power at 40 GHz *2015 Optical Fiber Communications Conf. and Exhibition (OFC)* (*Los Angeles, CA*) (http://doi.org/10.1364/OFC.2015.Th5B.7)

[257] Hulme J, Kennedy M J, Chao R-L, Komljenovic T, Shi J-W and Bowers J E 2016 Heterogeneously integrated InP

based evanescently-coupled high-speed and high-power p-i-n photodiodes on silicon-on-insulator (SOI) substrate *2016 IEEE Int. Topical Meeting on Microwave Photonics (MWP)* (*Long Beach, CA*) (http://doi.org/10.1109/MWP.2016.7791322)
[258] Li Q, Li K, Fu Y, Xie X, Yang Z, Beling A and Campbell J C 2016 High-power flip-chip bonded photodiode with 110 GHz bandwidth *J. Lightwave Technol.* **34** 2139–44
[259] Chandrakasan A P, Sheng S and Brodersen R W 1992 Low-power CMOS digital design *IEEE J. Solid-State Circuits* **27** 473–84
[260] Reed G T, Mashanovich G, Gardes F Y and Thomson D J 2010 Silicon optical modulators *Nat. Photon.* **4** 518–26
[261] Soref R A and Bennett B R 1987 Electrooptical effects in silicon *IEEE J. Quantum. Electron.* **23** 123–9
[262] Reed G T and Png J C E 2005 Silicon optical modulators *Mater. Today* **8** 40–50
[263] Yu H *et al* 2012 Performance tradeoff between lateral and interdigitated doping patterns for high speed carrier-depletion based silicon modulators *Opt. Express* **20** 12926–38
[264] Liu A, Liao L, Rubin D, Nguyen H, Ciftcioglu B, Chetrit Y, Izhaky N and Paniccia M 2007 High-speed optical modulation based on carrier depletion in a silicon waveguide *Opt. Express* **15** 660–8
[265] Park J W, You J-B, Kim I G and Kim G 2009 High-modulation efficiency silicon Mach-Zehnder optical modulator based on carrier depletion in a PN Diode *Opt. Express* **17** 15520–4
[266] Sacher W D, Green W M J, Assefa S, Barwicz T, Pan H, Shank S M, Vlasov Y A and Poon J K S 2013 Coupling modulation of microrings at rates beyond the linewidth limit *Opt. Express* **21** 9722–33
[267] van Engelen J P, Shen L, Roelkens G, Jiao Y, Smit M K and van der Tol J J G M 2018 A novel broadband electro-absorption modulator based on bandfilling in n-InGaAs: design and simulations *IEEE J. Sel. Top. Quantum Electron.* **24** 3300108
[268] Van Gasse K, Verbist J, Li H, Torfs G, Bauwelinck J and Roelkens G 2019 Silicon photonics radio-over-fiber transmitter using GeSi EAMs for frequency up-conversion *IEEE Photonics Technol. Lett.* **31** 181–4
[269] Yamanaka T, Tsuzuki K, Kikuchi N, Yamada E, Shibata Y, Fukano H, Nakajima H, Akage Y and Yasaka H 2006 High-performance InP-based optical modulators *2006 Optical Fiber Communication Conf. and the National Fiber Optic Engineers Conf.* (*Anaheim, CA*) (http://doi.org/10.1109/OFC.2006.215454)
[270] Hui-Tao W, Dai-Bing Z, Rui-Kang Z, Dan L, Ling-Juan Z, Hong-Liang Z, Wei W and Chen J 2015 Optimization of 1.3-μm InGaAsP/InP electro-absorption modulator *Chin. Phys. Lett.* **32** 084203-1–5
[271] Gasulla I and Capmany J 2011 Analytical model and figures of merit for filtered microwave photonic links *Opt. Express* **19** 19758–74
[272] Liu K, Ye C R, Khan S and Sorger V J 2015 Review and perspective on ultrafast wavelength-size electro-optic modulators *Laser Photonics Rev.* **9** 172–94
[273] Li Z-Y, Xu D-X, McKinnon W R, Janz S, Schmid J H, Cheben P and Yu J-Z 2009 Silicon waveguide modulator based on carrier depletion in periodically interleaved PN junction *Opt. Express* **17** 15947–58
[274] Cohen R A, Amrani O and Ruschin S 2015 Linearized electro-optic racetrack modulator based on double injection method in silicon *Opt. Express* **23** 2252–61
[275] Degli-Eredi I and Heck M J R 2020 Experimental demonstration of a novel microwave photonics ring modulator with reduced driving power *IEEE J. Quantum. Electron.* **56** 5200111
[276] Li G, Krishnamoorthy A V, Shubin I, Yao J, Luo Y, Thacker H, Zheng X, Raj K and Cunningham J E 2013 Ring resonator modulators in silicon for interchip photonic links *IEEE J. Sel. Top. Quantum Electron.* **19** 3401819
[277] Janner D, Tulli D, Belmonte M and Pruneri V 2008 Waveguide electro-optic modulation in micro-engineered $LiNbO_3$ *J. Opt. A: Pure Appl. Opt.* **10** 104003
[278] Maldonado. T A 1995 Electro-optic modulators *Handbook of Optics: Devices, Measurements, and Properties* vol 2 2nd edn (New York: McGraw-Hill) p 13.30
[279] Lauermann M 2018 Electro-optic bandwidth measurement *Silicon-Organic Hybrid Devices for High-Speed Electro-Optic Signal Processing* ed C Koos, W Freude and S Randel (Karlsruhe: KIT Scientific Publishing) p 125
[280] Reed G T, Mashanovich G Z, Gardes F Y, Nedeljkovic M, Hu Y, Thomson D J, Li K, Wilson P R, Chen S-W and Hsu S S 2014 Recent breakthroughs in carrier depletion based silicon optical modulators *Nanophotonics* **3** 229–45
[281] Witzens J 2018 High-speed silicon photonics modulators *Proc. IEEE* **106** 2158–82
[282] Li M, Wang L, Li X, Xiao X and Yu S 2018 Silicon intensity Mach–Zehnder modulator for single lane 100 Gb/s applications *Photonics Res.* **6** 109–16
[283] DeRose C T, Trotter D C, Zortman W A and Watts M R 2012 High speed travelling wave carrier depletion silicon Mach-Zehnder modulator *2012 Optical Interconnects Conf.* (*Santa Fe, NM*)
[284] Zhou J, Wang J, Zhu L, Zhang Q and Hong J 2019 Silicon photonics carrier depletion modulators capable of 85Gbaud 16QAM and 64Gbaud 64QAM *2019 Optical Fiber Communications Conf. and Exhibition (OFC)* (*San Diego, CA*) (http://doi.org/10.1364/OFC.2019.Tu2H.2)
[285] Patel D, Samani A, Veerasubramanian V, Ghosh S and Plant D V 2015 Silicon photonic segmented modulator-based electro-optic DAC for 100 Gb/s PAM-4 generation *IEEE Photonics Technol. Lett.* **27** 2433–6
[286] Romero-García S, Moscoso-Mártir A, Sharif Azadeh S, Müller J, Shen B, Merget F and Witzens J 2017 High-speed resonantly enhanced silicon photonics modulator with a large operating temperature range *Opt. Lett.* **42** 81–84
[287] Müller J, Merget F, Sharif Azadeh S, Hauck J, Romero García S, Shen B and Witzens J 2014 Optical peaking enhancement in high-speed ring modulators *Sci. Rep.* **4** 6310
[288] Sharif Azadeh S, Müller J, Merget F, Romero-García S, Shen B and Witzens J 2014 Advances in silicon photonics segmented electrode Mach-Zehnder modulators and peaking enhanced resonant devices *Proc. SPIE* **9288** 928817
[289] Zhang C, Morton P A, Khurgin J B, Peters J D and Bowers J E 2016 Highly linear heterogeneous-integrated Mach-Zehnder interferometer modulators on Si *Opt. Express* **24** 19040–7
[290] Song M, Zhang L, Beausoleil R G and Willner A E 2010 Nonlinear distortion in a silicon microring-based electro-optic modulator for analog optical links *IEEE J. Sel. Top. Quantum Electron.* **16** 185–91
[291] Ding J, Shao S, Zhang L, Fu X and Yang L 2016 Method to improve the linearity of the silicon Mach-Zehnder optical modulator by doping control *Opt. Express* **24** 24641–8
[292] Xiao X, Xu H, Li X, Li Z, Chu T, Yu Y and Yu J 2013 High-speed, low-loss silicon Mach-Zehnder modulators with doping optimization *Opt. Express* **21** 4116–25
[293] Kim Y, Takenaka M, Osada T, Hata M and Takagi S 2015 Strain-induced enhancement of plasma dispersion effect

and free-carrier absorption in SiGe optical modulators *Sci. Rep.* **4** 4683
[294] Nguyen H C, Hashimoto S, Shinkawa M and Baba T 2012 Compact and fast photonic crystal silicon optical modulators *Opt. Express* **20** 22465–74
[295] Gao Y, Wen A, Tu Z, Zhang W and Lin L 2016 Simultaneously photonic frequency downconversion, multichannel phase shifting, and IQ demodulation for wideband microwave signals *Opt. Lett.* **41** 4484–7
[296] Luo X, Tu X, Song J, Ding L, Fang Q, Liow T-Y, Yu M and Lo G-Q 2013 Slope efficiency and spurious-free dynamic range of silicon Mach-Zehnder modulator upon carrier depletion and injection effects *Opt. Express* **21** 16570–7
[297] Cardenas J, Morton P A, Khurgin J B, Griffith A, Poitras C B, Preston K and Lipson M 2013 Linearized silicon modulator based on a ring assisted Mach Zehnder inteferometer *Opt. Express* **21** 22549–57
[298] Gutiérrez A M *et al* 2012 Silicon-based electro-optic modulators for linear and nonlinear radio-over-fiber applications *2012 IEEE Int. Topical Meeting on Microwave Photonics* (*Noordwijk, Netherlands*) (http://doi.org/10.1109/MWP.2012.6474083)
[299] Zhang C, Morton P A, Khurgin J B, Peters J D and Bowers J E 2016 Ultralinear heterogeneously integrated ring-assisted Mach–Zehnder interferometer modulator on silicon *Optica* **3** 1483–8
[300] Li J, Zhang Y-C, Yu S, Jiang T, Xie Q and Gu W 2013 Third-order intermodulation distortion elimination of microwave photonics link based on integrated dual-drive dual-parallel Mach–Zehnder modulator *Opt. Lett.* **38** 4285–7
[301] Zhou Y, Zhou L, Wang M, Xia Y, Zhong Y, Li X and Chen J 2016 Linearity characterization of a dual-parallel silicon Mach-Zehnder modulator *IEEE Photonics J.* **8** 7805108
[302] Jiang W, Tan Q, Qin W, Liang D, Li X, Ma H and Zhu Z 2015 A linearization analog photonic link with high third-order intermodulation distortion suppression based on dual-parallel Mach-Zehnder modulator *IEEE Photonics J.* **7** 7902208
[303] Streshinsky M, Ayazi A, Xuan Z, Lim A E-J, Lo G-Q, Baehr-Jones T and Hochberg M 2013 Highly linear silicon traveling wave Mach-Zehnder carrier depletion modulator based on differential drive *Opt. Express* **21** 3818–25
[304] Zhou Y, Zhou L, Su F, Xie J, Zhu H, Li X and Chen J 2015 Linearity measurement of a silicon single-drive push-pull Mach-Zehnder modulator *2015 Conf. on Lasers and Electro-Optics (CLEO)* (*San Jose, CA*) (http://doi.org/10.1364/CLEO_SI.2015.SW3N.6)
[305] Morton P A, Morton M J, Zhang C, Khurgin J B, Peters J, Morton C D and Bowers J E 2019 High-power, high-linearity, heterogeneously integrated III–V on Si MZI modulators for RF photonics systems *IEEE Photonics J.* **11** 5501310
[306] Ayazi A, Baehr-Jones T, Liu Y, Lim A E-J and Hochberg M 2012 Linearity of silicon ring modulators for analog optical links *Opt. Express* **20** 13115–22
[307] Chen L, Chen J, Nagy J and Reano R M 2015 Highly linear ring modulator from hybrid silicon and lithium niobate *Opt. Express* **23** 13255–64
[308] Shen Y, Hraimel B, Zhang X, Cowan G E R, Wu K and Liu. T 2010 A novel analog broadband RF predistortion circuit to linearize electro-absorption modulators in multiband OFDM radio-over-fiber systems *IEEE Trans. Microw. Theory Tech.* **58** 3327–35
[309] Chen S, Deng L, Ye Y, Chen X, Cheng M, Tang M, Fu S, Luo F and Liu D 2017 Experimental investigation on improved predistortion circuit for directly modulated radio over fiber system *IEEE Photonics J.* **9** 5502509
[310] Zhu R, Zhang X, Hraimel B, Shen D and Liu T 2013 Broadband predistortion circuit using zero bias diodes for radio over fiber systems *IEEE Photonics Technol. Lett.* **25** 2101–4
[311] Zhang X, Lee B, Lin C-Y, Wang A X, Hosseini A and Chen R T 2012 Highly linear, broadband optical modulator based on electro-optic polymer *IEEE Photonics J.* **4** 2214–28
[312] Burla M, Hoessbacher C, Heni W, Haffner C, Fedoryshyn Y, Elder D L, Dalton L R and Leuthold J 2017 Plasmonic-organic hybrid Mach-Zehnder modulators: experimental characterization of intermodulation distortions *32nd URSI GASS* (*Montreal, Canada*)
[313] Liu Y, Hotton J, Choudhary A, Eggleton B J and Marpaung D 2017 All-optimized integrated RF photonic notch filter *Opt. Lett.* **42** 4631–4
[314] Tao Y, Shu H, Jin M, Wang X, Zhou L and Zou W 2019 Numerical investigation of the linearity of graphene-based silicon waveguide modulator *Opt. Express* **27** 9013–31
[315] Zhang X, Zhu R, Shen D and Liu T 2014 Linearization technologies for broadband radio-over-fiber transmission systems *Photonics* **1** 455–72
[316] Napoli A *et al* 2018 Digital pre-compensation techniques enabling high-capacity bandwidth variable transponders *Opt. Commun.* **409** 52–65
[317] Zhalehpour S, Lin J, Sepehrian H, Shi W and Rusch L A 2018 Mitigating pattern dependent nonlinearity in SiP IQ-modulators via iterative learning control predistortion *Opt. Express* **26** 27639–49
[318] Duan R, Xu K, Dai J, Lan M, Wu J and Lin J 2011 Suppression of third-order intermodulation distortion based on digital post compensation in intensity-modulation direct-detection analog optical links *Int. Summer Session: Lasers and Their Applications* (http://doi.org/10.1364/SUMSESSION.2011.Th28)
[319] Niu Z, Yu H, Chen M, Li P, Chen H and Xie S 2014 High linearity downconverting analog photonic link based on digital signal post-compensation *Optical Fiber Communication Conf.* (*San Francisco, CA*) (http://doi.org/10.1364/OFC.2014.W2A.37)
[320] Poberaj G, Hu H, Sohler W and Günter P 2012 Lithium niobate on insulator (LNOI) for micro-photonic devices *Laser Photonics Rev.* **6** 488–503
[321] Boes A, Corcoran B, Chang L, Bowers J and Mitchell A 2018 Status and potential of lithium niobate on insulator (LNOI) for photonic integrated circuits *Laser Photonics Rev.* **12** 1700256
[322] He M *et al* 2019 High-performance hybrid silicon and lithium niobate Mach–Zehnder modulators for 100 Gbit s−1 and beyond *Nat. Photon.* **13** 359–64
[323] Weigel P O *et al* 2018 Bonded thin film lithium niobate modulator on a silicon photonics platform exceeding 100 GHz 3-dB electrical modulation bandwidth *Opt. Express* **26** 23728–39
[324] Rabiei P, Ma J, Khan S, Chiles J and Fathpour S 2013 Heterogeneous lithium niobate photonics on silicon substrates *Opt. Express* **21** 25573–81
[325] Chen L, Wood M G and Reano R M 2013 12.5 pm/V hybrid silicon and lithium niobate optical microring resonator with integrated electrodes *Opt. Express* **21** 27003–10
[326] Qi Y and Li Y 2020 Integrated lithium niobate photonics *Nanophotonics* **9** 1287–320
[327] Sun S, He M, Xu M, Zhang X, Ruan Z, Liu L and Cai X 2020 120 Gb s-1 hybrid silicon and lithium niobate modulators with on-chip termination resistor *2020 Optical*

Fiber Communications Conf. and Exhibition (OFC) (*San Diego, CA*) (http://doi.org/10.1364/OFC.2020.M2B.7)
[328] Wang X, Weigel P O, Zhao J, Ruesing M and Mookherjea S 2019 Achieving beyond-100-GHz large-signal modulation bandwidth in hybrid silicon photonics Mach Zehnder modulators using thin film lithium niobate *APL Photonics* **4** 096101-1–8
[329] Wang C, Zhang M, Chen X, Bertrand M, Shams-Ansari A, Chandrasekhar S, Winzer P and Lončar M 2018 Integrated lithium niobate electro-optic modulators operating at CMOS-compatible voltages *Nature* **562** 101–4
[330] Mercante A J, Shi S, Yao P, Xie L, Weikle R M and Prather D W 2018 Thin film lithium niobate electro-optic modulator with terahertz operating bandwidth *Opt. Express* **26** 14810–6
[331] Jian J, Xu M, Liu L, Luo Y, Zhang J, Lin L, Zhou L, Chen H, Yu S and Cai X 2019 High modulation efficiency lithium niobate Michelson interferometer modulator *Opt. Express* **27** 18731–9
[332] Heni W *et al* 2017 Silicon-organic and plasmonic-organic hybrid photonics *ACS Photonics* **4** 1576–90
[333] Koos C *et al* 2016 Silicon-organic hybrid (SOH) and plasmonic-organic hybrid (POH) integration *J. Lightwave Technol.* **34** 256–68
[334] Haffner C *et al* 2016 Plasmonic organic hybrid modulators-scaling highest speed photonics to the microscale *Proc. IEEE* **104** 2362–79
[335] Hoessbacher C *et al* 2017 Plasmonic modulator with >170 GHz bandwidth demonstrated at 100 GBd NRZ *Opt. Express* **25** 1762–8
[336] Heni W *et al* 2016 108 Gbit/s plasmonic Mach-Zehnder modulator with >70-GHz electrical bandwidth *J. Lightwave Technol.* **34** 393–400
[337] Liu M, Yin X, Ulin-Avila E, Geng B, Zentgraf T, Ju L, Wang F and Zhang X 2011 A graphene-based broad-band optical modulator *Nature* **474** 64–67
[338] Luo S, Wang Y, Tong X and Wang Z 2015 Graphene-based optical modulators *Nanoscale Res. Lett.* **10** 1–11
[339] Phare C T, Lee Y-H D, Cardenas J and Lipson M 2015 Graphene electro-optic modulator with 30 GHz bandwidth *Nat. Photon.* **9** 511–4
[340] Dalir H, Xia Y, Wang Y and Zhang X 2016 Athermal broadband graphene optical modulator with 35 GHz speed *ACS Photonics* **3** 1564–8
[341] Shu H-W, Jin M, Tao Y-S and Wang X-J 2019 Graphene-based silicon modulators *Front. Inf. Technol. Electron. Eng.* **20** 458–71
[342] Tonouchi M 2007 Cutting-edge terahertz technology *Nat. Photon.* **1** 97–105
[343] Zouaghi W, Thomson M D, Rabia K, Hahn R, Blank V and Roskos H G 2013 Broadband terahertz spectroscopy: principles, fundamental research and potential for industrial applications *Eur. J. Phys.* **34** S179–99
[344] Ghann W and Uddin J 2017 Terahertz (THz) spectroscopy: a cutting-edge technology *Terahertz Spectroscopy - A Cutting Edge Technology* (London: IntechOpen) (http://doi.org/10.5772/62805)
[345] Dhillon S S *et al* 2017 The 2017 terahertz science and technology roadmap *J. Phys. D: Appl. Phys.* **50** 043001
[346] Rommel S, Raddo T R and Tafur Monroy I 2018 Data center connectivity by 6G wireless systems *Proc. 2018 Photonics in Switching and Computing, PSC 2018* (*Limmasol, Cyprus*) (http://doi.org/10.1109/PS.2018.8751363)
[347] Nagatsuma T, Ducournau G and Renaud C C 2016 Advances in terahertz communications accelerated by photonics *Nat. Photon.* **10** 371–9
[348] Correas-Serrano D and Gómez-Díaz J S 2017 Graphene-based antennas for terahertz systems: a review *Forum for Electromagnetic Research Methods and Application Technologies*
[349] Pavlov S G, Zhukavin R K, Orlova E E, Shastin V N, Kirsanov A V, Hübers H-W, Auen K and Riemann H 2000 Stimulated emission from donor transitions in silicon *Phys. Rev. Lett.* **84** 5220–3
[350] Bründermann E, Chamberlin D R and Haller E E 2000 High duty cycle and continuous terahertz emission from germanium *Appl. Phys. Lett.* **76** 2991–3
[351] Hübers H-W, Pavlov S G and Shastin V N 2005 Terahertz lasers based on germanium and silicon *Semicond. Sci. Technol.* **20** S211–21
[352] Kadow C, Jackson A W, Gossard A C, Matsuura S and Blake G A 2000 Self-assembled ErAs islands in GaAs for optical-heterodyne THz generation *Appl. Phys. Lett.* **76** 3510–2
[353] Köhler R, Tredicucci A, Beltram F, Beere H E, Linfield E H, Davies A G, Ritchie D A, Iotti R C and Rossi F 2002 Terahertz semiconductor-heterostructure laser *Nature* **417** 156–9
[354] Bates R *et al* 2003 Interwell intersubband electroluminescence from Si/SiGe quantum cascade emitters *Appl. Phys. Lett.* **83** 4092–4
[355] Chung P-K and Yen S-T 2014 Enhanced thermal radiation in terahertz and far-infrared regime by hot phonon excitation in a field effect transistor *J. Appl. Phys.* **116** 183101
[356] Pavlov S G *et al* 2014 Terahertz stimulated emission from silicon doped by hydrogenlike acceptors *Phys. Rev.* X **4** 021009
[357] Jones R, Cohen O, Paniccia M, Fang A W, Park H and Bowers J E 2007 A hybrid silicon laser *Photonics Spectra* **41** 54–6
[358] Fang A W, Park H, Cohen O, Jones R, Paniccia M J and Bowers J E 2006 Electrically pumped hybrid AlGaInAs-silicon evanescent laser *Opt. Express* **14** 9203–10
[359] Koos C *et al* 2009 All-optical high-speed signal processing with silicon–organic hybrid slot waveguides *Nat. Photon.* **3** 216–9
[360] Fasching G, Benz A, Zobl R, Andrews A M, Roch T, Schrenk W, Strasser G, Tamosiunas V and Unterrainer K 2006 Microcavity THz quantum cascade laser *Physica* E **32** 316–9
[361] Gmachl C, Capasso F, Sivco D L and Cho A Y 2001 Recent progress in quantum cascade lasers and applications *Rep. Prog. Phys.* **64** 1533–601
[362] Jung S, Kim J H, Jiang Y, Vijayraghavan K and Belkin M A 2017 Terahertz difference-frequency quantum cascade laser sources on silicon *Optica* **4** 38–43
[363] Nguyen-Van H *et al* 2018 Quantum cascade lasers grown on silicon *Sci. Rep.* **8** 1–8
[364] Vijayraghavan K, Adams R W, Vizbaras A, Jang M, Grasse C, Boehm G, Amann M C and Belkin M A 2012 Terahertz sources based on Čerenkov difference-frequency generation in quantum cascade lasers *Appl. Phys. Lett.* **100** 1–4
[365] Yang H, Zhao D, Chuwongin S, Seo J-H, Yang W, Shuai Y, Berggren J, Hammar M, Ma Z and Zhou W 2012 Transfer-printed stacked nanomembrane lasers on silicon *Nat. Photon.* **6** 615–20
[366] Justice J, Bower C, Meitl M, Mooney M B, Gubbins M A and Corbett B 2012 Wafer-scale integration of group III-V lasers on silicon using transfer printing of epitaxial layers *Nat. Photon.* **6** 610–4
[367] Spott A *et al* 2016 Quantum cascade laser on silicon *Optica* **3** 545–51

[368] Spott A *et al* 2016 Heterogeneously integrated distributed feedback quantum cascade lasers on silicon *Photonics* **3** 35-1–10

[369] Liu M Y, Chou S Y, Alexandrou S, Wang C C and Hsiang T Y 1993 110 GHz Si MSM photodetectors *IEEE Trans. Electron Devices* **40** 2145–6

[370] Liu M Y, Chen E and Chou S Y 1994 140-GHz metal-semiconductor-metal photodetectors on silicon-on-insulator substrate with a scaled active layer *Appl. Phys. Lett.* **65** 887–8

[371] Chen L and Lipson M 2009 Ultra-low capacitance and high speed germanium photodetectors on silicon *Opt. Express* **17** 7901–6

[372] Lacombe E, Gianesello F, Durand C, Ducournau G, Luxey C and Gloria D 2017 Sub-THz source integrated in industrial silicon photonic technology targeting high data rate wireless applications *2017 IEEE 17th Topical Meeting on Silicon Monolithic Integrated Circuits in RF Systems (SiRF)* (*Phoenix, AZ*) (http://doi.org/10.1109/SIRF.2017.7874361)

[373] Bowers S M, Abiri B, Aflatouni F and Hajimiri A 2014 A compact optically driven travelling-wave radiating source *OFC 2014* (*San Francisco, CA*) (http://doi.org/10.1364/OFC.2014.Tu2A.3)

[374] Schuster F, Coquillat D, Videlier H, Sakowicz M, Teppe F, Dussopt L, Giffard B, Skotnicki T and Knap W 2011 Broadband terahertz imaging with highly sensitive silicon CMOS detectors *Opt. Express* **19** 7827–32

[375] Tanoto H *et al* 2012 Greatly enhanced continuous-wave terahertz emission by nano-electrodes in a photoconductive photomixer *Nat. Photon.* **6** 121–6

[376] Preu S, Döhler G H, Malzer S, Wang L J and Gossard A C 2011 Tunable, continuous-wave terahertz photomixer sources and applications *J. Appl. Phys.* **109** 061301

[377] Gregory I S, Tribe W R, Cole B E, Evans M J, Linfield E H, Davies A G and Missous M 2004 Resonant dipole antennas for continuous-wave terahertz photomixers *Appl. Phys. Lett.* **85** 1622–4

[378] Pilla S 2007 Enhancing the photomixing efficiency of optoelectronic devices in the terahertz regime *Appl. Phys. Lett.* **90** 161119

[379] Safian R, Ghazi G and Mohammadian N 2019 Review of photomixing continuous-wave terahertz systems and current application trends in terahertz domain *Opt. Eng.* **58** 110901

[380] Burford N M and El-Shenawee M O 2017 Review of terahertz photoconductive antenna technology *Opt. Eng.* **56** 010901

[381] Chen P, Hosseini M and Babakhani A 2016 An Integrated germanium-based optical waveguide coupled THz photoconductive antenna in silicon *Conf. on Lasers and Electro-Optics 2016* (http://doi.org/10.1364/CLEO_SI.2016.STh3I.2)

[382] Withayachumnankul W, Yamada R, Fumeaux C, Fujita M and Nagatsuma T 2017 All-dielectric integration of dielectric resonator antenna and photonic crystal waveguide *Opt. Express* **25** 14706–14

[383] Withayachumnankul W, Yamada R, Fujita M and Nagatsuma T 2018 All-dielectric rod antenna array for terahertz communications *APL Photonics* **3** 051707

[384] Yata M, Fujita M and Nagatsuma T 2016 Photonic-crystal diplexers for terahertz-wave applications *Opt. Express* **24** 7835–49

[385] Headland D, Withayachumnankul W, Yamada R, Fujita M and Nagatsuma T 2018 Terahertz multi-beam antenna using photonic crystal waveguide and Luneburg lens *APL Photonics* **3** 126105

[386] Tsuruda K, Fujita M and Nagatsuma T 2015 Extremely low-loss terahertz waveguide based on silicon photonic-crystal slab *Opt. Express* **23** 31977–90

[387] Withayachumnankul W, Fujita M and Nagatsuma T 2018 Integrated silicon photonic crystals toward terahertz communications *Adv. Opt. Mater.* **6** 1800401

[388] Okamoto K, Tsuruda K, Diebold S, Hisatake S, Fujita M and Nagatsuma T 2017 Terahertz sensor using photonic crystal cavity and resonant tunneling diodes *J. Infrared Millim. Terahertz Waves* **38** 1085–97

[389] Urbanowicz A, Adomavičius R, Krotkus A and Malevich V L 2005 Electron dynamics in Ge crystals studied by terahertz emission from photoexcited surfaces *Semicond. Sci. Technol.* **20** 1010–5

[390] Kang C, Leem J W, Maeng I, Kim T H, Lee J S, Yu J S and Kee C-S 2015 Strong emission of terahertz radiation from nanostructured Ge surfaces *Appl. Phys. Lett.* **106** 261106

[391] Wang X and Gan X 2017 Graphene integrated photodetectors and opto-electronic devices—a review *Chin. Phys.* B **26** 034201

[392] Gosciniak J, Rasras M and Khurgin J B 2020 Ultrafast plasmonic graphene photodetector based on the channel photothermoelectric effect *ACS Photonics* **7** 488–98

[393] Koike Y and Gaudino R 2013 Chapter 10 - plastic optical fibers and Gb/s data links *Optical Fiber Telecommunications (Sixth Edition): Components and Subsystems* vol Optics and Photonics (New York: Academic Press) pp 353–76

[394] Siokis A, Christodoulopoulos K and Varvarigos E 2017 *Optical Interconnects for Data Centers* (: Cambridge: Woodhead) pp 3–41, 375–93

[395] Tang J, Hao T, Li W, Domenech D, Baños R, Muñoz P, Zhu N, Capmany J and Li. M 2018 Integrated optoelectronic oscillator *Opt. Express* **26** 12257–65

[396] Tønning P and Heck M J R 2018 Feasibility study of integrated photonic oscillators with 5 fs timing jitter *2018 European Conf. on Integrated Optics* (*Valencia, Spain*)

[397] Do P T, Alonso-Ramos C, Le Roux X, Vivien L, Ledoux I, Cassan E and Journet B 2019 Tunable optoelectronic oscillator based on silicon micro-ring resonator *2019 European Conf. on Integrated Optics* (*Ghent, Belgium*)

[398] Sun K and Beling A 2019 High-speed photodetectors for microwave photonics *Appl. Sci.* **9** 1–15

[399] Serafino G, Porzi C, Falconi F, Pinna S, Puleri M, D'Errico A, Bogoni A and Ghelfi P 2018 Photonics-assisted beamforming for 5G communications *IEEE Photonics Technol. Lett.* **30** 1826–9

[400] Friis H T 1946 A note on a simple transmission formula *Proc. IRE* **34** 254–6